Master of Science Thesis

Preliminary structural design of a tanker spacecraft for on-orbit refueling purposes

Panagiotis Trifa

National Technical University of Athens

Master of Science Thesis

Computational Mechanics in Solids

Preliminary Structural Design of a Tanker Spacecraft for On-Orbit Refueling Purposes

Author:

Panagiotis Trifa

Thesis supervisor:

Ass. Professor V. Papadopoulos

National Technical
University of Athens

Heron Engineering

Athens, June 2019

The research in this thesis was supported and supervised by Associate Professor Vissarion Papadopoulos at Laboratory of Structural Analysis and Anti-seismic Research and Heron Engineering company. Their cooperation is hereby gratefully acknowledged.

Dedicated to my parents for their endless love...

Acknowledgements

The following research is the result of my involvement in Laboratory of Structural Analysis and Anti-seismic Research as well as my partnership with Heron Engineering Company, in the area of computational structural analysis and finite element method. That work has motivated me to delve into the structural design process of spacecraft systems. Appreciating this successful partnership throughout the duration of this thesis work, I would like to acknowledge and express my heartfelt gratitude to the following persons for their continuous support, guidance and motivation.

I would like to thank my thesis supervisor, Ass. Professor Vissarion Papadopoulos who guided me with insightful directions on this project and contributed to my better understanding on computational structural mechanics aspects.

Special thanks go to the engineers from Heron Engineering Company, Ms. Georgia Psoni and Mr. Dimitris Rellakis for their trust and confidence in me; for all of their advices concerning spacecraft design disciplines and their technical assistance in performing finite element analysis.

Finally, I would like to express my deepest gratitude to my sister Ileana for her assistance during writing and reviewing this thesis work.

Abstract

In the past two decades, some of the most extraordinary breakthroughs in space exploration have emphasized the growing importance of on-orbit servicing. The current challenges concerning the space sector have moved beyond simply launching complex systems. Consequently, the aerospace industry faces the need of exploiting the flight systems already launched, constructing structures in situ to assist new scientific projects while providing services to systems that reliably and cost-effectively support the next steps in space exploration. Being inspired from the satellite's life extension concept and focusing specifically on the on-orbit refueling applications, this thesis suggests the implementation of a tanker spacecraft in order to satisfy this specific need and delves into the conceptual and structural design of a structure of this particular concept.

The attention of this work is mainly focused on the spacecraft's primary structure and its payload. The design proceeds by performing separate sizing procedures for the above structures, examining both static and dynamic environments. The computation of the structural response of the tanker spacecraft is carried out through finite element analysis, considering the most critical load cases, which correspond to the most severe environments that both structures will encounter throughout their operational lifetime.

The design process incorporates multiple types of finite element analysis, such as linear static, linear buckling and nonlinear elastoplastic for the preliminary sizing of both structural modules. Afterwards, the design proceeds with modal analysis and is finalized via sinusoidal vibration analysis for the low operational frequency range of the spacecraft by suggesting proper design modifications and finalizing the sizing procedure.

In conclusion, the analysis provides the structural design process with encouraging results which satisfy simultaneously mass, strength and stiffness requirements, preventing the proposed structure from the most common material failures, structural instability or dynamic coupling and resonance effects.

Table of Contents

List of Figures

List of Tables

List of Diagrams

1. Introduction

1.1. On-orbit refueling concept

For more than two decades, on-orbit servicing is one of the most revolutionary and promising challenges, concerning the space industry. On-orbit servicing, refers to operations conducted to assist an operating satellite 'in need' by preventing and solving a wide range of performance anomalies. Prime examples of on-orbit services, which are applied on a spacecraft, are the in-situ inspections of possible damages, the robotic manipulations for assisting release of stuck antennas or solar arrays, adjusting out-of-space thermal blankets, collecting space debris etc. However, this work focuses on an alternative aspect of on-orbit servicing, that corresponds to the satellite's life extension. Life extension refers to the process of lengthening the period of time of a space asset, enabling a satellite to continue operating for its intended purpose, while staying within its licensed and operational boundaries. Considering that the propellant is a fundamental key for crucial phases of a space mission-such as station keeping or orbit and attitude control-it is obvious that propellant exhaustion is the main reason for the ending of a satellite's useful lifetime, despite the fact that the rest of its subsystems might be fully functional. There are two different technologies proposed to provide on-orbit life extension services. The first one involves tug services, where a vehicle is attached to the 'dying' satellite and thus becoming its new power source and booster module. ViviSat proposed the Mission Extension Vehicle (MEV) concept for providing tug services. [1]

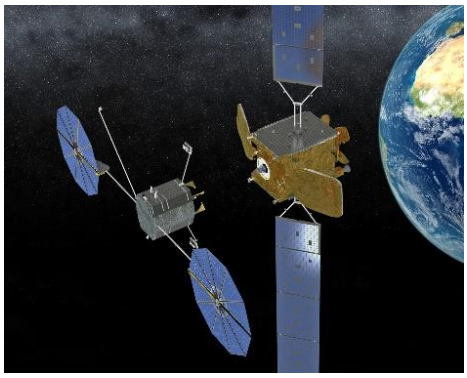

Figure 1.1 Client Satellite Receives Tug Services [Credits: ViviSat]

The second one consists of refueling services. The most common approaches for this technology are the concept of propellant in-space depot and the propellant tanker delivery. Delving deeper into the second concept, propellant tanker delivery refers to the implementation of a tanker spacecraft, which rendezvous and docks with the on-obit client, refuels it and disengages from it, in order to continue refueling the upcoming clients. USG Agencies, such as NASA and DARPA have been conducting research on providing refueling services. [2]

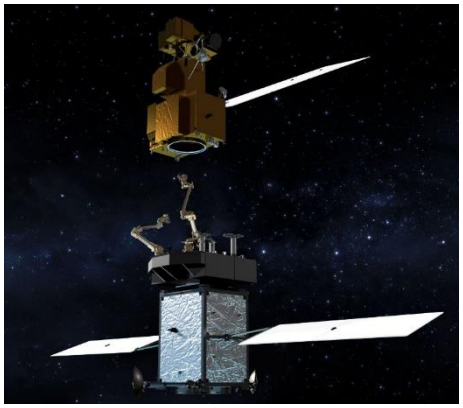

Figure 1.2 Client Satellite Receives Refueling Services [Credits: NASA]

Being inspired from the aforementioned philosophy, the present study focuses on the conceptual and preliminary structural design of a tanker spacecraft.

1.2. Master's Thesis Aims

The multiple challenges arising from the on-orbit refueling concept lead the aerospace industry to invest on relevant research and innovation development in designing spacecraft systems for these particular applications. This thesis work suggests a preliminary configuration for an innovative tanker spacecraft, focusing mainly on its structural analysis and design. The analysis of the tanker spacecraft is being conducted using finite element method while investigating its structural response against the most severe operational environments, in order to size its most critical structural modules.

1.3. Master's Thesis Objectives

The present study investigates an on-orbit refueling application by focusing on the development of a tanker spacecraft concept. More specifically, it focuses on the structural analysis and design of its primary structure and payload. It is important to mention that the frame of the spacecraft and the storage tank are considered the primary structure and the payload of the spacecraft, respectively. All the steps needed for the design of the tanker spacecraft are strictly relied on the requirements and constraints introduced by VEGA Launcher with regards to auxiliary mini passengers. Moreover, it must be clearly stated that, generally, the design of a spacecraft structure is strongly dependent on the entirety of its subsystems, such as propulsion, thermal, power, attitude control, communication, trajectory etc. This study is limited in examining the tanker spacecraft only from the structural point of view due to the complexity, that arises from combining principles and requirements of the above-mentioned systems and their disciplines.

The first objective of this thesis consists of the definition and the design of the structural configuration of the spacecraft's frame and storage tank and a proper material selection, in to order to provide a combination of mass, stiffness and strength efficiency for each module.

The second objective concerns the development of the mathematical representation of the proposed structure and the correct computation of its structural response against the most conservative magnitudes of the encountered predominant environments.

The third objective emphasizes the development of an iterative design process which focuses on sizing the storage tank and the frame structure, taking into consideration that the spacecraft is subjected not only to static loads, but also to dynamic loads. Consequently, it is of great importance the most critical load cases be defined and incorporated to the mathematical model of the structure. The ultimate goal is to determine the minimum thickness of the tank and the minimum preliminary dimensions of the cross-sectional profiles of the frame members, ensuring the structural integrity of both structures while preventing material failure, structural instabilities or unacceptable operational events.

Finally, the finalized product of the structural design process must be accessed so as to examine if the design constraints, such as the position of the center of gravity and the mass restrictions, are met or not.

2. Tanker Spacecraft's Structural Configuration Design

2.1. Usable Volume and Mechanical Interface of the Tanker Spacecraft

The first step in defining spacecraft's configuration, is to realize and respect the requirements and the constraints induced by the Launch Vehicle, which refer to both mass and volume. As it was already pointed out, the proposed tanker spacecraft concept is considered and designed as an auxiliary mini passenger, compatible with VEGA Launcher. This particular type of passenger is included in a launch vehicle, in case of extra performance and volume on a main passenger mission. VEGA Launcher offers additional volume for only a single mini passenger customer to be delivered into orbit. The classification for small spacecrafts according to the Arianespace User's Manual defines the mini passenger, as a small spacecraft with a mass between 200 and 400 (kg). [3] It should be pointed out that all of the following data in this section are collected from the aforementioned User's Manual. Apart from the mass constraints, special attention must be paid on Center of Gravity position of the tanker spacecraft. It is required that the distance between the mounting plane of the spacecraft and its center of gravity position does not exceed 900(mm). Moreover, the static unbalance of the Center of Gravity position must stay within 15 (mm). VEGA Launcher provides the VESPA system as a carrying structure in which the mini passenger is placed internally. As a result, VESPA structure dictates the available usable volume and the type of the mechanical interface between the mini passenger and the VEGA. The VESPA is manufactured by AIRBUS DS CASA and consists of the upper part, the boat tail, the inner cone and the inner platform. The separation of the upper part of the VESPA structure is achieved through clamp band with 8 springs.

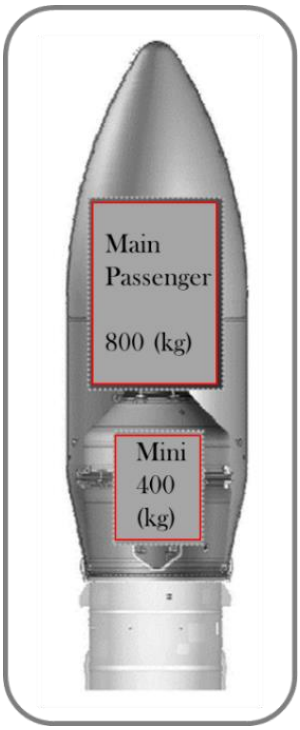

Figure 2.1 VEGA Launcher Configuration [Credits: Arianespace]

It is noteworthy that among the different versions of VESPA, the stretched one is implemented for carrying the tanker spacecraft. The dimensions of the usable volume provided by this particular version is presented below. The maximum height of the usable volume is 2150 (mm) and its maximum diameter reaches 1700 (mm).

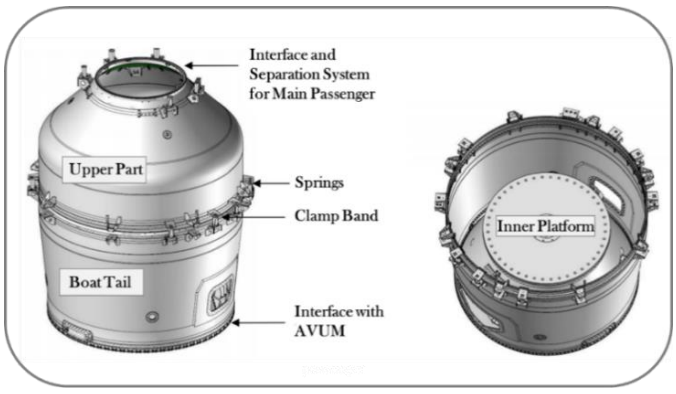

Figure 2.2 VESPA Configuration [Credits: Arianespace]

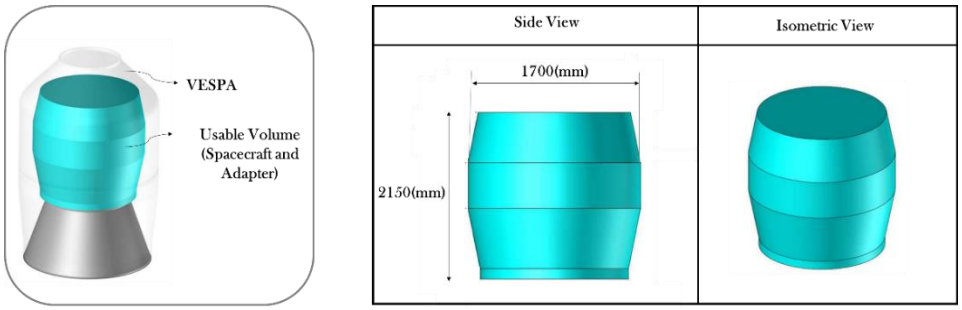

Figure 2.3 Usable Volume Dimensions [Credits: Arianespace]

Examining the internal of the VESPA structure, it can be observed that an off-the-shelf adapter is attached at the upper surface of the inner platform. The adapter provides the mechanical interface between the spacecraft and the carrying structure. Depending on each auxiliary passenger, Arianespace offers a wide variety of compatible adapters. Each adapter is equipped with a payload separation system and brackets for electrical connectors. The tanker spacecraft incorporates the PAS 432 RUAG Space AB. This specific structure comprises the passive ring, which is the interface on the remaining part on the spacecraft, and the active ring, that is the interface remaining part on the carrying structure respectively. The spacecraft is secured to the adapter interface ring by a clamping device. The clamp band consists of a band with one connecting point. The tension applied to the band provides pressure on the clamp as it attaches the spacecraft to the VESPA structure. Release is obtained by means of a Clamp-Ring Separation System, which initiates pyrotechnically. This kind of circular interface is widely used and preferred because it induces uniform load distribution along the contact surfaces.

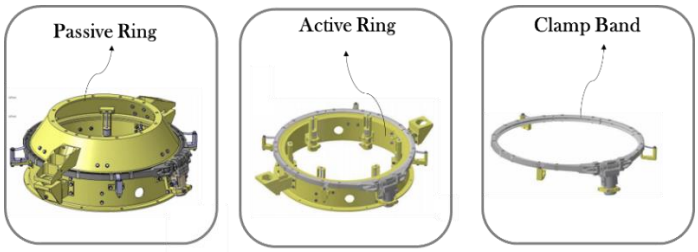

Figure 2.4 PAS 432 RUAG Space AB Adapter [Credits: Arianespace]

2.2. Tank Structure Configuration

The storage tank is obviously the most critical mission-specific equipment of the tanker spacecraft and thus the most definitive design factor for the spacecraft configuration. A major consideration when designing a storage tank, is to avoid embedding a single spherical storage tank or a combination of spheres into a non-spherical spacecraft envelope, because several mass and volume penalties might arise. [4] Hence, for the preliminary design process, a cylindrical body combined with two hemispherical ends is proposed. At this point, due to mass considerations, it is worth noting that hemispherical ends for a cylindrically shaped tank are preferred over ellipsoidal ones. Preliminary dimensions, such as the length of the cylinder and the inner radius, are defined with the perspective of leveraging the maximum given usable volume of the VESPA, and thus pursuing a maximum tank capacity for propellant storage. The length of the cylinder is 400(mm) and its inner radius is 360 (mm). Thickness of the tank's wall is selected as the design variable of the problem and its final value is going to be defined through strength analysis, which is going to be described on later chapters.

It is notable that the wall thickness of the tank is uniform throughout the structure and its preliminary value is assumed 4 (mm).

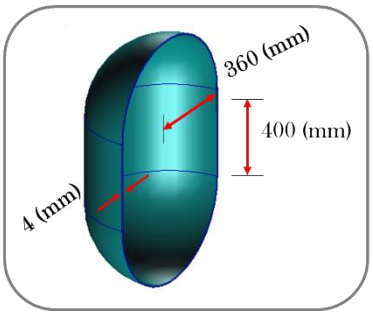

Figure 2.5 Tank Dimensions

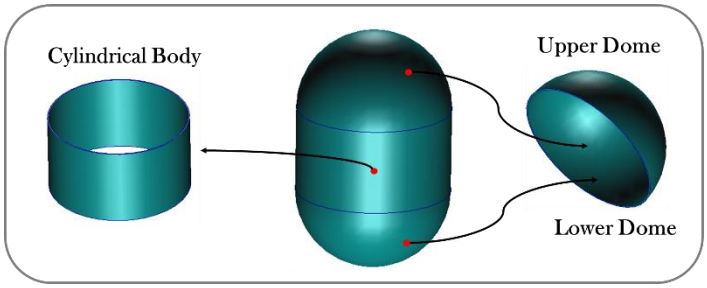

Figure 2.6 Tank Configuration

2.3. Frame Structure Configuration

Frame is considered to be the spacecraft's backbone, which provides the major load path between spacecraft's components and the Launch Vehicle. As a result, it is designed as a primary structure. Its main objective is to support the payload with enough strength and stiffness so as to prevent any type of failure, such as yielding, excessive deformation, rupture and buckling. The proposed frame, actually incorporates a skeletal network of beams that are capable of carrying combined axial, shear, torsion loads and bending moments. Considering previous successful structural design concepts, there is a notable preference for implementing symmetrical shapes in designing small spacecrafts. Following this particular philosophy, the proposed frame for the tanker spacecraft is characterized as a combination of beams which form a hexagonal box at the upper part, and the interface tower of conical shape at the lower part of the spacecraft. It should be emphasized that a major consideration upon designing the geometry of thee frame, is to ensure that the storage tank is properly mounted. As it is illustrated below, perfect compatibility between the tank and the frame is achieved via the respective mounting rings. The beam members of the frame, depending on their specific location and function, are categorized into seven groups. The hexagonal box consists of upper and lower bulkhead, longerons, diagonal struts, main deck struts, main deck ring and upper struts. On the other hand, the interface tower consists of support struts, support mounting ring and adapter ring. The bonding of the upper and the lower part of the spacecraft is obtained via connection struts.

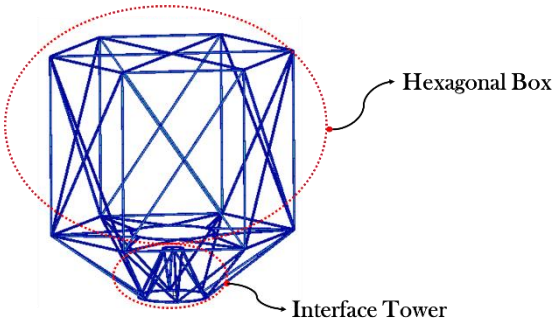

Figure 2.7 Frame Configuration

Frame Beam Groups	Number of Beam Members
Upper Struts	6
Support Struts	6
Diagonal Struts	24
Mounting Struts	12
Connect Struts	12
Main Deck Struts	12
Upper/Lower Bulkhead	12
Longerons	6
Rings	3

Table 2.1 Number of Beam Members

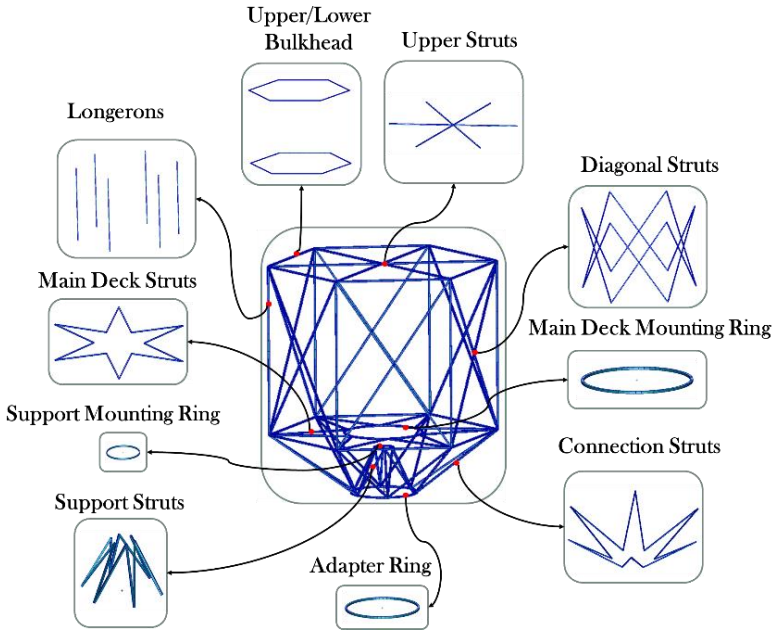

Figure 2.8 Categories of Beam Members

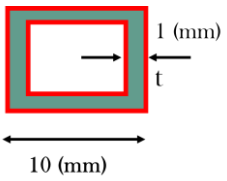

Figure 2.9 Square Tube Cross-Sectional Area

Proceeding with a lightweight design of the spacecraft frame, thin walled square beams have been incorporated due to their high stiffness to weight ratios. Indicative cross-sectional dimensions of 10x1 have been selected for the entirety of the beam groups before initiating the design process. Width and thickness of the thin-walled square tube are selected as the design variables of the problem. Similar to the tank sizing procedure, strength analysis is going to be performed so as to finalize the appropriate values of the design variables. It must be pointed out that each change of the design variable is applied to the entire beam group and not to individual beams. Moreover, it is important to underline that the length dimensions of the beam members be defined so as to provide the tank with a proper enclosure, respecting and taking advantage of the maximum usable volume restrictions induced by the VESPA structure.

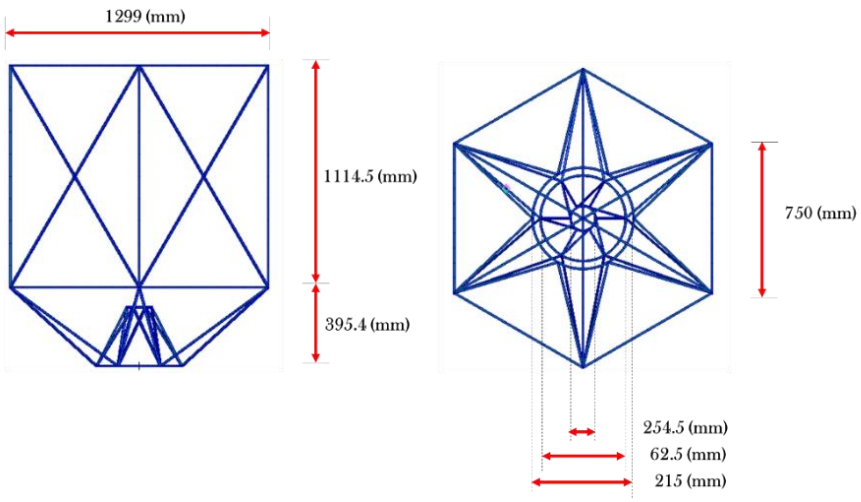

Figure 2.10 Frame Dimensions

2.4. Material Selection

Material selection plays a vital role in structural design process of the tanker spacecraft structures, indicating specific criteria that must be met in order to satisfy all the requirements induced throughout their operational lifetime. The selected materials must provide a combination of various mechanical properties and features, [5] such as high specific strength and stiffness with high resistance against fatigue and stress corrosion and ease of manufacturing and welding. The most commonly used metallic materials on spacecraft applications are the aluminum alloys and especially series 2000 and 6000, which satisfy the above criteria and operate successfully under the most severe mechanical environments, combining both mass and stiffness efficiency. Aluminum alloy 6061 meets the aforementioned requirements and as a result it is selected as the construction material for the spacecraft's frame. On the other hand, a closer examination on the material selection for the storage tank indicates the importance of ensuring a long-term chemical compatibility between the propellant and the construction material of the tank. Within the scope of the tanker spacecraft concept, hydrazine is assumed as the storable liquid propellant. Among aluminum alloys, 6066-T6 is one of the most widely used materials for hydrazine storage tank applications. Tables of operational properties of hydrazine and mechanical properties of aluminum alloys 6061 and 6066-T6 are presented below.

Properties	
Density	1.021 ($g \cdot cm^3$)
Boiling Point	114 (°C)
Storage Temperature	-37 (°C)-71 (°C)
Operating Pressure	4.10 (MPa)

Table 2.2 Hydrazine Operational Properties [Wikipedia]

Mechanical Properties	Al-6061	Al-6066-T6
Tensile Yield Strength (MPa)	276	359
Compressive Yield Strength (MPa)	-276	-359
Ultimate Tensile Strength (MPa)	310	
Elongation at Break (%)	12	12
Modulus of Elasticity (MPa)	68900	68900
Poisson's Ratio	0.33	0.33
Density $\left(Mg / mm^3\right)$	$2.70 \cdot 10^{-9}$	$2.72 \cdot 10^{-9}$

Table 2.3 Mechanical Properties of 6061 and 6066-T6 Aluminum Alloys [Matweb]

3. Development of the Mathematical Model

3.1. Analysis Methods and Software Selection

There is a wide range of critical operational events during a space mission, such as handling, transportation, ground, launch and orbital operations, that must be taken into account when designing spacecraft's components. Among the above-mentioned operations, launch events induce the most severe environments and the maximum load regimes upon the spacecraft, mainly because of the propulsion system operation. Launch consists of a series of events, [6] each of which has several independent load sources for the launch vehicle and the passenger. Among them, only static acceleration and low-frequency dynamic response is being examined in this study. The procedure followed for validating the structural integrity of a specific spacecraft component subjected to the above load sources, requires, initially, the mathematical representation of its structure. This particular representation is achieved through a mathematical model which caters significantly to the overall design process, such as the calculation of the most critical natural frequencies of the structure and the prediction of the structural response to static and dynamic loads.

Figure 3.1 VEGA Launcher at the Launch Phase [Credits: Arianespace]

It is more than obvious that a mathematical model, representing a pressurized storage tank, mounted on a complex spacecraft frame, cannot be approached accurately either by closed form solutions known from theory of elasticity or by practical stress analysis approximate solutions. The complexity induced by this particular engineering problem is counteracted using Finite Element Method, which enjoys predominance among the numerical methods in solving complex structural mechanics problems.

For the scope of this thesis work, finite element procedures, have been carried out via the academic version of MSC Patran and Nastran Software, 2018, for evaluating the tanker spacecraft's mechanical behavior and for sizing each of the spacecraft's structural modules. A major limitation of this version is that the models are restricted to only 5000 computational nodes. It is also noted that Patran is the pre-processor and post-processor software and Nastran is the solver software. The development of the finite element model requires the sequential application of specific pre-processing steps. The process starts with the creation of the model's geometry which depicts the actual configuration of the structure. Afterwards, the geometry of each structural module included in the model, is discretized and consequently the finite element mesh is generated. An essential issue encountered in this step, is that the model's mesh must be generated in such a way that the incorporated elements respect and properly discretize the geometry of the structure so as to enable the solver to provide sufficient and accurate nodal and elemental results. The following steps depend on the type of the finite element analysis. They generally consist of the application of the boundary conditions, the application of the external

loads, the input of material and elemental properties and finally the submission of the completed model to the Nastran through its input .bdf file. Subsequently, Nastran solves the problem-specific system of equations for the requested outputs by creating specific data recovery files. Files such as .f04, .f06, .MASTER, .xdb contain analysis results. Afterwards they are brought back in Patran for post-processing actions. The final step concerns the interpretation and the evaluation of the results via deformation and stress fringe plots, reports, graphs and output data that record the progress of the analysis.

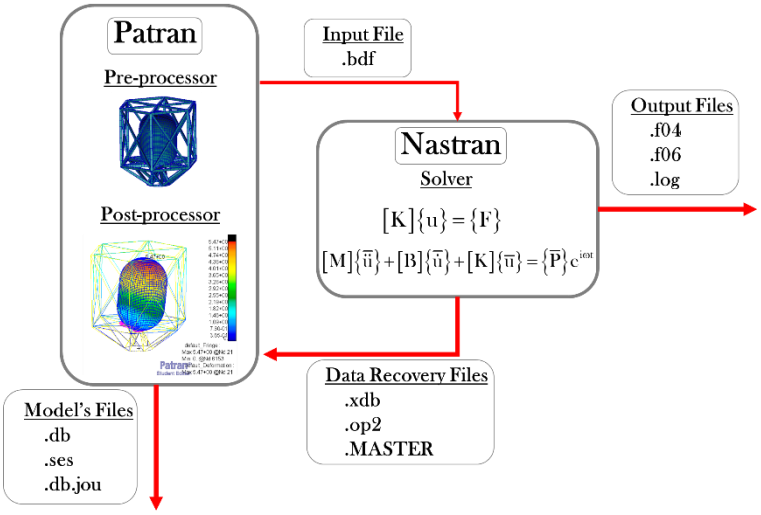

Figure 3.2 Patran/Nastran File Exchange

3.2. Geometry Development of the Finite Element Model

Upon building finite element model for the preliminary design of the tanker spacecraft, it is of great importance that the model should be developed in such a manner that the analysis can suggest feasible modifications on the initial geometry. As a result, special attention must be paid in creating geometry that represents the actual structure, combining both simplicity and accuracy. The first step in developing the analytical geometry of the model in Patran, is to create points which are zero-dimensional CAD entities, representing certain locations in space. Examining the tank case, six points have been created in order to represent a hemi-section of the tank. Specifically, the hemi-section consists of the top and the lowest regions of tank's cylindrical body and its hemispherical domes including the frame's attachment locations. However, from the frame's point of view each created point represents the end of a beam member. The following step consists of connecting the previously created points with curves,

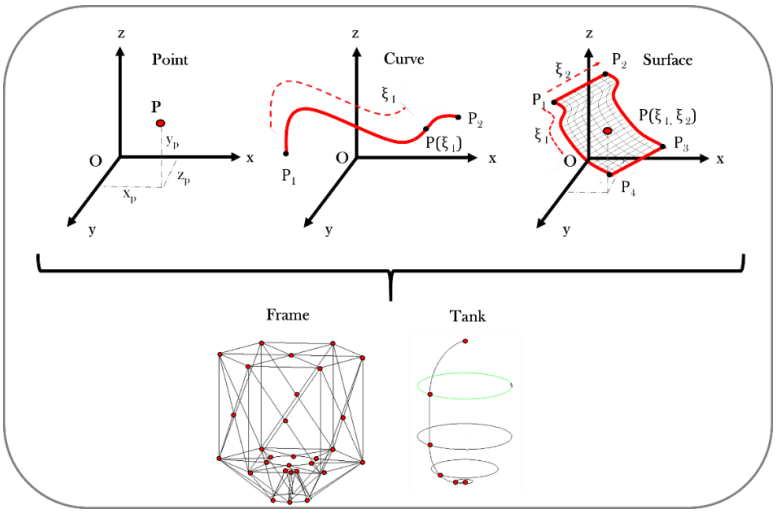

Figure 3.3 Geometric Model of the Frame and the Tank of the Tanker Spacecraft

which are general vector functions of a single parametric variable ξ_1. Meshing curves results into generating one-dimensional finite elements. The hemi-section of the tank is completed by connecting the proper side points with quarter circles and the intermediate points with a straight line, as to form the hemi-sectional domes and the main body of the tank, respectively. On the other hand, the geometry of the frame is obtained by connecting the points, which correspond to beam ends with a straight line and with proper arcs, so to form the circular adapter and mounting rings. The last step refers exclusively to the completion of the tank geometry and implies a revolution of 360° for the hemi-section of the tank. Therefore, the appropriate cylindrical and hemispherical surfaces of the tank are created. Surfaces are general vector functions of two parametric variables ξ_1 and ξ_2. The generated mesh upon them, results in creating two dimensional finite elements. In conclusion, the created geometry, as described, provides simplicity in modifying the values of the design variables for structures, facilitating the iterative trial and error process for the preliminary design of the tanker spacecraft.

3.3. Finite Element Type Selection

The philosophy upon selecting the most appropriate finite element types for a successful structural model is based on combining two features concurrently. The first feature requires that the shape of each element type must satisfy the geometry of each structural module. The second one implies that the mathematical formulation of each element type is sufficient for the development of the correct load path within the structure, ensuring its realistic response upon external loading.

Starting from the first structural module, it is crucial that the storage tank be considered as a thin-walled pressure vessel, consisting of curved surfaces, such as the cylindrical main body and the hemispherical domes. The most commonly used finite elements for modelling curved surfaces with much lower thickness than the rest dimensions, are the shell elements. There are two major categories of shell elements in Nastran. CTRIA3 are three-nodded isoparametric shell elements that correspond to the unstructured grid layer, developed circumferentially to the poles of the two tank domes. On the other hand, CQUAD4 are four nodded isoparametric shell elements which correspond to the structured of the rest tank structure. The nodes of both CTRIA3 and CQUAD4 coincide with the grid points that define the corners of each element. Additionally, both elements are elastically connected to only five of the six elemental degrees of freedom at their grid points, due to the

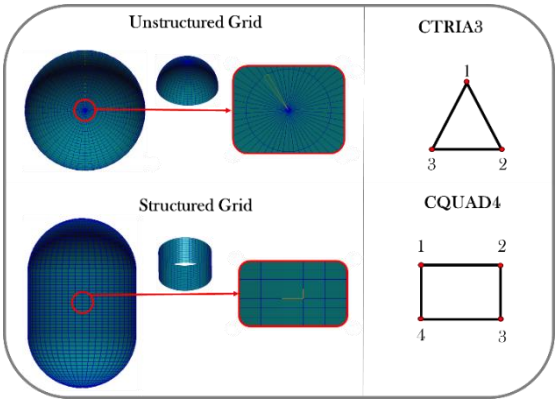

Figure 3.4 Tank Modelling with Shell Elements

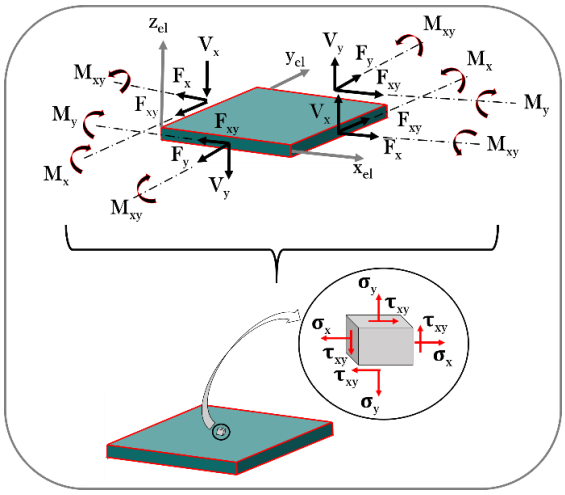

Figure 3.5 Forces, Moments and Stresses in Shell Elements

absence of the direct elastic stiffness at the rotational degree of freedom, about the surface normal.

Figure 3.5 depicts the forces, the moments and the stresses on a shell element. Shell elements are formulated according the assumption of small deflections. This implies that during bending the mid-surface remains unstrained upon the action of lateral out-of-plane loads. Finally, it is of great importance that shell elements orientation be pointed out. This particular feature is defined upon each surface via its normal vector. Determining the proper direction of the normal vectors is the most critical step for applying correctly the pressure loads to tank's surfaces.

As far as the frame structure is concerned, it must be capable of carrying both longitudinal and lateral loads. As a result, axial, torsion and bending loads are developed on its beam members. The simplest Nastran beam element, which is capable of resisting against the combination of axial, shear forces and bending moments, is the CBAR element. This particular element is connected to two grid points and its formulation is derived from the classical beam theory, in which the plane sections of the beam remain plane even after the deformation. Moreover, similar to the shell elements, there is a need for defining normal vectors for the beam elements depending on their orientation, in order to capture the correct stiffness contribution of each beam member. Additional features of the CBAR elements include the automatic calculation of the transverse shear stiffness and the capability of creating beam members with principal moments of inertia axis that do not need to coincide with the element axis or with their neutral axis offset from the grid points. On the other hand, there are significant limitations introduced because of the CBAR element. For example, the beam member must be prismatic. Hence, its properties remain constant along its length. Furthermore, the shear center and the neutral axis of the element must coincide. This requirement is satisfied by selecting a rectangular hollow cross section for the design process. However, it is important that channel or angle sections must be avoided. Last but not least it is worth noting that the effect of cross-sectional warping is neglected.

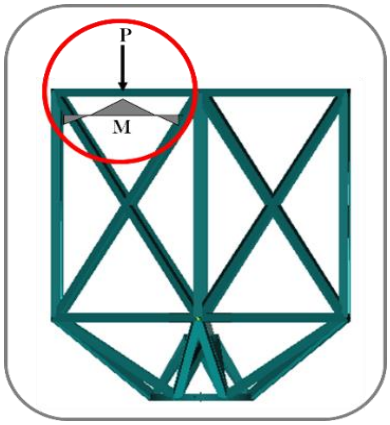

Figure 3.6 Need for Lateral and Longitudinal Frame Strength

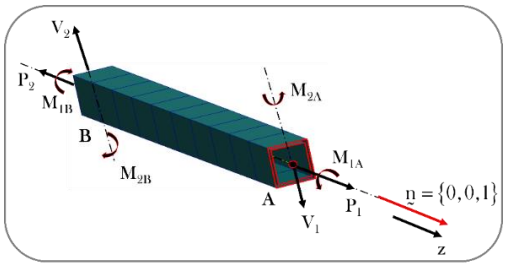

Figure 3.7 Beam Element Forces and Orientation

The bonding between the aforementioned structural modules is achieved by implementing rigid elements. Among them, RBE2 are the most suitable elements for providing a realistic approach of the load transfer between the frame and the storage tank. RBE2 elements connect an independent grid to one or multiple dependent grids, ensuring that stiffness, mass and loads are transferred from the dependent degrees of freedom to the independent degrees of freedom. Their formulation is derived from the small displacement theory, generating the respective multi-point-constraint equations.

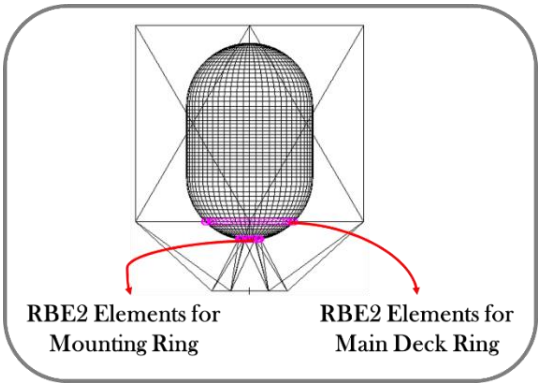

Figure 3.8 Bonding Frame and Tank Structures via RBE2 Elements

3.4. Units

The pre-processing process of a finite element model in MSC Patran requires that the user determines a specific system of units, used for the inputs of the model. Therefore, a consistent system of units must be selected so as to procced correctly with the results post-processing. For the purposes of this work, a variation of SI Units has been incorporated, using the millimeter (mm) as a unit for length. The unit of force is Newton (N) and the unit of time is second (s). The consistency of the selected unit system is checked by ensuring that Newton's Second Law is satisfied.

$$F = m \cdot a \rightarrow$$

$$\{1 \text{ unit force}\} = \{1 \text{ unit force}\} \cdot \{1 \text{ unit acceleration}\} \rightarrow$$

$$\{1\ (\mathrm{N})\} = \{1\ (\mathrm{Mg})\} \cdot \left\{1\ \left(\frac{\mathrm{mm}}{\mathrm{s}^2}\right)\right\}$$

The satisfaction of Newton's Second Law indicates that the units of mass must be expressed in Megagrams (Mg), which coincides with the metric ton (t). A detailed list of the most common inputs that are used upon developing the finite element model is presented below.

Inputs/Outputs	SI-mm Units
Length/Rotation	mm/rad
Mass	Mg
Forces/Moments	$\mathrm{N/N \cdot mm}$
Density	$\frac{\mathrm{Mg}}{\mathrm{mm}^3}$
Stress/Pressure	$\frac{\mathrm{N}}{\mathrm{mm}} = \mathrm{MPa}$
Frequency	Hz
Gravitational Acceleration	$9.81 \cdot 10^3 \frac{\mathrm{mm}}{\mathrm{s}^2}$

Table 3.1 Unit at SI-mm

4. Static Analysis of Tanker Spacecraft and Sizing Procedure

4.1. Static and Quasi-Static Loads Acting on the Tanker Spacecraft

The first consideration upon designing a tanker spacecraft, is to ensure that its structural modules are capable of withstanding the maximum quasi-static loads. [7] In particular, quasi-static loads are the most severe combinations of accelerations acting on that specific spacecraft. Reviewing the Ariane User's Manual for Auxiliary Passengers leads to two critical load cases. The first load case consists of the combination of longitudinal and lateral accelerations which subject the spacecraft under compression state. The second load case indicates an alternative combination of longitudinal and lateral acceleration that stresses the whole structure under tension. Between the two load cases, the design process will be determined by the one which induces the most conservative results.

	Quasi-Static Loads (g) (Static + Dynamic)		
Ground and Flight Load Cases	Lateral	Longitudinal	
	+2.6	Tension	Compression
		+5	-7.5

Table 4.1 Acceleration Acting on the Spacecraft

$$\begin{cases} a_{long}^{ten} = a_z = a_{long}^{ten} \cdot g = 5 \cdot 9.81 = 49.05 \left(\dfrac{m}{s^2} \right) \\ a_{long}^{com} = a_z = a_{long}^{com} \cdot g = -7.5 \cdot 9.81 = 73.58 \left(\dfrac{m}{s^2} \right) \\ a_{lat} = a_x = a_y = n_{lat} \cdot g = 2.6 \cdot 9.81 = 25.51 \left(\dfrac{m}{s^2} \right) \end{cases}$$

The resultant shear acceleration is given by: $a_{res} = \sqrt{a_{long}^2 + a_{lat}^2}$

Where:

- a_{long} : Longitudinal Acceleration
- a_{lat} : Lateral Acceleration
- a_{res} : Resultant Shear Acceleration
- n_{long} : Factor of Longitudinal Acceleration
- n_{lat} : Factor of Lateral Acceleration
- g : Gravitational Acceleration

Regarding structural design of the tank, the additional static and quasi-static loads, that are taken into account, are the internal overpressure, the hydrostatic pressure and the extra weight due to the contained propellant. The tank is designed to operate safely under the maximum magnitude of burst pressure. Burst pressure is obtained by multiplying the operating pressure with the burst factor, which equals to 1.25 for pressurized structures, assuming an unmanned mission.

$$P_{bur} = n_{bur} P_{oper} = 1.25 \cdot 4.10 = 5.125(\text{MPa})$$

Where:

- P_{bur} : Burst Pressure
- n_{bur} : Burst Factor
- P_{oper} : Operating Pressure

The weight of the propellant is an additional quasi-static load, which is evenly distributed throughout the hemispherical surface of the lower dome. Its inertial effect on the tank is further increased when considering the launch phase, where the tanker spacecraft is moving collinearly along its longitudinal axis with the acceleration $n_{long} \cdot g$ of the Launch Vehicle.

$$w_p = \frac{W_p}{A_h} = \frac{m_p \cdot (ng)}{A_h} = \frac{266 \cdot 7.5 \cdot 9.81}{0.814} \left(\frac{N}{m^2} \right) = 0.024(\text{MPa})$$

Where:

- P_{bur} : Burst Pressure
- n_{bur} : Burst Factor
- P_{oper} : Operating Pressure

Including the hydrostatic pressure among the external loads of the finite element model, multiple assumptions have been considered in its computation, for the sake of simplicity. First of all, it is assumed that the tank is filled with a specific quantity of propellant that corresponds to the internal volumes of the lower hemispherical dome and the cylindrical body. As a result, the internal volume of the upper dome coincides with the ullage volume of the tank. Considering that the ullage volume is neither in a vacuum state nor pressurized by any pressurization gas, it is estimated that the pressure at the surface of the propellant coincides with the external pressure, acting on the tank. A typical value of this type of pressure is 0.034 (MPa). Moreover, because of the fact that the liquid hydrazine is considered an incompressible fluid, it is reasonably estimated that its density is constant throughout the volume of the fluid. Finally, it is noted that the curved surface of the lower dome of the tank is not taken into account for the computation of the hydrostatic pressure. Consequently, the maximum hydrostatic pressure located on the bottom of the tank, is calculated via the following formula:

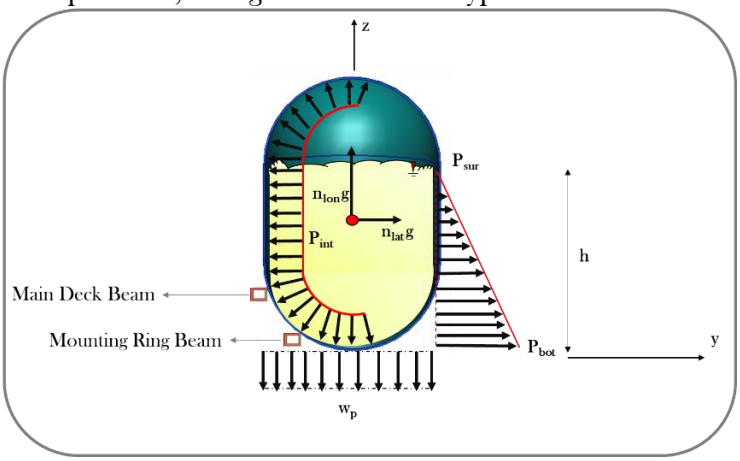

Figure 4.1 Static and Quasi-Static Loads Acting on the Tank

$$P_{bot} = P_{sur} + p_h \cdot (n_{long} g) \cdot h = 0.034(\text{MPa}) + 1.2 \cdot 10^{-9} \left(\frac{Mg}{mm^3} \right) \cdot 7.5 \cdot 9.81 \cdot 10^3 \left(\frac{mm}{s^2} \right) \cdot 400 \left(mm \right) = 0.064(\text{MPa})$$

Where:

- P_{bot} : Hydrostatic pressure on the bottom of the tank
- P_{sur} : Pressure on the surface of the propellant
- p_h : Hydrazine density
- h: Height of the test area

On the other hand, except from the combination of longitudinal and lateral accelerations, the design of the frame structure, is also determined by the combination of constraint forces and moments due to the attached storage tank.

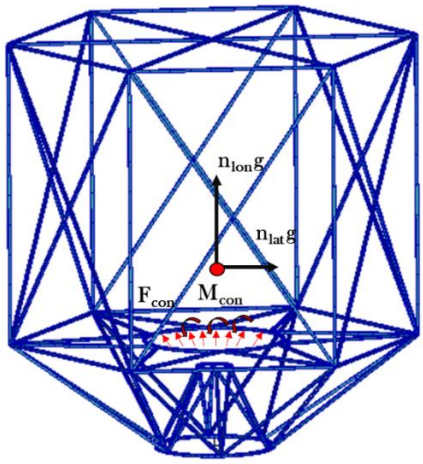

Figure 4.2 Static and Quasi-Static Loads Acting on the Frame

It should be pointed out that the qualification loads are obtained by multiplying all of the above quasi-static loads with a safety factor which equals to 1.25.

Quasi-Static Loads	Limit	Qualification (x1.25)
Longitudinal Acceleration Tension $\left(m/s^2\right)$	49.05	61.31
Longitudinal Acceleration Compression $\left(m/s^2\right)$	-73.58	-91.98
Lateral Acceleration $\left(m/s^2\right)$	25.51	31.38
Internal Pressure (MPa)	5.13	6.41
Hydrostatic Pressure (MPa)	0.06	0.08
Propellant's Weight (MPa)	0.02	0.03

Table 4.2 Limit and Qualification Loads

4.2. Static Strength Analysis for Sizing the Tank Structure

The preliminary sizing of the tank utilizes an iterative trial and error procedure of performing linear static finite element analysis for the two major load cases. The ultimate goal of the iterative design procedure of the tank is to determine its minimum wall thickness, ensuring that the structure is strong enough to withstand the entirety of the previously described loads while preventing it from failing due to yielding. The tank is considered a pressurized structure and according to ECSS Standards, a factor of safety of 1.1 has been applied against yielding. [8] It is reminded from Chapter 3, that yield strength of Al-6066-T6 is 359 (MPa) and thus the stresses developed throughout the tank must not exceed the maximum allowable Von Mises stress value of 327 (MPa). For each design iteration, tank's thickness and critical areas where the maximum Von Mises stresses occur, are listed below. The respective Margins of Safety are calculated using the formula: $M.o.S. = \frac{F.L.}{(D.L.)x(F.o.S.)} - 1$

- M.o.S. : Margin of Safety
- F.L. : Failure Load
- D.L. : Design Load
- F.o.S. : Factor of Safety

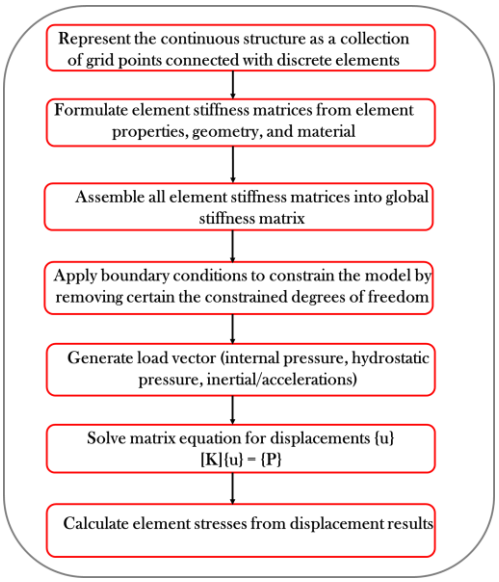

Figure 4.3 Flow Chart of Setting Up a Linear Static Analysis

Setting up the linear static analysis for both load cases requires specific steps to be followed as shown in Figure 4.3. The geometry modelling and mesh generation have already been described on Chapter 4. For the sake of completeness, it is mentioned that the tank structure is modeled incorporating 100 CTRIA3 and 3150 CQUAD4 shell elements, inducing approximately 18,912 degrees of freedom. The next step concerns the creation of the material and elemental properties by inputting the Elastic Modulus and Poisson Ratio of the tank's construction material and the thickness of the shell elements respectively. The following actions entail the application of the external loads and the boundary conditions of the model. It should be clearly established that in the static analysis the accelerations are inputted as inertial loads, which act at the center of gravity of the finite element model. The longitudinal and lateral components of acceleration are applied simultaneously on the respective axes. With regards to the boundary conditions, translational displacements of the common nodes between the tank and the frame have been constrained about the three axes. Finally, the displacements and the stresses are selected as output requests. The completion of the finite element model is obtained by submitting the linear static analysis to Nastran, which solves the required matrix equation for displacements.

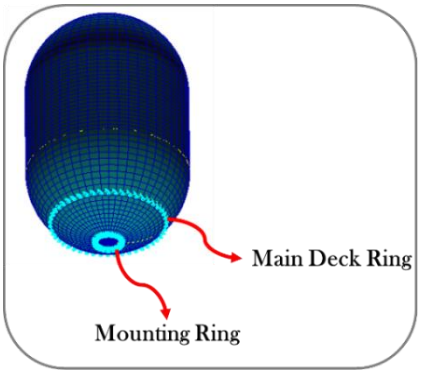

Figure 4.4 Boundary Conditions of the Tank

4.2.1. Static Strength Analysis Results for the Load Case of Compression

The results of the iterative tank sizing procedure, considering the load case of compression, are presented in the following tabular form (Table 4.3). The design process is terminated after 5 iterations where a maximum allowable Von Mises stress of 323 (MPa) is developed, indicating a minimum wall tank thickness of 6.5(mm).

Design Iteration	Tank Thickness (mm)	Region	Maximum Von Mises Stress (MPa)	Margin of Safety	Acceptance /Reject
1	4	Cylindrical Body	527	-0.3807	✗
2	5	Cylindrical Body	422	-0.2265	✗
3	5.5	Cylindrical Body	383	-0.1478	✗
4	6	Cylindrical Body	351	-0.0701	✗
5	6.5	Cylindrical Body	323	0.0104	✓

Table 4.3 Results of the Tank Design Process for the Compression Load Case

Indicative diagrams of both translational and rotational displacement distribution as well as Von Mises stress distribution of the last design iteration are shown in Figure 4.5, Figure 4.6 and Figure 4.7.

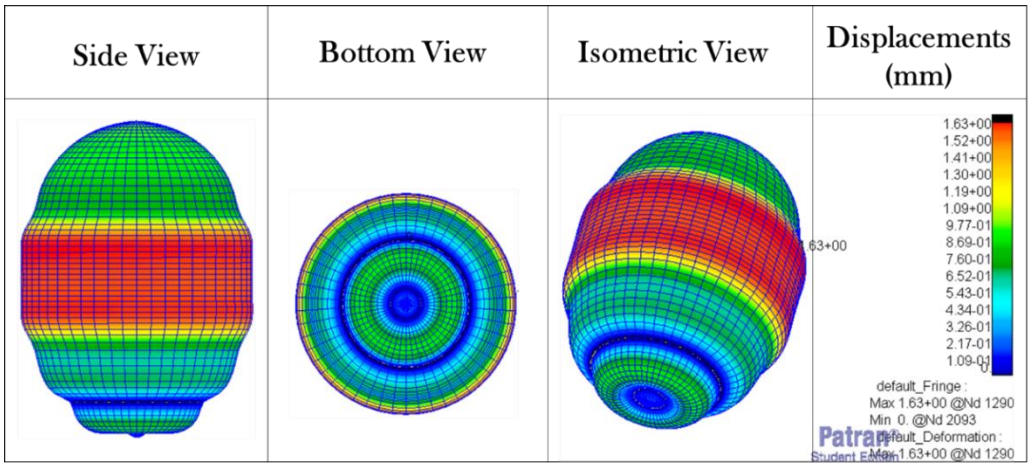

Figure 4.5 Translational Displacements Distribution

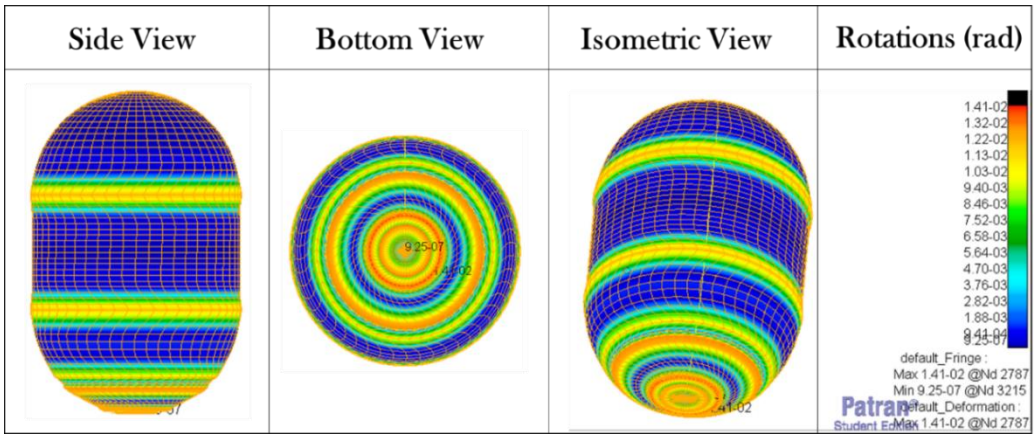

Figure 4.6 Rotational Displacements Distribution

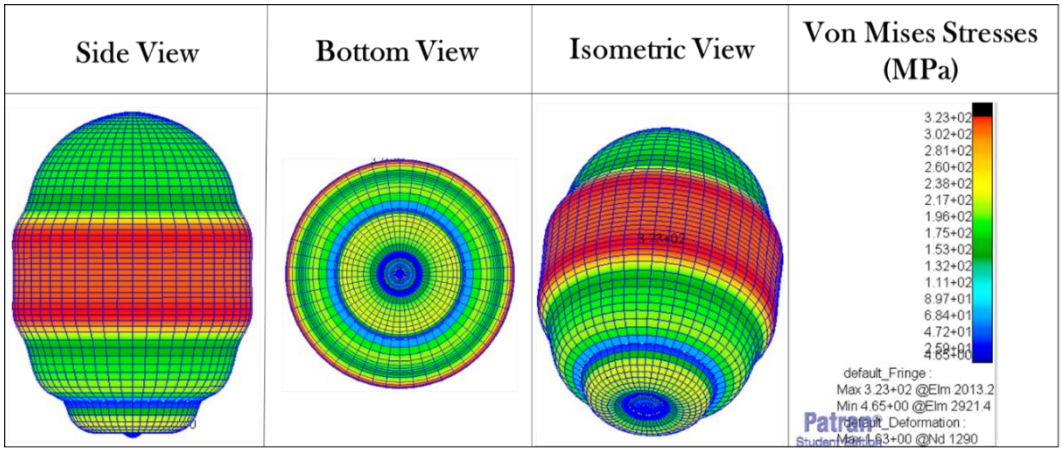

Figure 4.7 Von Mises Stress Distribution

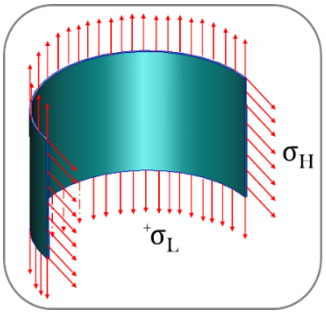

Figure 4.8 Hoop and Longitudinal Stresses

Observing the results of the iterative design process, significant remarks are reported. First of all, it can be observed that the maximum Von Mises stresses always occur at the cylindrical body of the tank. This observation is totally reasonable due to the simultaneous development of both hoop and longitudinal stresses at that particular region of the tank. It is reminded that the hoop stresses are twice the longitudinal ones. Furthermore, upon the hemispherical part of the tank, as there are no hoop stresses, only longitudinal stresses are developed.

An additional noteworthy observation that can be made, is that the highest stress jumps occur at the lower dome and more specifically along the attachment regions. This situation is completely justifiable due to the application of boundary conditions at these particular regions of the tank structure. The maximum stress jump equals to 140 (MPa) and occurs at the lower mounting region.

Finally, a vital conclusion drawn upon post-processing the results, is that there are no significant differences between averaged and unaveraged stress plots as shown, in Figure 4.10. As a result, the mesh density of the finite element model is of good quality and there is no need for any additional mesh refinement.

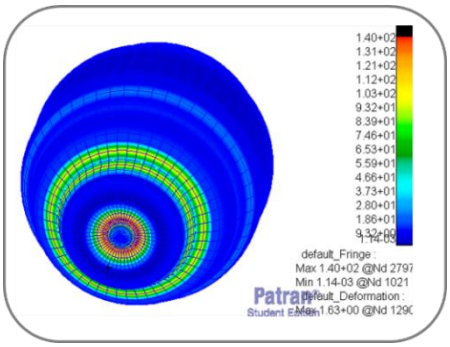

Figure 4.10 Stress Jumps on the Tank

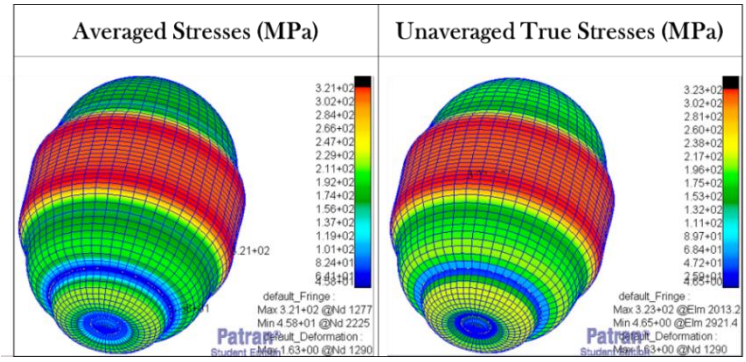

Figure 4.9 Averaged and Unaveraged Von Mises Stresses

4.2.2. Static Strength Analysis Results for the Load Case of Tension

The results of the iterative tank sizing procedure, considering the load case of tension, are presented in the following tabular form (Table 4.4). The design process is terminated after five iterations where a maximum allowable Von Mises stress of 324 (MPa) is developed, indicating the same minimum wall tank thickness of 6.5 (mm) as the previous load case.

Design Iteration	Tank Thickness (mm)	Region	Maximum Von Mises Stress (MPa)	Margin of Safety	Acceptance /Reject
1	4	Cylindrical Body	527	-0.3807	✗
2	5	Cylindrical Body	422	-0.2265	✗
3	5.5	Cylindrical Body	383	-0.1478	✗
4	6	Cylindrical Body	351	-0.0701	✗
5	6.5	Cylindrical Body	324	0.0072	✓

Table 4.4 Results of the Tank Design Process for the Tension Load Case

Indicative diagrams of both translational and rotational displacement distribution as well as Von Mises stress distribution of the last design iteration are shown in Figure 4.11, Figure 4.12 and Figure 4.13.

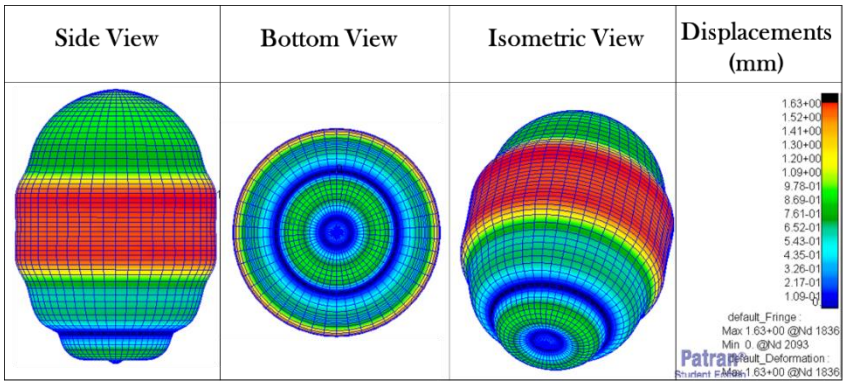

Figure 4.11 Translational Displacements Distribution

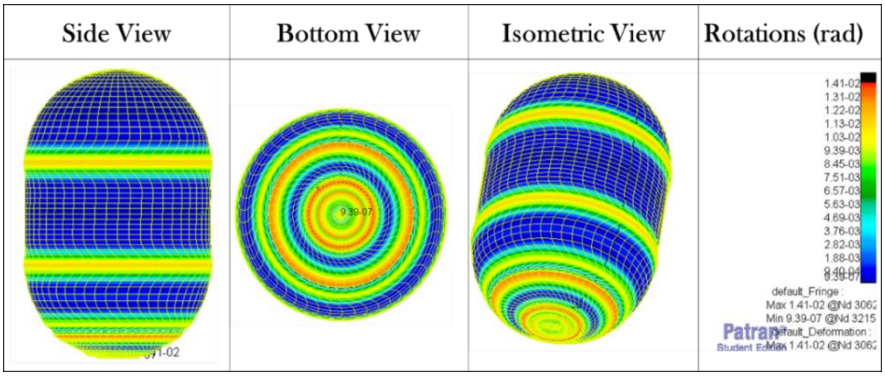

Figure 4.12 Rotational Displacements Distribution

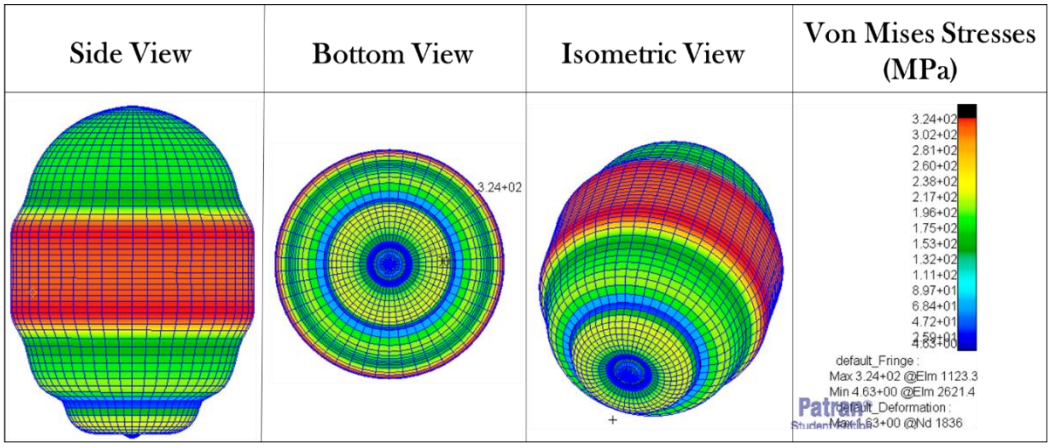

Figure 4.13 Von Mises Stress Distribution

Comparing the results between the compression and tension load case, the iterative trial and error design process of the tank leads to almost identical displacement and stress results, the same number of design iterations and the same value of the tank wall thickness. Consequently, the distinction of the direction in which the acceleration of the spacecraft is applied, does not influence the results drawn from the linear static analysis.

4.2.3. Results Validation

While trying to validate the reliability of the results drawn from the previous analysis of the shell element tank model, a supplemental three-dimensional solid element model has been developed. This particular three-dimensional finite element model has two orthogonal planes of symmetry; a fact which enables the tank to be captured with the one fourth of its initial geometry.

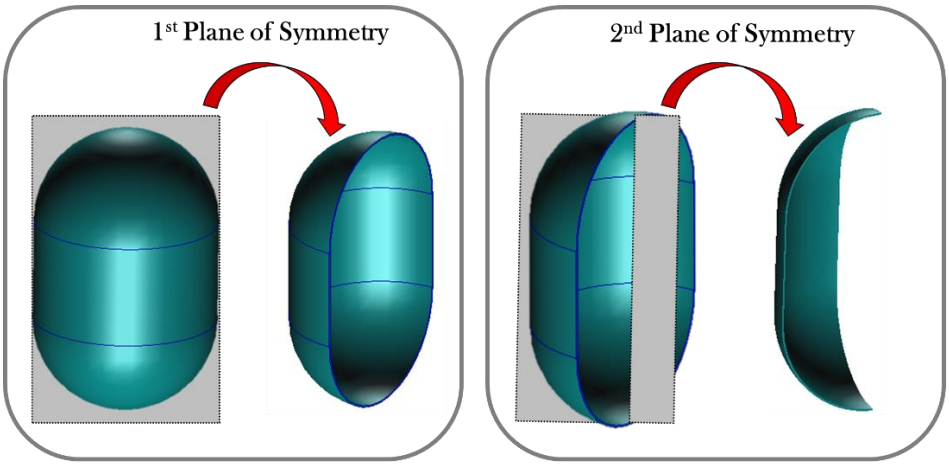

Figure 4.14 Orthogonal Planes of Symmetry

The mesh of the model is generated automatically incorporating 4870 ten-nodded tetrahedral solid elements with approximately 14,035 degrees of freedom. It is worth noting, that the thickness at a given height of the tank is modelled via a single element, as it is shown below.

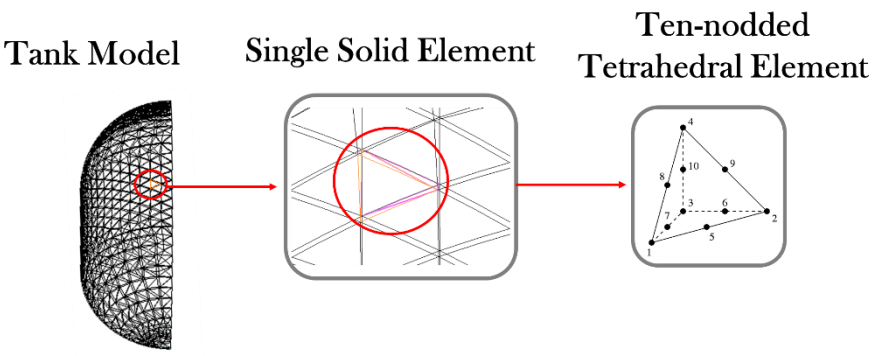

Figure 4.15 Tank's Modelling via Solid Elements

The major simplification of this model is that the hydrostatic pressure and the propellant's weight are excluded from the list of the applied loads on the tank due to their low magnitude in comparison with the magnitude of the internal pressure. Therefore, only the internal pressure and the inertial loads caused by the accelerations are included in this particular model. Moreover, it is important to mention that the boundary conditions have been applied on the reduced geometry of the tank by selecting the proper tangential, radial and attachment constraints, as shown in Figure 4.17. Leveraging the symmetry of the model-considering the fact that the geometry, the applied loads and finally the boundary conditions do not vary circumferentially-linear static analysis has been performed for cross-checking the results drawn from the shell element tank model.

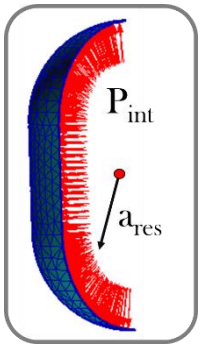

Figure 4.16 Loads Acting on the Tank

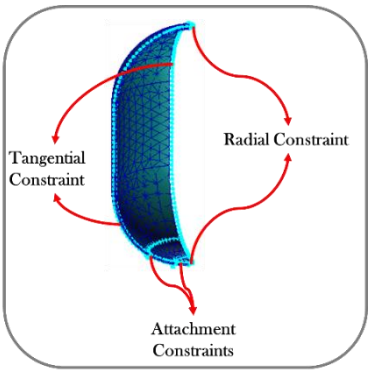

Figure 4.17 Boundary Conditions of the Model

Examining the results of the symmetrical solid model of the tank, it is observed, from the particular plots, that Von Mises stress results are almost identical to the shell element model. Indicative results, concerning the load case of compression, are presented in the Figure 4.18, verifying that the maximum stresses are developed on the cylindrical body of the tank with a magnitude of 323 (MPa). A simplistic but significant conclusion extracted from comparing the results between the two models is both hydrostatic pressure and propellant's weight do not play a dominant role on the developed stresses throughout the tank structure.

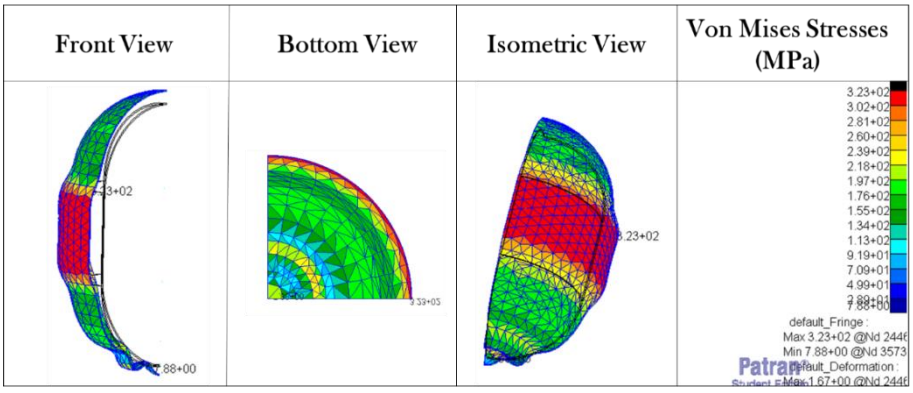

Figure 4.18 Von Mises Stress Distribution

4.3. Static Strength Analysis for Sizing the Frame Structure

The preliminary procedure for sizing the frame structure is divided into two parts. The first part initiates the iterative design process, taking into account the structural interaction between the frame and the tank. Its ultimate goal is to determine the minimum cross-sectional profile area of each beam member, ensuring that neither of the two structures will fail because of the action of the previously described loads. The design iterations cease only when the magnitude of the developed stresses for both structures satisfy concurrently the yielding requirements for each construction material for the two load cases. It is noteworthy that throughout the sizing procedure, the maximum combined stresses, developed on beam members of the frame, have been examined against yielding in both tension and compression state. It is reminded that the construction material selected for the frame is Al-6061, which entails a tensile and compressive yield strength of 276 (MPa). Additionally, it is reminded that the frame of the spacecraft is considered as a primary metallic structure and therefore a factor of safety of 1.1 against yielding has been applied according to ECSS Standards. [8] As a result, the magnitude of the combined axial and bending stresses, must not exceed the maximum allowable stress of 259 (MPa). For each design iteration, cross-sectional dimensions as well as the most critical beam member groups, where the maximum stresses occur, are listed below. The respective Margins of Safety are calculated. The steps for setting up the analysis are identical to the previously described model. The number of CTRIA3 and CQUAD4 elements of the tank remain the same as above and the frame structure is modeled using 660 CBAR elements. Moreover, 120 RBE2 elements have been utilized in order to achieve the welded type of connection between the common nodes of the two structures. Therefore, the completed model includes approximately 27,702 degrees of freedom. In respect to the load application, it is mentioned that only the internal pressure and the combination of longitudinal and lateral acceleration (as inertial loads), are included in the model. Regarding the boundary conditions, both translational and rotational displacements of the adapter rings nodes have been constrained about the three axes.

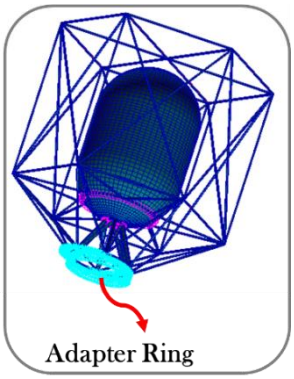

Figure 4.19 Boundary Conditions of the Frame

4.3.1.1. Static Strength Analysis Results for the Load Case of Compression

The results of the initial iterative procedure for sizing the frame structure, considering the compression load case, are presented in the following tabular form (Table 4.5). The design process is terminated after four iterations, indicating cross-sectional area modifications for the mounting ring and the support struts.

	Tank				Frame Beams							
D.I.	Tank Stress (MPa)	Region	M.O.S.	A/R	Maximum Tensile Stresses (MPa)	Region	M.O.S.	A/R	Minimum Compressive Stresses (MPa)	Region	M.O.S.	A/R
1	321	Cylindrical Body	0.0104	✔	390	Mounting Ring	-0.3566	✗	-437	Mounting Ring	-0.4258	✗
2	321	Cylindrical Body	0.0104	✔	311	Mounting Ring	-0.1932	✗	-439	Mounting Ring	-0.4284	✗
3	321	Cylindrical Body	0.0104	✔	290	Mounting Ring	-0.1347	✗	-432	Mounting Ring	-0.4191	✗
4	321	Cylindrical Body	0.0104	✔	211	Mounting Ring	0.1891	✔	-308	Mounting Ring	-0.1853	✗
5	321	Cylindrical Body	0.0104	✔	183	Mounting Ring	0.3710	✔	-133	Mounting Ring	0.8865	✔

Table 4.5 Results of the Frame Design Process for the Compression Load Case

Two cross-sectional modifications have been applied for the mounting ring and the support struts. The finalized cross-sectional area for both beam member groups is 20x2.

Design Iteration	Member Modification	Cross-sectional Modification
1	Mounting Ring	(10x1) → (15x1)
2	Mounting Ring	(15x1) → (20x2)
3	Support Struts	(10x1) → (15x1)
4	Support Struts	(15x1) → (20x2)
5	-	-

Table 4.6 Cross-sectional Modifications

The design sequence of the iterative sizing process is illustrated in Figure 4.20. For each design iteration the particular beam member groups requiring cross-sectional area modifications, are marked.

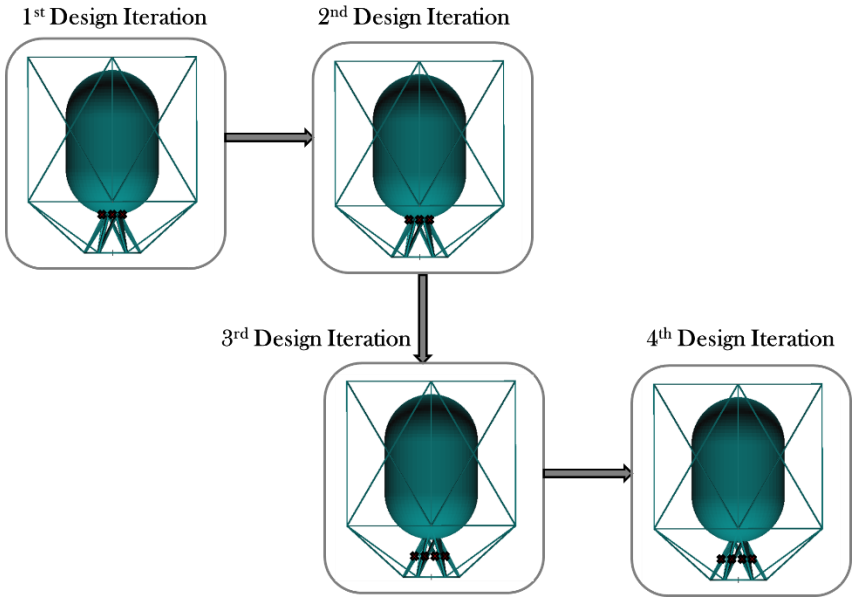

Figure 4.20 Design Sequence of the Frame Sizing for the Compression Load Case

For the last design iteration indicative diagrams of stress distribution throughout the tank and the frame are shown in Figure 4.21, Figure 4.22 and Figure 4.23.

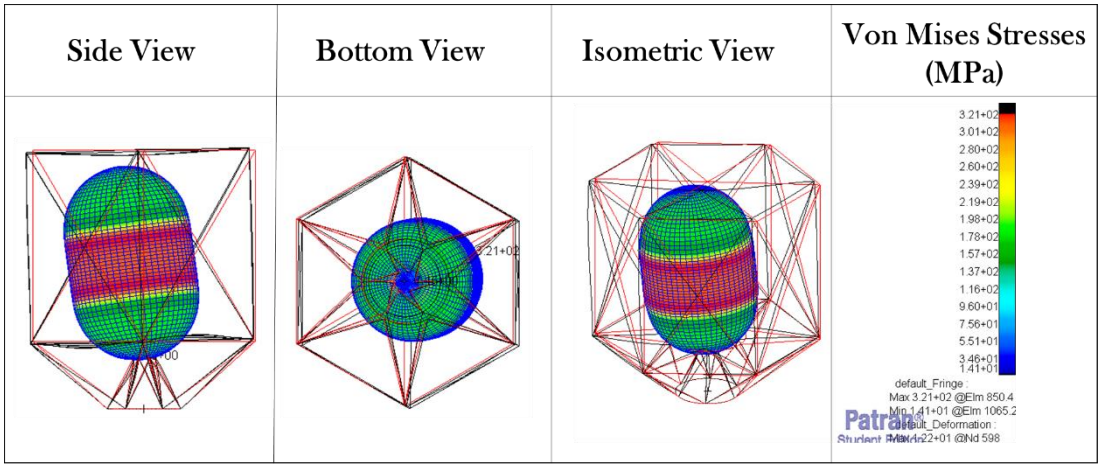

Figure 4.21 Von Mises Stress Distribution on the Tank

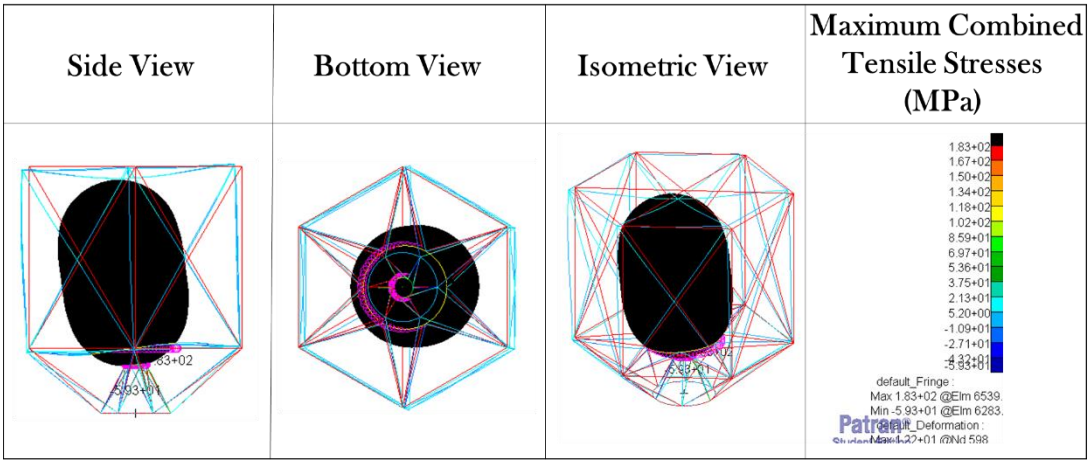

Figure 4.22 Maximum Combined Tensile Stresses of the Beam Members

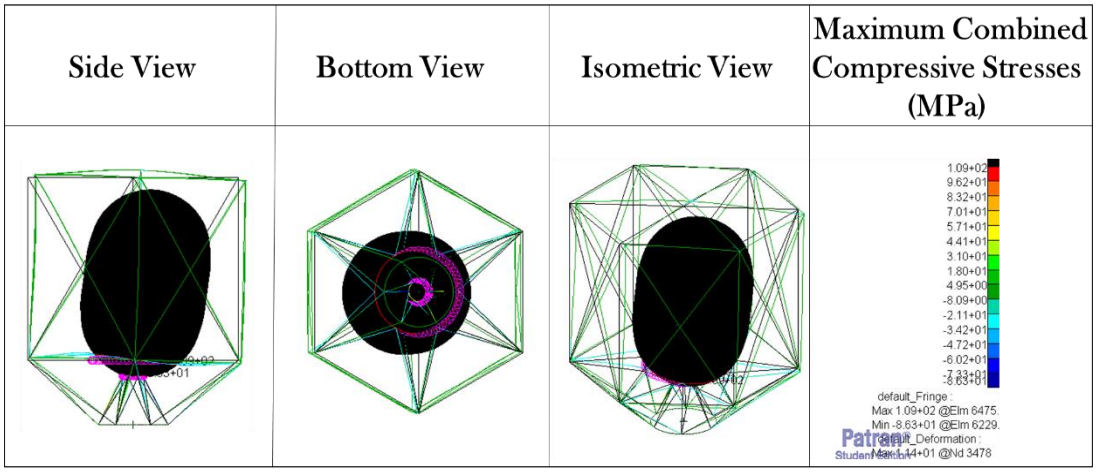

Figure 4.23 Maximum Combined Compressive Stresses of the Beam Members

4.3.1.2. Static Strength Analysis Results for the Load Case of Tension

The results of the initial iterative frame sizing procedure, considering the tension load case, are presented in the following tabular form (Table 4.7). The design process is terminated after three iterations, indicating cross-sectional area modifications for the mounting ring.

	Tank				Frame Beams							
D.I.	Tank Stress (MPa)	Region	M.O.S.	A/R	Maximum Tensile Stresses (MPa)	Region	M.O.S.	A/R	Minimum Compressive Stresses (MPa)	Region	M.O.S.	A/R
1	357	Attachment Points	-0.858	✗	264	Mounting Ring	-0.0495	✗	-87.9	Mounting Ring	1.8544	✓
2	345	Attachment Points	-0.540	✗	222	Mounting Ring	0.1302	✓	-87.3	Mounting Ring	1.8741	✓
3	329	Attachment Points	-0.080	✗	166	Mounting Ring	0.5115	✓	-86.2	Mounting Ring	1.9107	✓
4	323	Attachment Points	0.0104	✓	150	Mounting Ring	0.6727	✓	86.3	Mounting Ring	1.9074	✓

Table 4.7 Results of the Frame Design Process for the Tension Load Case

Three cross-sectional modifications have been applied exclusively for the mounting ring. The finalized cross-sectional area for this specific beam member group is 34x3.

Design Iteration	Member Modification	Cross-sectional Modification
1	Mounting Ring	(20x2) → (25x2)
2	Mounting Ring	(25x2) → (30x3)
3	Mounting Ring	(30x3) →(34x3)
4	-	-

Table 4.8 Cross-sectional Modifications

The design sequence of the iterative process is illustrated at Figure 4.24. For each design iteration, the particular beam member group requiring cross-sectional modifications is marked.

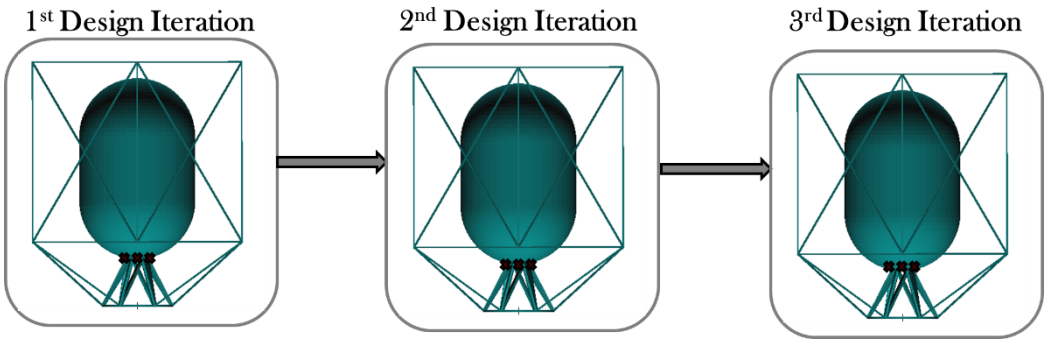

Figure 4.24 Design Sequence of the Frame Sizing for the Tension Load Case

For the last design iteration indicative diagrams of stress distribution throughout the tank and the frame are shown in Figure 4.25, Figure 4.26 and Figure 4.27.

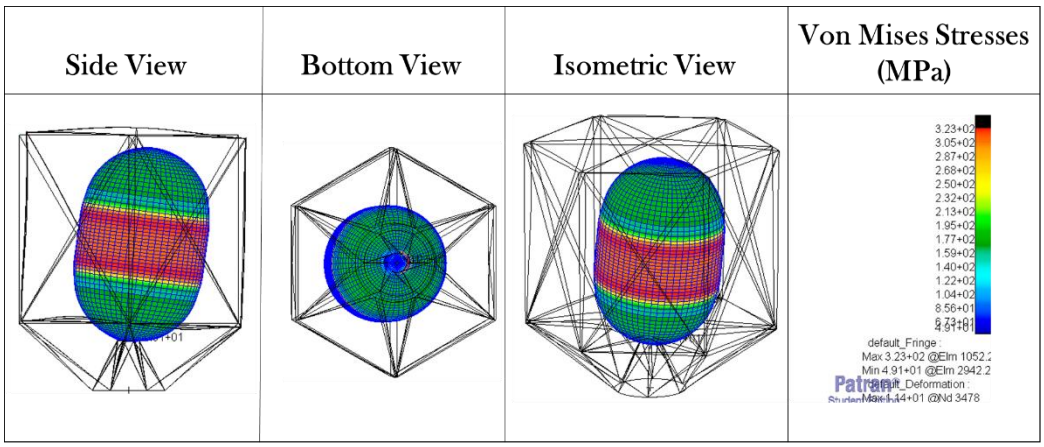

Figure 4.25 Von Mises Stress Distribution on the Tank

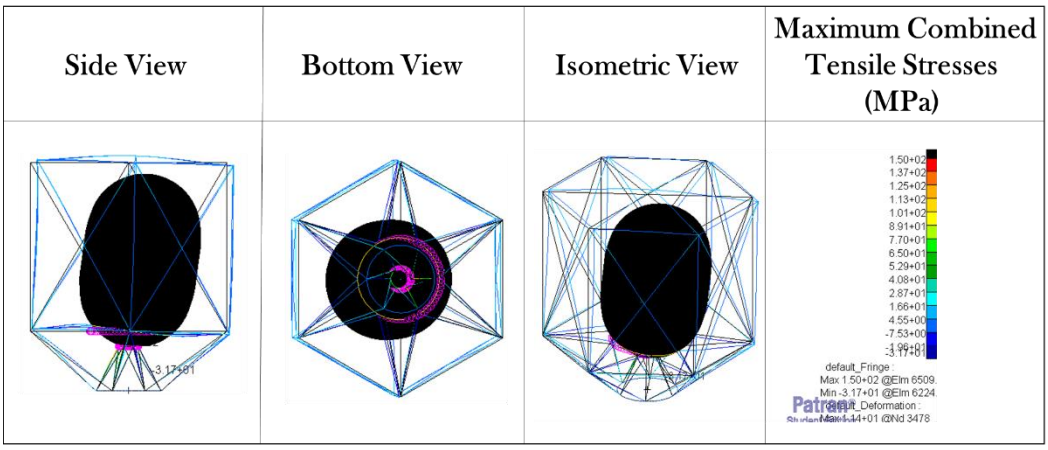

Figure 4.26 Maximum Combined Tensile Stresses of the Beam Members

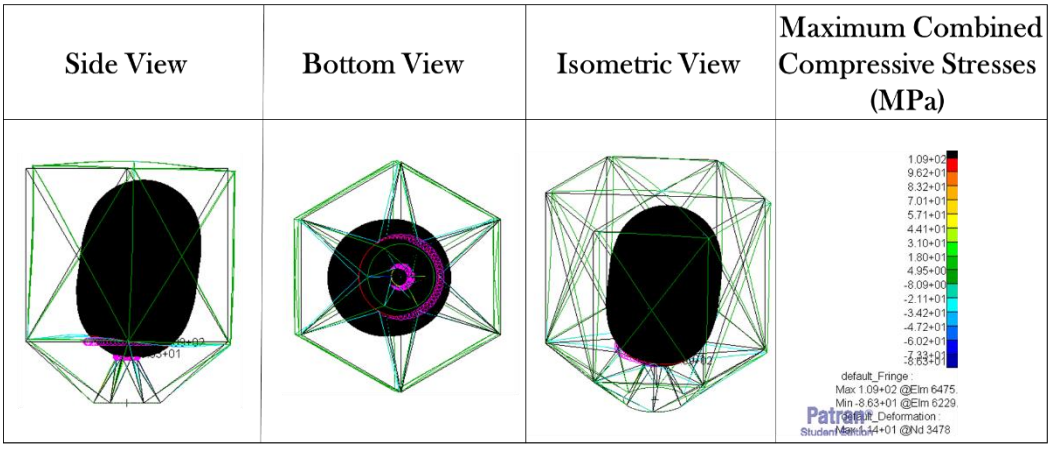

Figure 4.27 Maximum Combined Compressive Stresses of the Beam Members

Once the first part of the frame sizing procedure is established, it is ensured that the structural interaction between the frame and the tank is acceptable and does not put either structure in jeopardy of failing, considering both load cases. A closer examination to the previous analysis shows that the structural response of the tank is more sensitive in the tension load case. In this particular load case, even if maximum values of combined stresses are acceptable for the beam members of the frame, the developed stresses on the tank exceed the maximum allowable stress value for the Al-6066-T6. Indicative stress distribution of the first iteration for the tension load case is presented in Figure 4.28, where the unacceptable value of 357 (MPa) is developed along the attachment region of the tank.

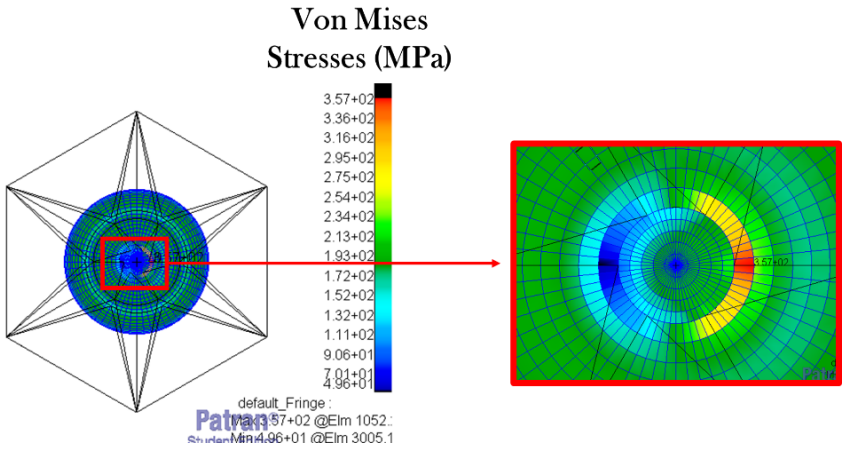

Figure 4.28 Von Mises Stresses on the Tank

Hence, the second part of the frame design process initiates with a priority given to the tension load case. Afterwards, the maximum constraint forces and moments are inputted in a new finite element model, which focuses on the frame structure exclusively.

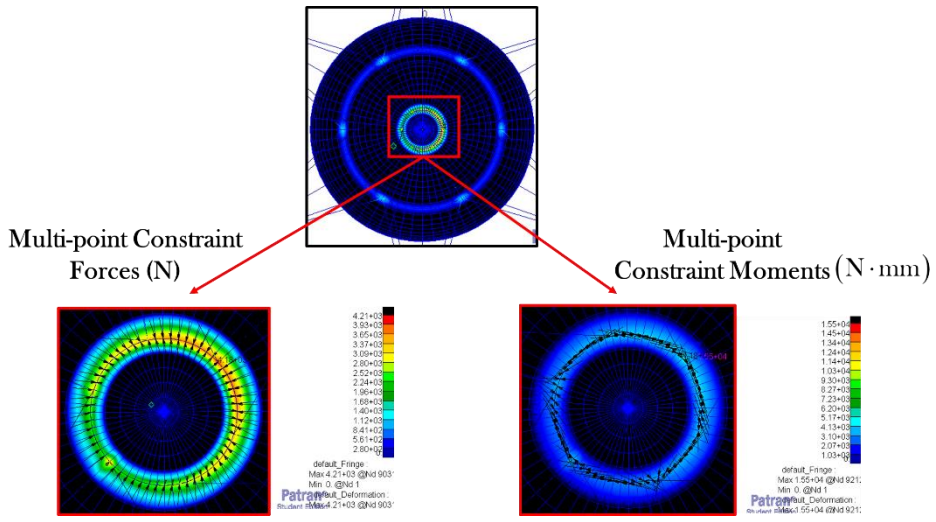

Figure 4.29 Multi-Point-Constraint Forces and Moments

However, upon obtaining accurate results, it is of great importance that the model of the frame includes a mathematical representation of the attached tank. Consequently, the tank structure is replaced with a nodal lumped mass idealization, which is located at the center of gravity of the tank and is connected to both attachment ring and mounting ring of the frame, using a rigid element. An obvious observation that can be made in this

model, is that the mass of the tank structure rigidizes the entire spacecraft structure and as a result a 'stiff' load path occurs between the tank and the frame. Taking the above into account leads to the incorporation of rigid elements instead of interpolation elements. The nodes located at the attachment rings of the frame, are considered dependent and are connected to the independent node of the lumped mass via RBE2 element. It is worth noting that this type of mathematical representation of the tank requires its principle moments of inertia, as an input.

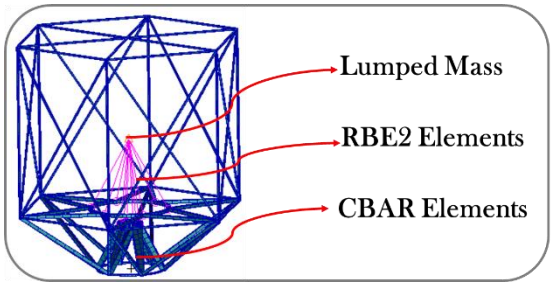

Figure 4.30 Frame Model

4.3.1.3. Static Strength Analysis Results for the Load Case of Tension

The results of the final iterative frame sizing procedure, considering the tension load case, are presented in the following tabular form (Table 4.9). The design process is terminated after four iterations, indicating modifications cross-sectional area modifications, for the connection struts, the main deck ring, the main deck struts and the support struts.

	Frame Beams							
D.I.	Maximum Tensile Stresses (MPa)	Region	M.O.S.	A/R	Minimum Compressive Stresses (MPa)	Region	M.O.S.	A/R
1	737	Main Deck Ring	-0.6595	✗	-492	Connection Struts	-0.4900	✗
2	503	Support Struts	-0.5011	✗	-360	Connection Struts	-0.3030	✗
3	314	Support Struts	-0.3939	✗	-250	Main Deck Struts	0.0036	✓
4	263	Support Struts	-0.2009	✗	-215	Main Deck Struts	0.1670	✓
5	215	Support Struts	0.1670	✓	-148	Main Deck Struts	0.6553	✓

Table 4.9 Results of the Frame Design Process for the Tension Load Case

Two cross-sectional modifications have been applied for the connection struts, the main deck ring, the main deck struts, and one for the support struts. The finalized cross-sectional area for the beam member groups are (20x2), (20x2), (20x2) and (30x3) respectively.

Design Iteration	Member Modification	Cross-sectional Modification
1	Connection Struts & Main Deck Ring	(10x1) → (15x1) & (10x1) → (15x1)
2	Connection Struts & Main Deck Ring	(15x1) → (20x2) & (15x1) → (20x2)
3	Support Struts & Main Deck Struts	(20x2) →(30x3) & (10x1) → (15x1)
4	Main Deck Struts	(15x1) → (20x2)
5	-	-

Table 4.10 Cross-sectional Modifications

The design sequence of the iterative process is illustrated at Figure 4.31 . For each design iteration, the particular beam member groups requiring cross-sectional modifications are marked.

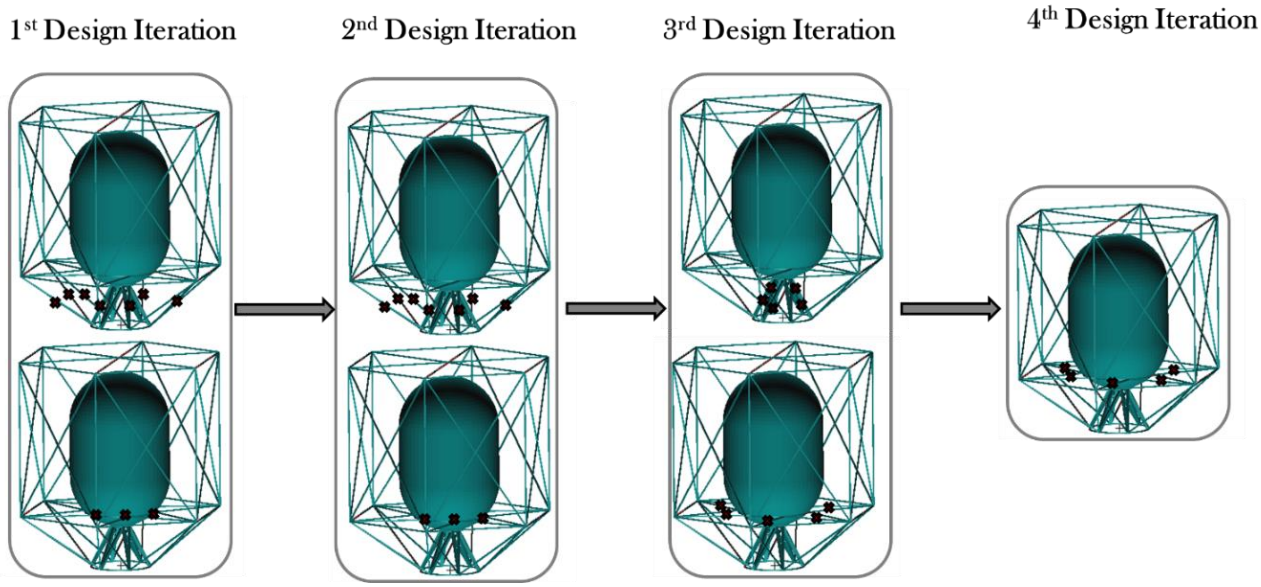

Figure 4.31 Design Sequence of the Frame Sizing for the Tension Load Case

For the last design iteration, indicative diagrams of displacements and stresses throughout the frame are shown in Figure 4.32, Figure 4.33, Figure 4.34 and Figure 4.35.

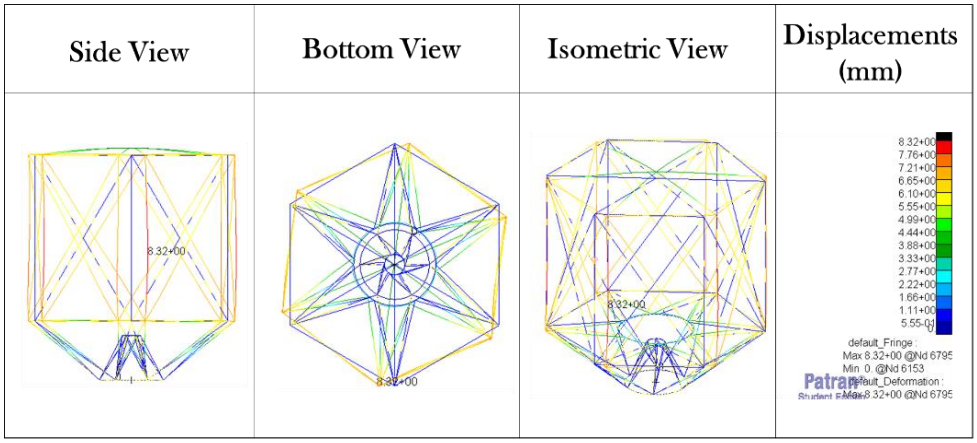

Figure 4.32 Translational Displacements of the Frame

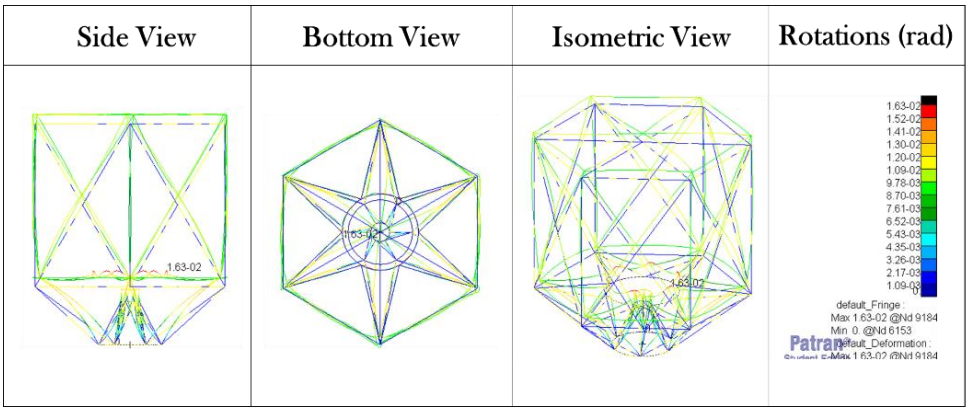

Figure 4.33 Rotational Displacements of the Frame

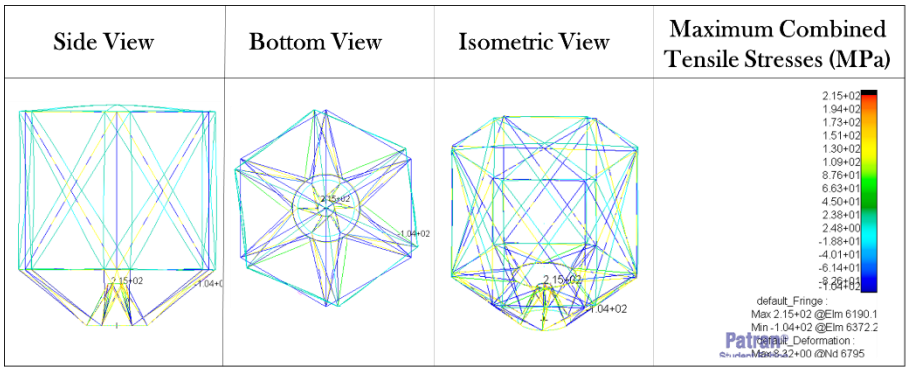

Figure 4.34 Maximum Combined Tensile Stresses of the Frame

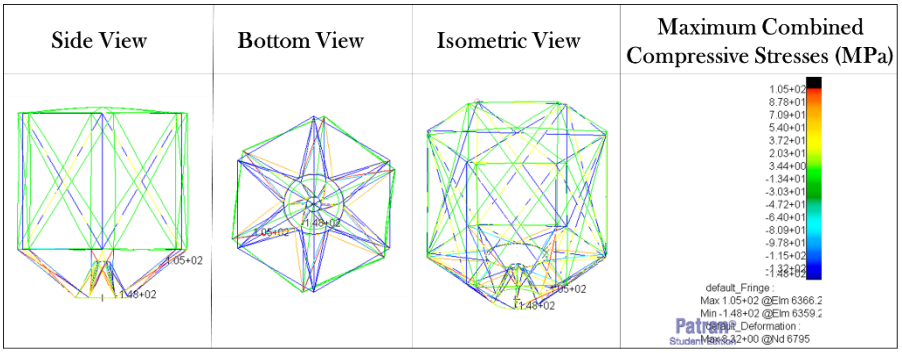

Figure 4.35 Maximum Combined Compressive Stresses of the Frame

4.3.1.4. Static Strength Analysis Results for the Load Case of Compression

The results of the final part of frame sizing procedure, considering the compression load case, are presented in the following tabular form (Table 4.11). The design process is terminated after one iteration, indicating no modifications upon the beam members.

	Frame Beams							
D.I.	Maximum Tensile Stresses (MPa)	Region	M.O.S.	A/R	Minimum Compressive Stresses (MPa)	Region	M.O.S.	A/R
1	214	Support Struts	-0.6595	✔	-147	Connection Struts	-0.4900	✔

Table 4.11Results of the Frame Design Process for the Compression Load Case

For this single design iteration, indicative diagrams of displacements and stresses throughout the frame are shown in Figure 4.36, Figure 4.37, Figure 4.38 and Figure 4.39.

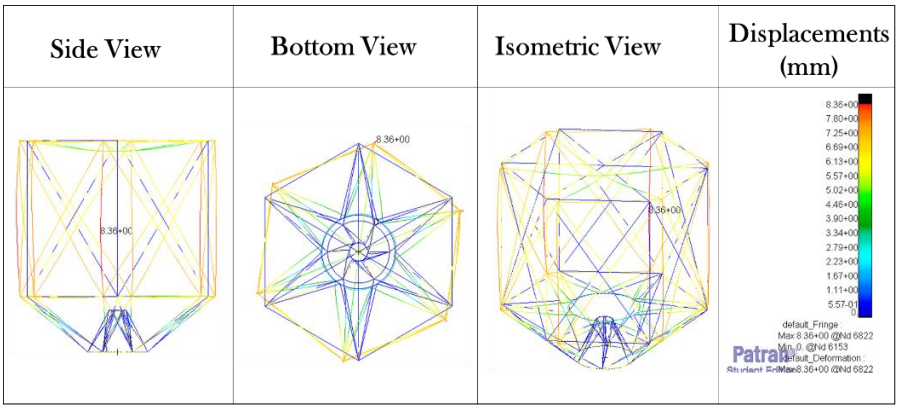

Figure 4.36 Translational Displacements of the Frame

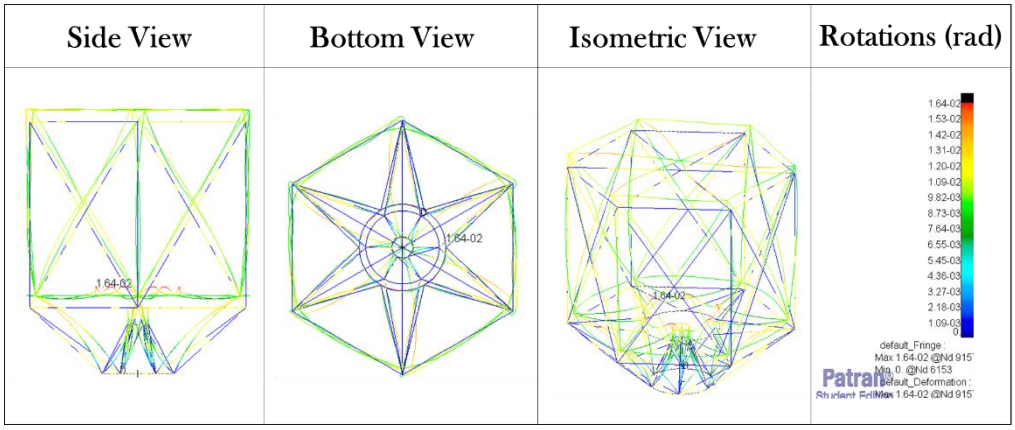

Figure 4.37 Rotational Displacements of the Frame

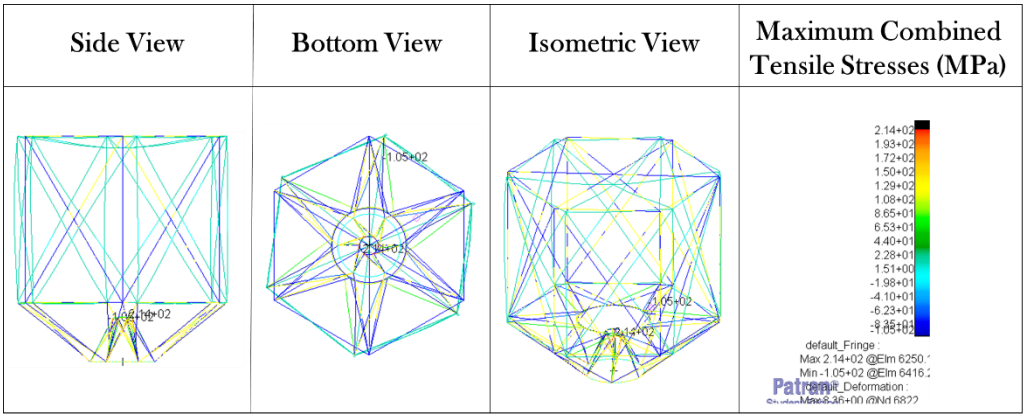

Figure 4.38 Maximum Combined Tensile Stresses of the Frame

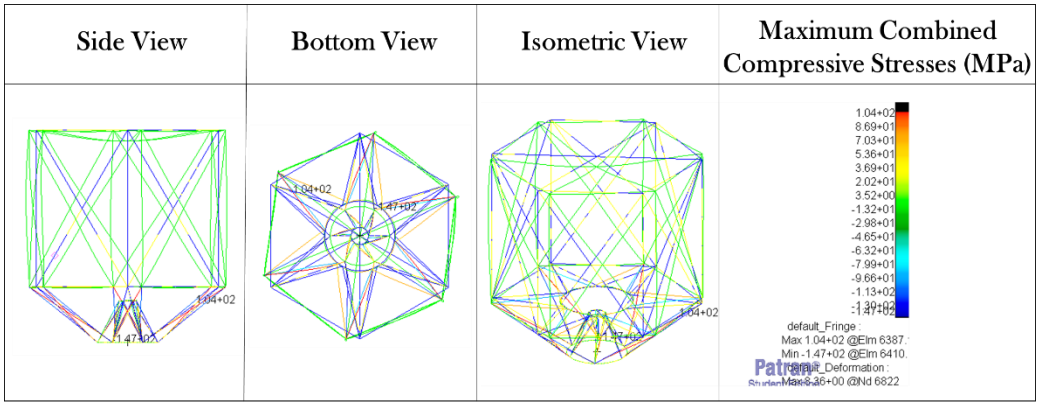

Figure 4.39 Maximum Combined Compressive Stresses of the Frame

4.4. Linear Buckling Analysis

From the previous analysis, it has been established that material yielding has been prevented for both structures. Apart from that, it is of great importance when designing lightweight structures to ensure that no elastic instabilities occur. The storage tank is associated with thin-walled shell structures and the frame with thin-walled hollow beams. A major design consideration, is that both structures are susceptible to buckling under critical loading conditions. In attempting to verify that the previously established design loads do not contribute to a buckling condition for both structures, linear buckling

analysis has been performed separately, considering material linearity and the absence of any pre-buckled deformations. A brief mathematical background of linear buckling is presented below.

The equilibrium equation of the structure subjected to a constant external force has the following form: [9]

$$[K]\{u\} = \{P\} \xrightarrow{[K]=[K_a]+[K_d]} \left[[K_a]+[K_d]\right]\{u\} = \{P\}$$

Where:

- $[K_a]$: Linear Stiffness Matrix.
- $[K_d]$: Differential Stiffness Matrix

The linear stiffness matrix can be represented as: $[K_a] = \sum_{i=1}^{n} K_{a_i}$, where the value 'i' stands for i-th element. Similarly, the differential stiffness matrix can be represented as: $[K_d] = \sum_{i=1}^{n} K_{d_i}$.

Differential stiffness matrix is a function of multiple factors, such as geometry, element type and the applied loads. It actually represents the structural stiffness due to higher order non-linear terms of the strain-displacement relations.
The total potential energy of the system is equal to:

$$[U] = \frac{1}{2}\{u\}^T [K_a]\{u\} + \frac{1}{2}\{u\}^T [K_d]\{u\}$$

In order to achieve static equilibrium for the system, its total potential energy must have a stationary value. As a result, the following equation must be satisfied:

$$\frac{\partial [U]}{\partial u_i} = [K_a]\{u\} + [K_d]\{u\} = \{0\}$$

Where:

- u_i : Displacement of the -ith degree of freedom

Rewriting the above equation and taking into account that the differential stiffness matrix is proportional to the internal forces of the structure:

$$\left[[K_a]+[K_d]\right]\{u\} = \{0\} \xrightarrow{[K_d]=P_a\left[\overline{K_d}\right]} \left[[K_a] + P_a\left[\overline{K_d}\right]\right]\{u\} = \{0\}$$

Where:

- P_a : Applied Load
- $\left[\overline{K_d}\right]$: Differential Stiffness Matrix modified by a distribution factor of the applied load

The trivial solution of the above equation occurs from $\{u\} = \{0\}$. For defining the non-trivial solution, the following relationship must be satisfied:

$$\left[\left[K_a\right]+P_a\left[\overline{K_d}\right]\right]=\{0\}\rightarrow\left|\left[K_a\right]+P_a\left[\overline{K_d}\right]\right|=[0]$$

The determinant of the matrix is zero, only for certain values of P_a, which are the critical buckling loads. A real structure is considered to be a continuous system and thus it has an infinite number of degrees of freedom. On the opposite side, the finite element model approximates the behavior of the structure via a finite number of degrees of freedom. As a result, the number of the buckling loads, obtained by the finite element model equals to the number of degrees of freedom of the model.

Hence $P_{cr}=\lambda_i\cdot P_a$ and the last equation takes the form of an eigenvalue problem.

$$\left|\left[K_a\right]+\lambda_i\left[K_d\right]\right|=[0]$$

It is noteworthy that the Lanczos method is utilized for the eigenvalue extraction. It uses Sturm sequence logic to ensure that all modes are found. The Sturm sequence check determines the number of eigenvalues below a trial eigenvalue, then finds all of the eigenvalues below this trial eigenvalue until all modes in the designated range are computed. This process helps to ensure that modes no are missed.

Once, the eigenvalues λ_i are obtained, they are used as a scale factor by which the applied load P_a is multiplied in order to produce the critical buckling loads.

4.4.1. Linear Buckling Analysis for the Tank Structure

The worst-case buckling scenario, considering the tank structure, is met at the compression load case when it is empty of propellant. As a result, the tank is subjected only to inertial loads-because of the accelerations acting on the whole spacecraft-and to external pressure which equals to the internal pressure of the spacecraft. This specific combination of loads induces the maximum compressive stresses on the cylindrical and the hemispherical shells of the tank. Indicatively, the first three buckling modes with the respective load factors are obtained via linear buckling analysis. Each mode is illustrated in Figure 4.41 .

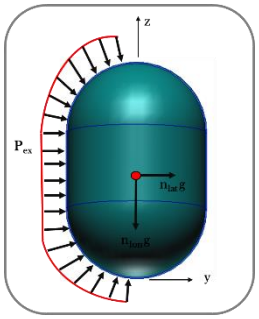

Figure 4.40 Empty Tank Subjected to External Pressure

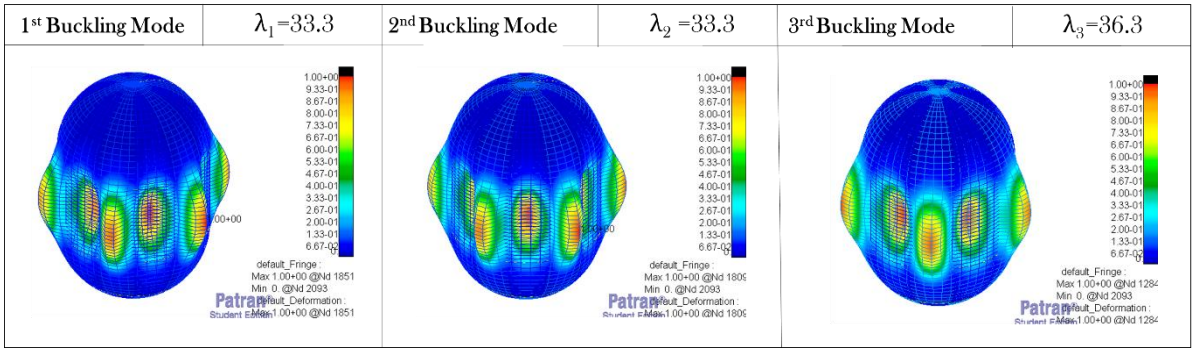

Figure 4.41 Tank Buckling Modes

Every unique load factor for each buckling mode is greater than one. This situation indicates that no buckling is going occur on the tank under the action of the assumed design loads. It can be observed that the cylindrical body of the tank is more susceptible to buckling.

4.4.2. Linear Buckling Analysis for the Frame Structure

The worst-case buckling scenario, considering the frame structure, is met at the compression load case when it supports a filled tank. This is the most significant load case which leads to the development of the maximum compressive stresses on the beam members of the frame. Indicatively, the first three buckling modes with the respective load factors are obtained via linear buckling analysis. Each mode is illustrated in Figure 4.43.

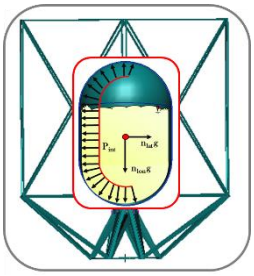

Figure 4.42 Frame Carrying a Filled Tank

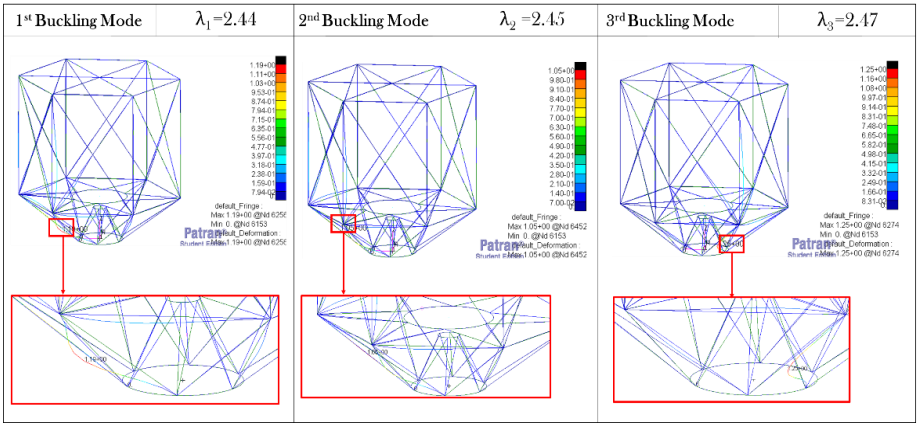

Figure 4.43 Frame Buckling Modes

Every unique of the load factor for each buckling mode is greater than one. This situation indicates that no buckling is going to occur on the frame under the action of the assumed design loads. Apparently, among the different beam groups of the frame, connection struts are more likely to buckle.

4.5. Elastoplastic Analysis for the tank

According to the previously established strength analysis of the tank structure, it is clear that the internal pressure, due to the pressurized propellant, is the most critical design load, influencing the tank design. Therefore, an important design consideration arises when the developed stresses approach or exceed the yield point of the construction material of the tank, causing permanent plastic strains. This event is inextricably linked with plasticity which is a common type of material nonlinearity, influencing the constitutive relations. A nonlinear analysis has been performed in order to predict the nonlinear behavior of Al-6066-T6 and to determine the maximum magnitude of the internal pressure that may lead to ultimate failure. According to ECSS Standards, a factor of safety of 1.25 is applied on pressurized structures against ultimate failure. [8] As a result, the stresses developed throughout the tank must not exceed the maximum allowable Von Misses stress of 314 (MPa).

It is noted that because of lack of material data, considering the stress-strain curve of Al-6066-T6, its elastoplastic behavior is represented through the following bilinear model.

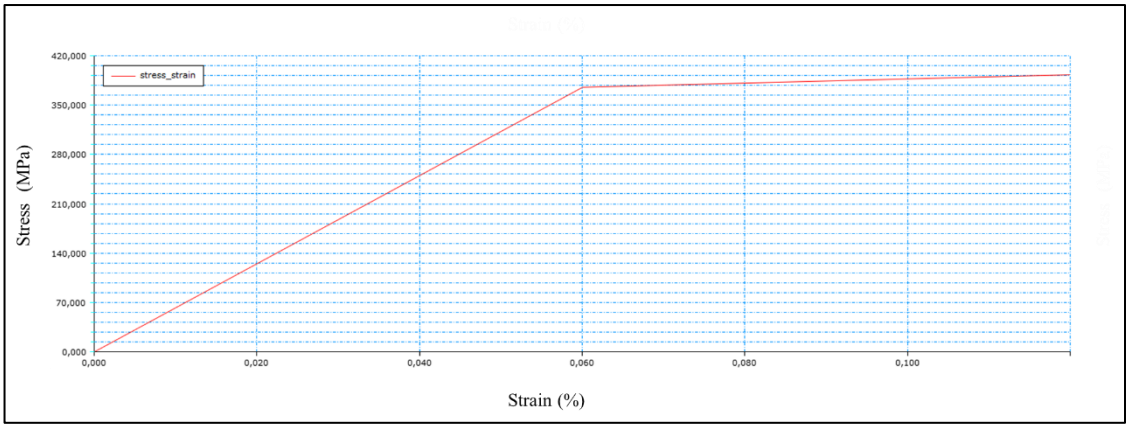

Diagram 4.1 Bilinear Elastoplastic Model

The next step required for defining the elastoplastic material model, is to select the type of yield condition which occurs in case of multiaxial state of stress. For ductile materials, such as isotropic metals, Von Mises is the most widely used yield criterion. The von Mises criterion states that yield occurs, when the effective or equivalent stress equals the yield stress as measured in a uniaxial test. [10] It is reminded that, for an isotropic material Von Mises Stress is given by the equation:

$$\sigma_{VM} = \sqrt{\frac{(\sigma_1 - \sigma_2)^2 + (\sigma_2 - \sigma_3)^2 + (\sigma_3 - \sigma_1)^2}{2}}$$

Where:

- $\sigma_1, \sigma_2, \sigma_3$: Principal Cauchy stresses

Yield condition can also be expressed in terms of non-principal Cauchy stresses and in terms of deviatoric stresses.

$$\sigma_{VM} = \sqrt{\frac{(\sigma_x - \sigma_y)^2 + (\sigma_y - \sigma_z)^2 + (\sigma_z - \sigma_x)^2 + 6(\tau_{xy}^2 + \tau_{yz}^2 + \tau_{zx}^2)}{2}} \text{ and } \sigma_{VM} = \sqrt{\frac{3}{2}\sigma_{ij}'\sigma_{ij}'}$$

Where:

- σ_{ij}' : Deviatoric Cauchy stress expressed as $\sigma_{ij}' = \sigma_{ij} - \frac{1}{3}\sigma_{kk}\delta_{ij}$.

In the two-dimensional principal stress space, the yield function is represented by an ellipse and in the deviatoric π plane, the yield function is a circle.

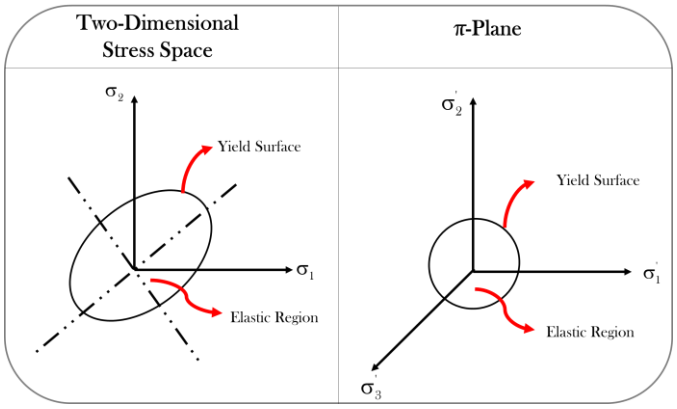

Figure 4.44 Von Mises Yield Surface

The subsequent input to be defined, is the type of workhardening rule, which determines how the material model responds to repeated stress reversals. A simple example of stress reversal occurs when switching the stress state between tension and compression. In case of the tank structure, the most suitable rule is the isotropic hardening model, which does not take into account the Bauschinger effect. Thus, the compressive yield always equals the tensile yield. Particularly, the work-hardening rule defines the way the yield surface changes with plastic straining. The isotropic

workhardening rule assumes that the center of the yield surface remains stationary in the stress space, but the size (radius) of the yield surface expands, due to workhardening. This type of hardening is appropriate when the straining is the same in all directions. A review of the load path, considering a uniaxial test that involves both the loading and unloading of a structure, is presented so as to describe the selected workhardening rule for the finite model of the tank.

The structure is first loaded from stress free (point 0) to initial yield at point 1. It is then continuously loaded to point 2. Afterwards, unloading from 2 to 3, following the elastic slope E (Young's modulus). Then elastic reloading from 3 to 2 takes place. Finally, the structure is plastically loaded again from 2 to 4 and elastically unloaded from 4 to 5. Reverse plastic loading occurs between 5 and 6. It is obvious that the stress at 1 is equal to the initial yield stress and stresses at points 2 and 4 are larger, due to workhardening. During unloading, the stress state can remain elastic (for example, point 3), or it can reach a subsequent (reversed) yield point (for example, point 5). The isotropic workhardening rule states that the reverse yield occurs at current stress level in the reversed direction.

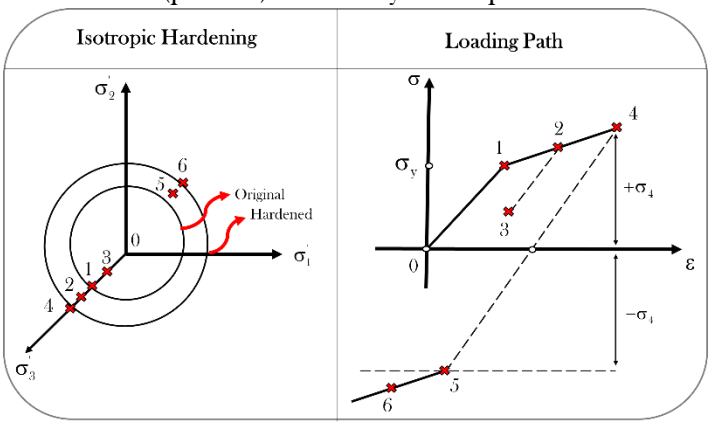

Figure 4.45 Isotropic Hardening Rule Scheme

Last but not least, it is important to note that the nonlinear solver uses the true stresses and true strains, taking into account changes in area due to finite deformations. True stress and true strain are defined below.

$$\begin{cases} \sigma_t = \dfrac{F}{A} \\ \varepsilon_t = \displaystyle\int_{l_0}^{l} \frac{dl}{l} = \ln\left(\frac{l}{l_0}\right) \end{cases}$$

Where:

- A: 'Instantaneous' area
- l_0 : Initial length
- l : 'Instantaneous' length.

As the elastoplastic model is completed, an iterative procedure of nonlinear static finite element analysis is performed, considering the previously established thickness of the tank and a gradual increase of the internal pressure magnitude. The results are obtained and presented for both load cases.

4.5.1. Elastoplastic Analysis Results for the Load Case of Compression

The results of the nonlinear elastoplastic runs regarding the compression load case, are presented in the following tabular form (Table 4.12). It is shown that under 6.4 (MPa) of internal pressure, the thickness of 6.5 (mm) is sufficient against ultimate failure and consequently there is no need for sizing it again. By increasing the magnitude of the internal pressure above 6.4 (MPa), the tank exhibits unacceptable stresses. Specifically, it should be pointed out that when the internal pressure reaches 7.2 (MPa), plastic

deformations initiate along the attachment region of the tank which correspond to the mounting ring of the frame.

Internal Pressure (MPa)	Nonlinear Stresses (MPa)	Region	Plastic Strains	Area	M.O.S.	Acceptance /Reject
6.4	312	Cylindrical Body	0	-	0.076	✔
6.8	332	Cylindrical Body	0	-	-0.5030	✗
7.2	351	Cylindrical Body	$7.63 \cdot 10^{-5}$	Attachment Points	-0.1042	✗
7.6	362	Cylindrical Body	$7.97 \cdot 10^{-3}$	Cylindrical Body	-0.1314	✗
7.8	367	Cylindrical Body	$2.40 \cdot 10^{-2}$	Cylindrical Body	-0.1433	✗

Table 4.12Results Elastoplastic Analysis of the Tank for the Compression Load Case

For the last design iteration, indicative diagrams of nonlinear stresses and strains distribution throughout the tank are shown in Figure 4.46 and Figure 4.47. As it can be observed the maximum magnitude of both nonlinear stresses and nonlinear strains occur at the cylindrical body of the tank.

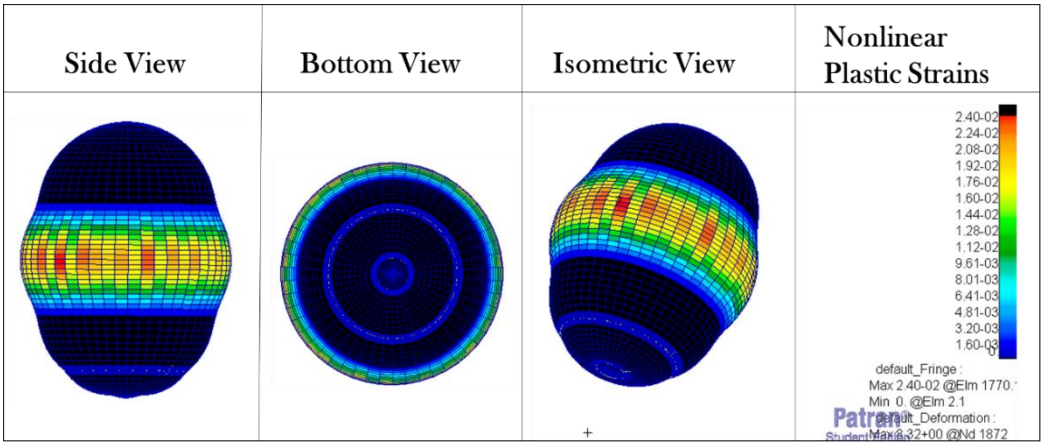

Figure 4.46 Nonlinear Strains on the Tank

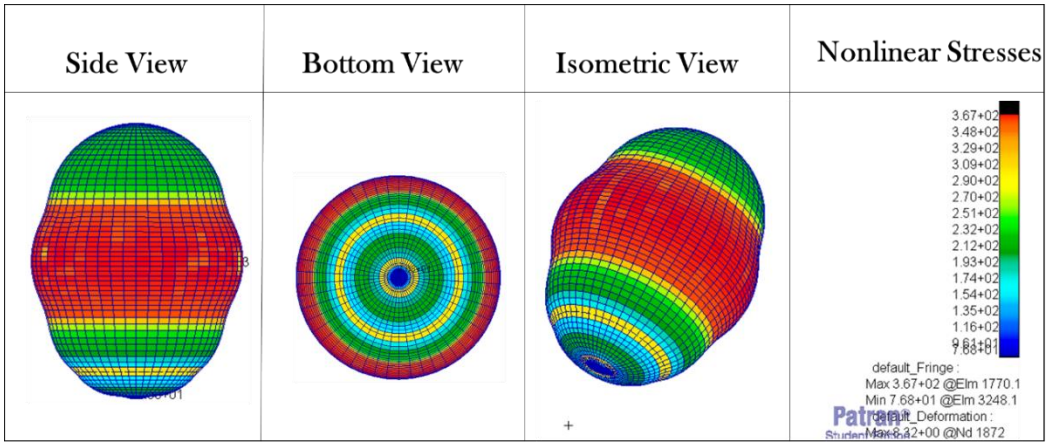

Figure 4.47 Nonlinear Stresses on the Tank

4.5.2. Elastoplastic Analysis Results for the Load Case of Tension

The results of the nonlinear elastoplastic runs, considering the compression load case, are presented in the following tabular form (Table 4.13). The results are almost identical, and thus no further conclusions can be drawn of the respective load case.

Internal Pressure (MPa)	Nonlinear Stresses (MPa)	Region	Plastic Strains	Area	M.O.S.	Acceptance /Reject
6.4	312	Cylindrical Body	0	-	0.076	✔
6.8	332	Cylindrical Body	0	-	-0.5030	✗
7.2	351	Cylindrical Body	$7.49 \cdot 10^{-5}$	Attachment Points	-0.1042	✗
7.6	362	Cylindrical Body	$8.35 \cdot 10^{-3}$	Cylindrical Body	-0.1314	✗
7.8	367	Cylindrical Body	$2.33 \cdot 10^{-2}$	Cylindrical Body	-0.1433	✗

Table 4.13 Results of the Frame Design Process for the Compression Load Case

For the last design iteration indicative diagrams of nonlinear stresses and strains distribution throughout the tank are shown in Figure 4.48 and Figure 4.49.

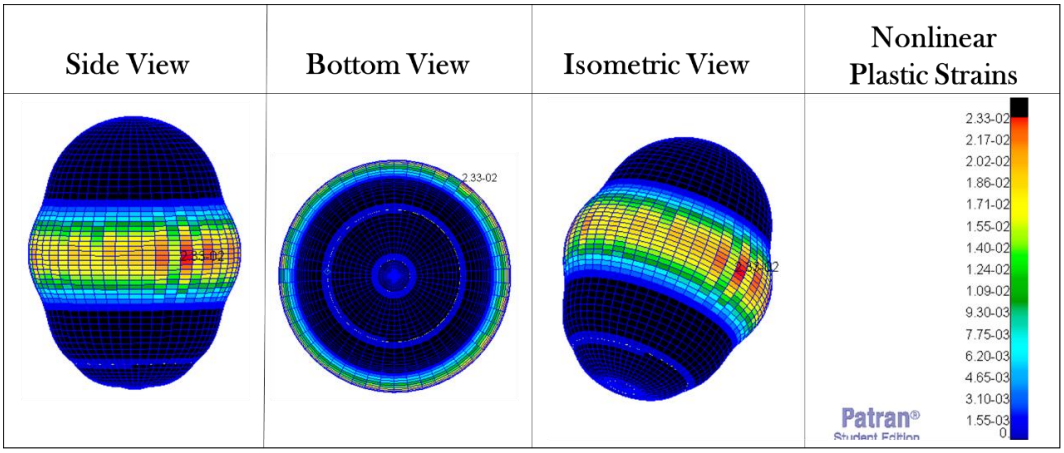

Figure 4.48 Nonlinear Strains on the Tank

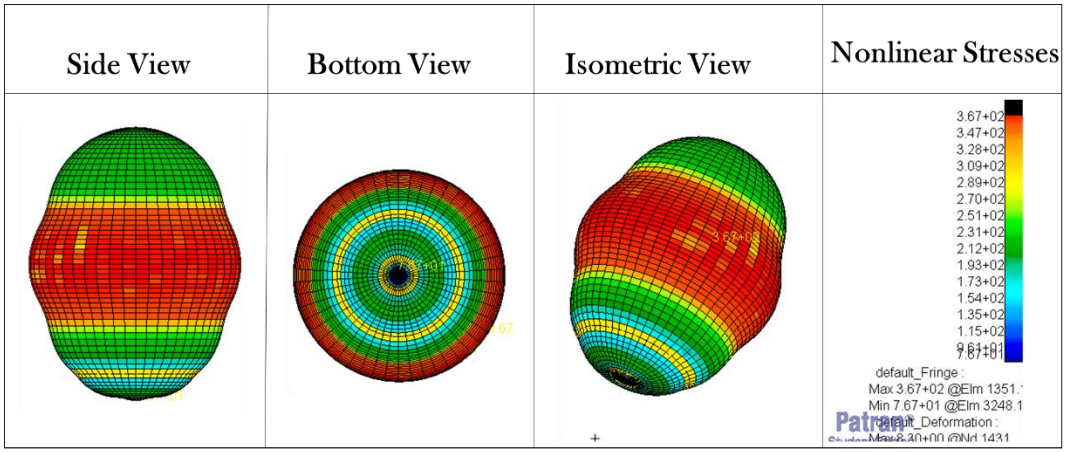

Figure 4.49 Nonlinear Stresses on the Tank

4.6. Evaluation of Static Analysis Results

After the completion of the sizing procedure for both structural modules of the tanker spacecraft through static strength analysis, mass properties are reported and evaluated in order to ensure that the design requirements for mini passengers are met. The mass and the center of gravity position of the tanker spacecraft are reported below:

Tank Modules	Thickness (mm)
Upper Dome	6.5
Lower Dome	6.5
Cylindrical Body	6.5
Total Structure Mass (kg)	44.41

Table 4.14Tank Structure Properties

Center of Gravity	
$x_{C.o.G}$ (mm)	0
$y_{C.o.G}$ (mm)	0
$z_{C.o.G}$ (mm)	748

Table 4.16Table 4.16 Center of Gravity Position

Frame Bram Groups	Cross-sectional Area
Adapter Ring	(10x1)
Support Struts	(30x3)
Mounting Ring	(34x3)
Connection Struts	(20x2)
Main Deck Struts	(20x2)
Main Deck Ring	(20x2)
Upper/Lower Bulkhead	(10x1)
Lateral Struts	(10x1)
Longerons	(10x1)
Upper Struts	(10x1)
Total Structure Mass (kg)	14.50

Table 4.15Frame Structure Properties

It can be observed that the combined mass of the storage tank and the frame is 58.91 (kg) which corresponds to the 14.72% of the maximum possible mass.

It should be pointed out that both constraints induced by Center of Gravity position of the structure are satisfied, as its height does not exceed 900(mm) from the mounting plane of the spacecraft, and its static unbalance does not exceed 15 (mm).

5. Dynamic Analysis for Tanker Spacecraft Sizing

5.1. Normal Modes of the Tanker Spacecraft

When proceeding with dynamic analysis of the tanker spacecraft, the first step is to compute its natural frequencies. The main reason for computing the natural frequencies, is to access the dynamic interaction between the spacecraft and the launch vehicle. The tanker spacecraft must be designed with the essential structural stiffness, ensuring the satisfaction of the frequency requirements listed at Table 5.1. It is noted that dynamic response of the structure at each frequency has a specific direction, which depends on the respective mode shape.

Direction	Frequency (Hz)
Longitudinal	>60
Lateral	>20

Table 5.1 Longitudinal and Lateral Frequency Requirements

It is vital that the above requirements must be respected in order to prevent any dynamic coupling between the spacecraft and the launch vehicle and suggest specific design modifications, if needed. A brief mathematical background of the normal modes computation is presented below: [11]

Considering a multi-degree-of- freedom system and neglecting damping and the applied loading, its equation of motion takes the following reduced form.

$$[M]\{\ddot{u}\}+[K]\{u\}=0$$

Where:

- $[M]$: Mass matrix of the model
- $[K]$: Stiffness matrix of the model
- $\{u\}$: Displacement matrix
- $\{\ddot{u}\}$: Acceleration matrix

This is the equation of motion for undamped free vibration. Solving this particular equation, defines natural frequencies and normal modes of the system. Assuming a harmonic solution of the form:

$$\{u\}=\{\varphi\}\sin(\omega t)=\{\varphi\}e^{i\omega t}$$

Where:

- $\{\varphi\}$: Eigenvector or mode shape
- ω: Circular natural frequency

The harmonic form of the solution entails that all the degrees of freedom of the vibrating structure move in a synchronous manner. The structural configuration does not change its basic shape during motion. However, its amplitude changes. Differentiating twice the assumed harmonic solution and substituting it into the equation of motion:

$$[M]\{\ddot{u}\}+[K]\{u\}=0 \xrightarrow[\{u\}=\{\varphi\}e^{i\omega t}]{\{\ddot{u}\}=-\omega^2\{\varphi\}e^{i\omega t}}$$
$$[M]\left(-\omega^2\{\varphi\}e^{i\omega t}\right)+[K]\left(\{\varphi\}e^{i\omega t}\right)=0 \rightarrow$$
$$e^{i\omega t}\left(-\omega^2[M]+[K]\right)\{\varphi\}=0 \rightarrow$$
$$\left(-\omega^2[M]+[K]\right)\{\varphi\}=0$$

This equation forms the standard eigenvalue problem. It is noteworthy that the stiffness matrix is constant. This means that deflections are small and the developed stresses and strains are defined by elastic material behavior.

There are two possible solution forms:

- If $\left|-\omega^2[M]+[K]\right|\neq 0$, the only possible solution is $\{\varphi\}=0$.
  The trivial solution, which does not provide any valuable information from a physical point of view due to the fact that represents the case of no motion.

- If $\{\varphi\}\neq 0$, then $\left|-\omega^2[M]+[K]\right|=0$.
  This is the non-trivial solution, which is satisfied only at a set of discrete eigenvalues. Hence the equation can be rewritten:
  $$\left(-\omega^2[M]+[K]\right)\{\varphi\}=0 \rightarrow$$
  $$\left[-\omega_i^2[M]+[K]\right]\{\varphi_i\}=0$$

Each eigenvalue and eigenvector define a free vibration mode of the structure. The eigenvalue is related to the natural frequency f_i where i refers to the i-th degree of freedom of the model. The number of possible eigenvalues and eigenvectors is equal to the number of degrees of freedom with a given value of mass. The most significant characteristic for a linear elastic structure-when vibrating in free or forced motion- is that its deflected shape at any given time, is a linear combination of all of its normal modes.

$$\{u\}=\sum_{i=1}^{i=n}\{\varphi_i\}\xi_i$$

Where:

- $\{u\}$: Vector of physical displacements
- $\{\varphi_i\}$: i-th mode shape
- ξ_i : i-th modal displacement

The majority of the most common structural elements, entail that both stiffness and mass matrices are real and symmetric. The following mathematical properties, which are known as the orthogonality property of normal modes must hold, ensuring that each normal mode differs from others. A natural mode of the structure can be represented by using its generalized mass and generalized stiffness.

$$\begin{cases} \{\varphi_i\}^T [M]\{\varphi_j\} = 0, \text{ if } i \neq j \\ \{\varphi_i\}^T [M]\{\varphi_j\} = m_j, \text{ for the } j-\text{th generalized mass} \end{cases}$$

and

$$\begin{cases} \{\varphi_i\}^T [K]\{\varphi_j\} = 0, \text{ if } i \neq j \\ \{\varphi_i\}^T [K]\{\varphi_j\} = k_j = \omega^2 m_j, \text{ for the } j-\text{th generalized stiffness} \end{cases}$$

Combining the above equations, Rayleigh equation is obtained:

$$\omega^2 = \frac{\{\varphi_i\}^T [K]\{\varphi_j\}}{\{\varphi_i\}^T [M]\{\varphi_j\}}$$

5.1.1. Normal Modes of the Tanker Spacecraft Considering Empty Tank

Initially, a preliminary normal modes analysis has been performed, examining the case in which the tank is empty. Table 5.2 presents the first ten natural frequencies and the directionality of the spacecraft dynamic response due to the corresponding shape modes.

Normal Modes	Frequency (Hz)	Modes Characterization	Direction	Acceptance /Rejection
1	18.61	1st Order Tank Bending	Lateral	✗
2	18.61	Symmetric by 90° to the 1st Bending	Lateral	✗
3	23.42	1st Order Upper Struts Breathing	Longitudinal	✗
4	32.87	1st Order Lateral Struts Breathing: -, +, -, +, -, +	Lateral	✓
5	33.08	1st Order Lateral Struts Breathing: -, +', +, +, -', -	Lateral	✓
6	33.08	1st Order Lateral Struts Breathing: -, -, -', +, +, +'	Lateral	✓
7	33.57	1st Order Lateral Struts Breathing: -, -', +, -, -', +	Lateral	✓
8	33.57	1st Order Lateral Struts Breathing: -, +, -', -, +, -'	Lateral	✓
9	34.73	1st Order Lateral Struts Breathing: -, -, -, -, -, -	Lateral	✓
10	47.34	1st Order Longerons Breathing	Lateral	✓

Table 5.2 Natural Frequencies of the Tanker Spacecraft Considering Empty Tank

As it can be observed from the Table 5.2, the first three natural frequencies violate the fundamental dynamic requirements for both lateral and longitudinal directions. The corresponding mode shapes are illustrated in Figure 5.1.

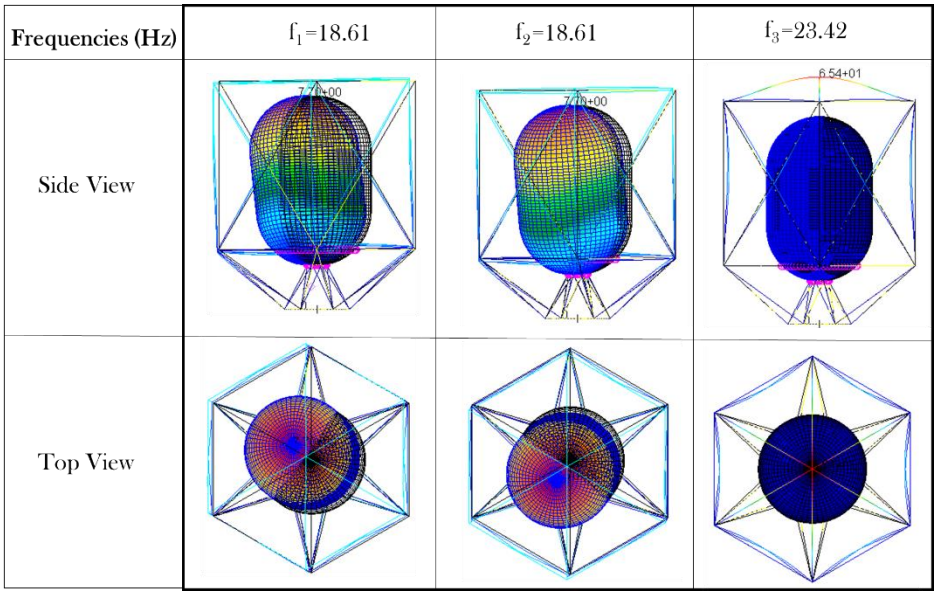

Figure 5.1 Mode Shapes of the Violative Natural Frequencies

5.1.2. Normal Modes of the Tanker Spacecraft Considering Half-Filled Tank

A more realistic approach on the normal modes computation of the tanker spacecraft, concerns the case in which the tank is half-filled with propellant. As a result, the storage tank is considered a pre-stiffened structure due to the internal pressure, induced by the contained propellant. Pressurization in a thin walled pressure vessel dominates stiffness and thus, the natural frequencies. Consequently, a static-preload should be considered for normal modes analysis. The objective of applying a static load to the structure is to obtain the stiffness matrix of the loaded structure and use it afterwards for modal analysis. Moreover, it is of great significance that the finite element model of the structure include the additional mass of the propellant as a non-structural mass acting at the surface of the tank's lower dome. Following the assumption of small deformations and material linearity, the standard eigenvalue problem is modified as shown below: [11]

$$\left(-\omega^2[M]^* + [K]^*\right)\{\varphi\} = 0 \xrightarrow[[M]^* = [M]_T + [M]_P]{[K]^* = [K] + [K]_D} \rightarrow$$

$$\left(-\omega^2\left([M] + [M]_P\right) + \left([K] + [K]_D\right)\right)\{\varphi\} = 0 \rightarrow$$

Where:

- $[M]$: Mass matrix of the model
- $[M]_P$: Non-structural mass matrix due to the mass of propellant
- $[K]$: Stiffness matrix of the model
- $[K]_D$: Differential stiffness matrix

The differential stiffness matrix is synthesized by the deformed structure. The basic approach for incorporating the pre-loaded stiffness in the normal modes analysis is to run a simulation with two subcases. The first is used to obtain the differential stiffness matrix from a linear static analysis and the second subcase is used to solve the eigenvalue problem, using the differential stiffness matrix from the prior subcase.

Table 5.3 presents the first ten natural frequencies and the directionality of the spacecraft dynamic response due to the corresponding mode shapes.

Normal Modes	Frequency (Hz)	Modes Characterization	Direction	Acceptance /Rejection
1	14.63	1st Order Tank Bending	Lateral	✗
2	14.63	Symmetric by 90° to the 1st Bending	Lateral	✗
3	23.17	1st Order Upper Struts Breathing	Longitudinal	✗
4	33.90	1st Order Lateral Struts Breathing: +, -, +, -, +, -	Lateral	✓
5	33.94	1st Order Lateral Struts Breathing: +, 0, -, -, -0, +	Lateral	✓
6	33.94	1st Order Lateral Struts Breathing: -, -, 0, +, +, 0	Lateral	✓
7	34.61	1st Order Lateral Struts Breathing: +, 0, -, +, 0, -	Lateral	✓
8	64.61	1st Order Lateral Struts Breathing: +, -, 0, +, -, 0	Lateral	✓
9	35.57	1st Order Lateral Struts Breathing: +, +, +, +, +, +	Lateral	✓
10	45.61	1st Order Longerons Breathing	Lateral	✓

Table 5.3 Natural Frequencies of the Tanker Spacecraft Considering Half-Filled Tank

Noticeably, the first three natural frequencies have decreased significantly in comparison with the previous case and consequently the requirements are once again violated. The corresponding mode shapes are illustrated at Figure 5.2.

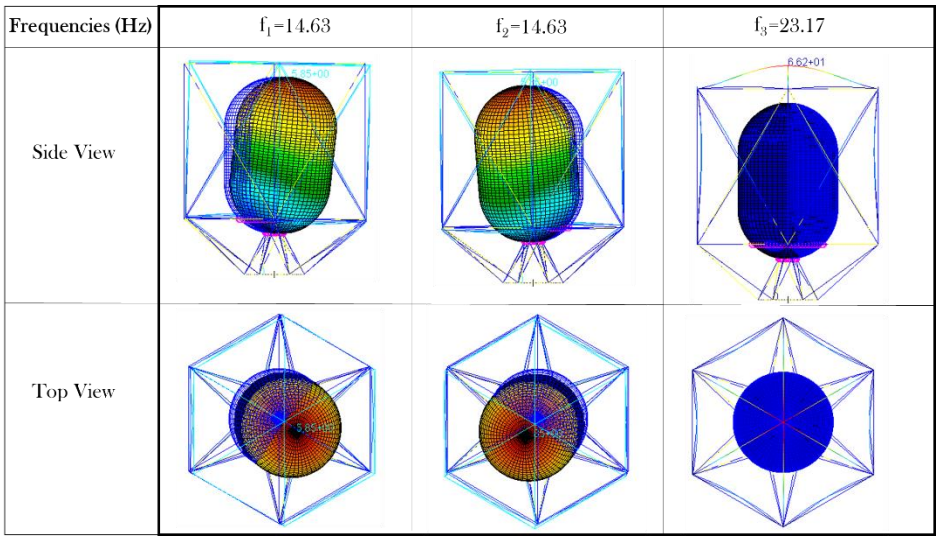

Figure 5.2 Mode Shapes of the Violative Natural Frequencies

5.1.3. Normal Modes Analysis for Sizing of the Tanker Spacecraft

The main conclusion drawn from the previous normal modes analysis indicates that the structural design process of the tanker spacecraft must proceed with continuation of the frame sizing, in order to increase the lowest frequencies of the overall structure, and thus increase its structural stiffness. Similar to the iterative design procedures performed via strength analysis in Chapter 4, the minimum cross-sectional area for each beam member group is determined through a normal modes trial and error procedure. The first

iteration suggests two design modifications. First of all, six supplemental support struts are placed between the adapter ring and the main deck ring. This modification contributes to increasing the lateral structural stiffness of the spacecraft. Secondly, it is clear by examining the mode shape, which corresponds to the third natural frequency, that the configuration of the upper struts provides insufficient structural stiffness on the longitudinal direction. The solution proposed to overcome this issue suggests the complete modification of the existing upper struts configuration to new one, which consists only of two parallel struts so as to eliminate the central weak point of the previous design.

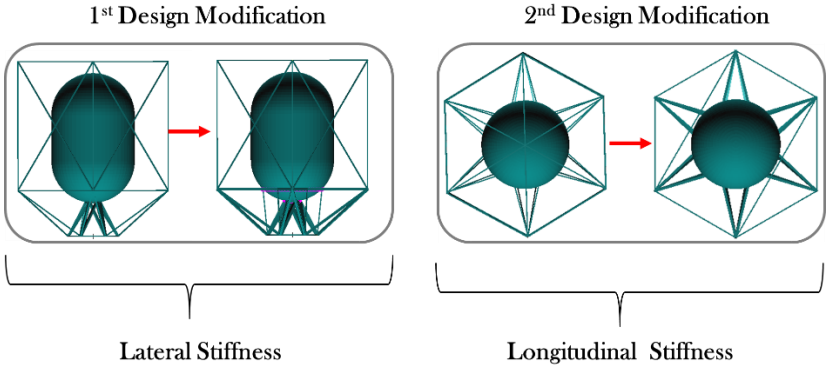

Figure 5.3 Design Modifications for the First Iteration

Table 5.4 presents the first ten natural frequencies of the first design iteration and the directionality of the spacecraft dynamic response due to the corresponding mode shapes.

Normal Modes	Frequency (Hz)	Modes Characterization	Direction	Acceptance /Rejection
1	29.12	1st Order Upper Struts Breathing +, +	Longitudinal	✗
2	29.30	1st Order Upper Struts Breathing +', -'	Longitudinal	✗
3	29.45	1st Order Lateral Struts Breathing: -, -, -, +, +, +	Lateral	✓
4	30.19	1st Order Upper Struts Breathing +', +'	Longitudinal	✗
5	31.18	1st Order Upper Struts Breathing -, +	Longitudinal	✗
6	33.40	1st Order Lateral Struts Breathing: -, +', -, -', +, -	Lateral	✓
7	33.84	1st Order Lateral Struts Breathing: -, 0, +, -, 0, +	Lateral	✓
8	33.91	1st Order Upper Struts Breathing -', +'	Longitudinal	✗
9	34.09	1st Order Lateral Struts Breathing: -', -, -', +', +, +'	Lateral	✓

Table 5.4 Natural Frequencies of the First Iteration

Apparently, the suggested design modifications have played a vital role upon increasing the lowest natural frequencies and thus the structural stiffness on both longitudinal and lateral direction have been affected. However, among the first ten natural frequencies of

the structure, six of them continue to violate, exclusively, the frequency requirements for the longitudinal direction. The corresponding mode shapes are illustrated in Figure 5.4.

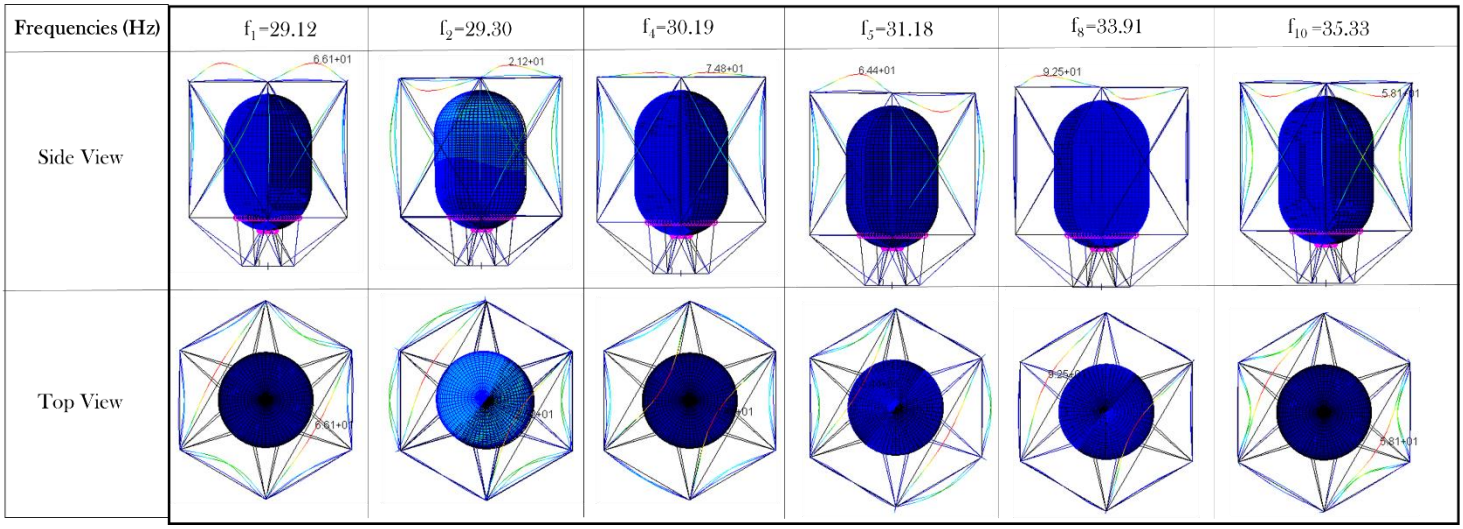

Figure 5.4 Mode Shapes of the Violative Natural Frequencies

The second design iteration, suggests modifications upon cross-section profiles of the upper struts, the bulkheads, the lateral struts and the longerons. Table 5.5 presents the first ten natural frequencies of the second design iteration and the directionality of the spacecraft dynamic response due to the corresponding mode shapes.

Normal Modes	Frequency (Hz)	Modes Characterization	Direction	Acceptance /Rejection
1	29.42	1st Order Tank Bending	Lateral	✔
2	29.43	Symmetric by 90° to the 1st Bending	Lateral	✔
3	44.39	1st Order Upper Struts Breathing +, +	Longitudinal	✗
4	46.13	1st Order Upper Struts Breathing -', -'	Longitudinal	✗
5	46.81	1st Order Upper Struts Breathing -, +	Longitudinal	✗
6	48.31	1st Order Frame-Tank Torsional	Vertical	-
7	49.69	1st Order Lateral Struts Breathing: +, -', +, -, +', -	Lateral	✔
8	49.76	1st Order Lateral Struts Breathing: -, 0, +, -, 0, +	Lateral	✔
9	50.67	1st Order Lateral Struts Breathing: +', +, +', -', -, -'	Lateral	✔
10	52.23	1st Order Upper Struts Breathing -'', +''	Longitudinal	✗

Table 5.5 Natural Frequencies of the Second Iteration

Frequencies (Hz)	f_3=44.39	f_4=46.13	f_5=46.81	f_{10} =52.23
Side View	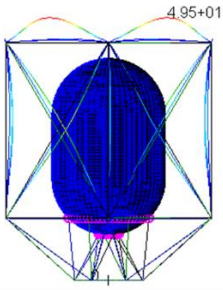	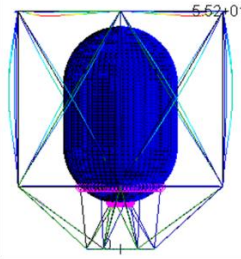	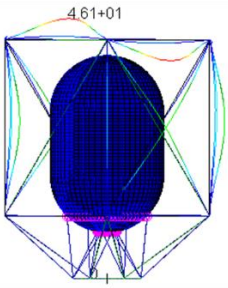	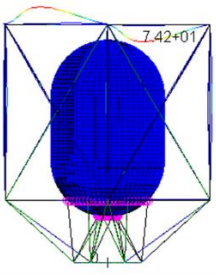
Top View	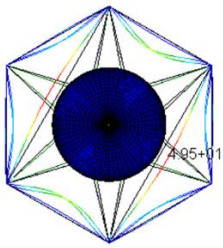	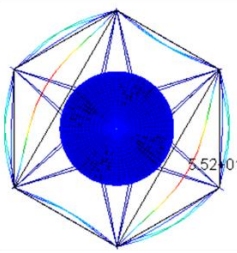	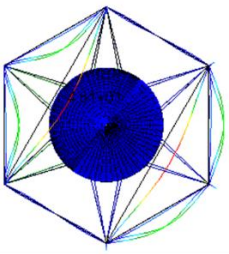	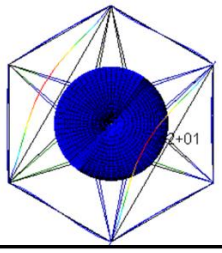

Figure 5.5 Mode Shapes of the Violative Natural Frequencies

For the second design iteration, it can be regarded that there are four unacceptable natural frequencies. The corresponding mode shapes are illustrated in Figure 5.5. Despite the fact that there is a continual increase of the structural stiffness after the two design iterations, the frequency requirements are still not satisfied. Consequently, there is a need for an additional iteration, proceeding with modifications upon cross-sectional area of the upper struts, the bulkheads and the longerons. Table 5.6 presents the first ten acceptable natural frequencies of the third design iteration and the directionality of the spacecraft dynamic response due to the corresponding mode shapes.

Normal Modes	Frequency (Hz)	Modes Characterization	Direction	Acceptance /Rejection
1	29.22	1st Order Tank Bending	Lateral	✔
2	29.28	Symmetric by 90° to the 1st Bending	Lateral	✔
3	46.72	1st Order Frame-Tank Torsional	Vertical	-
4	50.68	1st Order Lateral Struts Breathing: -, -, -, -, -, -	Lateral	✔
5	51.88	1st Order Lateral Struts Breathing: +, 0, -, -, 0, +	Lateral	✔
6	53.02	1st Order Lateral Struts Breathing: -, 0, +, -, 0, +	Lateral	✔
7	53.72	1st Order Lateral Struts Breathing: +, -, +, +, -, +	Lateral	✔
8	53.78	1st Order Lateral Struts Breathing: -, -', -, +, +', -'	Lateral	✔
9	54.41	1st Order Lateral Struts Breathing: +', -, +', -', +, -'	Lateral	✔
10	61.55	1st Order Upper Struts Breathing -, +	Longitudinal	✔

Table 5.6 Natural Frequencies of the Third Iteration

Finally, after the third design iteration the frequency requirements are satisfied and as a result the iterative design and sizing procedure design of the frame structure is terminated. The acceptable mode shapes are illustrated in their entirety in Figure 5.6.

Frequencies (Hz)	f_1=29.22	f_2=29.28	f_3=46.72	f_4=50.68	f_5=51.88
Side View	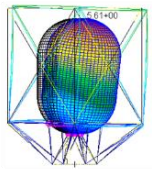	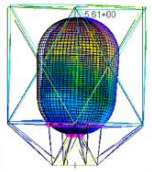	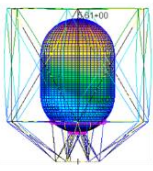	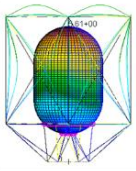	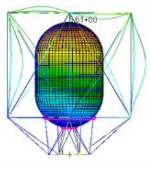
Top View	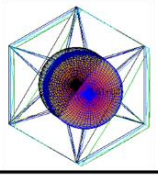	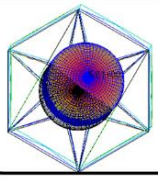	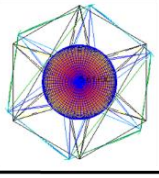	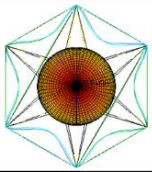	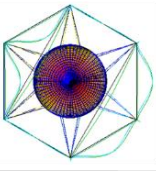
Frequencies (Hz)	f_6=53.02	f_7=53.72	f_8=53.78	f_9=54.41	f_{10}=61.55
Side View	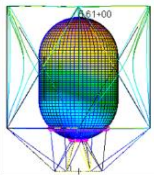	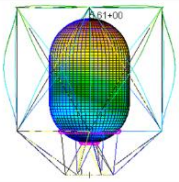	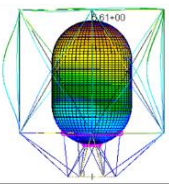	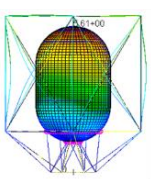	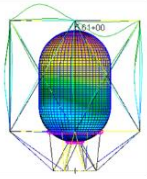
Top View	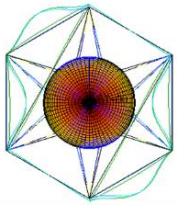	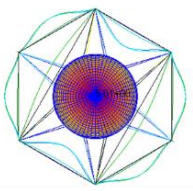	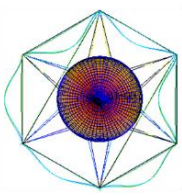	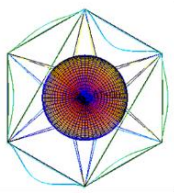	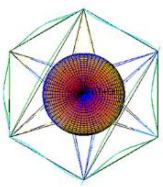

Figure 5.6 Mode Shapes and Natural Frequencies of the Final Iteration

In conclusion, two design modifications have been applied, including the addition of the supplemental support struts. Additionally, four cross-sectional modifications have been applied for the upper struts, the upper/lower bulkhead, the longerons and the lateral struts. The finalized cross-sectional area for the beam member groups are (20x2), (20x2), (20x2) and (15x1) respectively.

Design Iteration	Design Modification	Member Modification	Cross-sectional Modification
1	Supplemental Support Struts & Upper Struts Configuration	-	(-) → (10x1) & (-) → (10x1)
2	-	Upper Struts & Upper/Lower Bulkhead & Longerons & Lateral Struts	(10x1) → (15x1) & (10x1) → (15x1) & (10x1) → (15x1) & (10x1) → (15x1)
3	-	Upper Struts & Upper/Lower Frame & Longerons	(15x1) → (20x2) & (15x1) → (20x2) & (15x1) → (20x2)
4	-	-	-

Table 5.7 Cross-sectional Modifications

The design sequence of the iterative process is illustrated at Figure 5.7. For each design iteration, the particular beam member groups requiring cross-sectional modifications, are marked

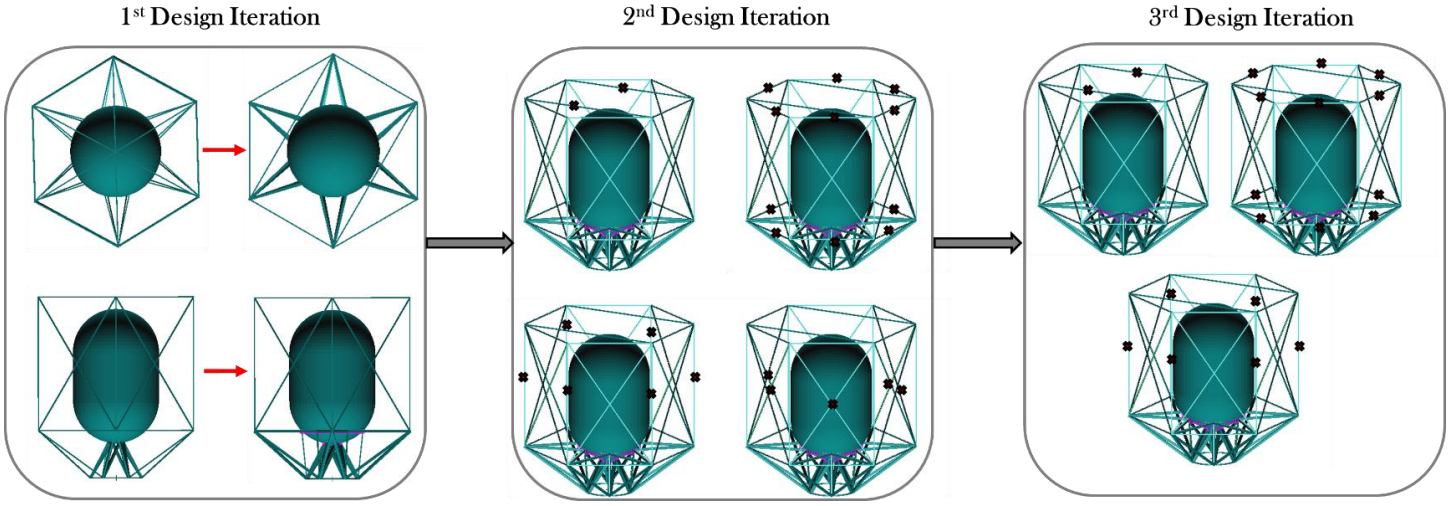

Figure 5.7 Design Sequence for the Frame Design and Sizing for Preventing Dynamic Coupling

5.2. Sinusoidal Vibration Analysis

The main purpose of performing a sinusoidal vibration analysis is to investigate whether the spacecraft structure is capable of withstanding all of the dynamic loads encountered during launch phase. It is of great significance that the analysis must lead to correct prediction of the dynamic behavior of the structure subjected to enforced vibration so as to prevent dynamic effects, such as resonance. Specifically, the idea of this frequency response analysis is to compute the structural response of the spacecraft at the low frequency domain. This frequency domain, considering a mini passenger, lies in the 5 to 125 (Hz) range. Acceleration amplitudes are considered the inputs for the enforced acceleration analysis. Their magnitudes are functions of frequency and they are presented at Table 5.8.

Sine	Frequency Range	Qualification Levels (x g)
Longitudinal	5-25	1.0
	25-45	1.0
	45-60	2.5
	60-110	1.25
	110-125	0.25
Lateral	5-25	1.0
	25-45	0.62
	45-60	1.87
	60-110	0.62
	110-125	0.25

Table 5.8 Sinusoidal Vibration Test Levels for a Mini Spacecraft

There are two approaches used for computing the frequency response of a structure. Direct method is considered the first approach. It is mostly applied in small finite element models. Its main characteristic is that the equation of motion of the damped forced

vibration is solved without computing the modes in the first place. On the other hand, the second approach implements the modal method. The modal method is particularly advantageous, if the natural frequencies and mode shapes have been computed during a previous stage of the analysis. The structural design process, established in this thesis work, benefits from the second approach and as a result the modal method is utilized in order to proceed with the dynamic analysis. A brief mathematical background of the modal method is presented below.

The forced response of the structure to an enforced motion, is proportional to the constraint forces at the same frequency as the one of the enforcing motion. Any one of the enforced displacements, velocity or acceleration must uniquely define the other two physical quantities because they differ only by multiples of frequency, with resultant constraint forces derived from a solution of a governing equation.

In the frequency domain, the damped forced vibration equation of motion with harmonic excitation has the following form: [11]

$$[M]\{\ddot{\bar{u}}\}+[B]\{\dot{\bar{u}}\}+[K]\{\bar{u}\}=\{\bar{P}\}e^{i\omega t}$$

Where:

- $\{\bar{P}\}$: Forcing Function Matrix
- $[B]$: Damping Matrix

The (Eq. 5.1) after multi-point constraint partitioning operations can be rewritten as:

$$\begin{bmatrix} M_{ff} & M_{fs} \\ M_{sf} & M_{ss} \end{bmatrix}\begin{Bmatrix} \ddot{\bar{u}}_f \\ \ddot{\bar{u}}_s \end{Bmatrix}+\begin{bmatrix} B_{ff} & B_{fs} \\ B_{sf} & B_{ss} \end{bmatrix}\begin{Bmatrix} \dot{\bar{u}}_f \\ \dot{\bar{u}}_s \end{Bmatrix}+\begin{bmatrix} K_{ff} & K_{fs} \\ K_{sf} & K_{ss} \end{bmatrix}\begin{Bmatrix} \bar{u}_f \\ \bar{u}_s \end{Bmatrix}=\begin{Bmatrix} \bar{P}_f \\ \bar{P}_s+\bar{Q}_s \end{Bmatrix}$$

The f-set and the s-set refer to the free and the constrained degrees of freedom respectively. P_s are the external loads applied to the s-set and Q_s are the corresponding forces of constraint. Similarly, P_f are the external loads applied to the f-set.

Considering the case in which enforced acceleration is applied, $\bar{u}_s \neq \{0\}$

- The f-set equation takes the form:

$$\left[-\omega^2 M_{ff}+i\omega B_{ff}+K_{ff}\right]\{\bar{u}_f\}=\{\bar{P}_f\}-\left[-\omega^2 M_{fs}+i\omega B_{fs}+K_{fs}\right]\{\bar{u}_s\}$$

- The s-set equation takes the form:

$$\{\bar{Q}_s\}=-\{\bar{P}_s\}+\left[-\omega^2 M_{sf}+i\omega B_{sf}+K_{sf}\right]\{\bar{u}_f\}+\left[-\omega^2 M_{ss}+i\omega B_{ss}+K_{ss}\right]\{\bar{u}_s\}$$

5.2.1. Enforced Acceleration Analysis for Sizing of the Tanker Spacecraft

Performing a sinusoidal vibration analysis is the final step of the preliminary structural design of the tanker spacecraft. Similar to the previous design steps, followed in strength and modal analysis, this final one must ensure that dynamic environment at that particular frequency domain will not lead any of the envisaged structures to failure. Therefore, an iterative sizing procedure is performed, utilizing enforced motion in longitudinal and

lateral axis of the spacecraft separately, in order to determine the finalized cross-sectional dimensions of the frame beam members.

It should be pointed out that in both load cases the acceleration input has been applied on the nodes of the adapter ring as shown in Figure 5.8.

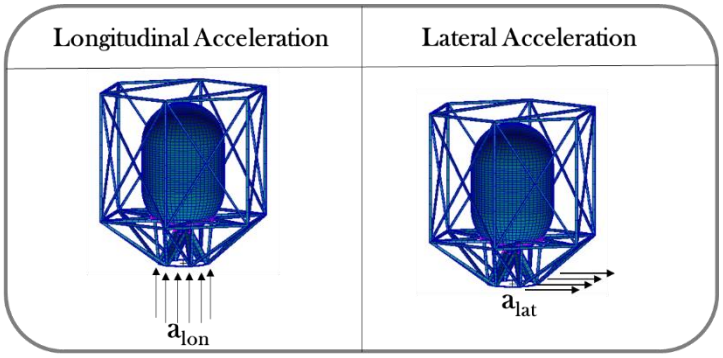

Figure 5.8 Enforced Acceleration of the Tanker Spacecraft

The completion of a realistic finite element model must proceed with the selection of the most appropriate option for modelling the damping effects. Among the available options provided by MSC Nastran, modal damping is used as to define damping as a function of frequency. Despite the fact that it is proportional to the stiffness matrix, its effect is viscous. The damping effects are distributed to the structure depending on the energy distribution in each mode shape. Modal damping is equal to 1% for all modes of the tanker spacecraft structure.

5.2.1.1. Longitudinal Enforced Acceleration

According to Table 5.8, Diagram 5.1 illustrates the longitudinal enforced acceleration input as a function of frequency, which is associated with the first load case of the frame sizing procedure with regards to the sinusoidal vibration analysis.

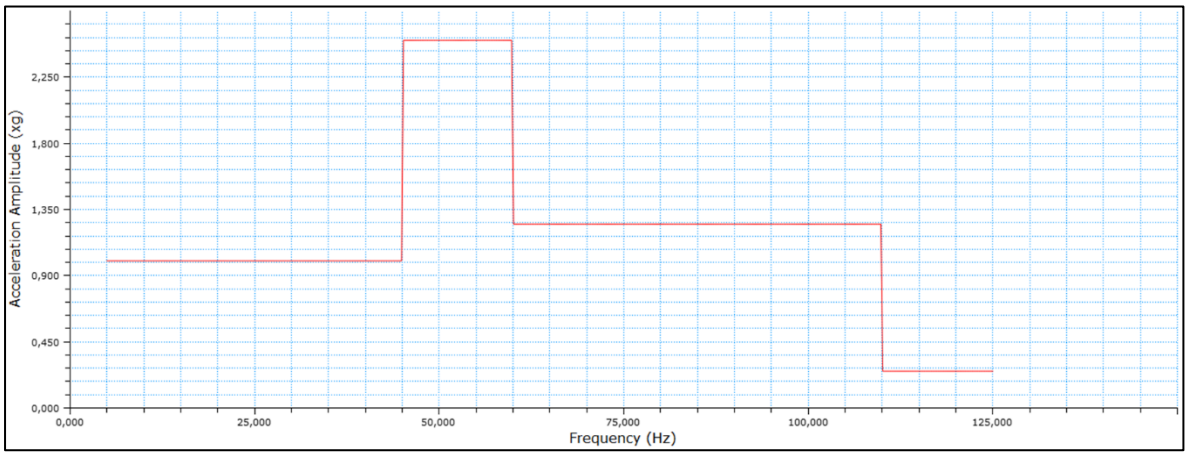

Diagram 5.1 Longitudinal Acceleration Amplitude vs Frequency [Credits: Arianespace]

The design process is terminated after the first iteration, verifying that tank's safe operation under the above acceleration input. Apparently, the maximum Von Mises stresses are developed on the cylindrical body of the tank.

Design Iteration	Maximum Von Mises Stress (MPa)	Frequency (Hz)	Region	Margin of Safety	Acceptance /Reject
1	324	∀	Cylindrical Body	0.042	✔

Table 5.9 Results of the Tank Response upon Longitudinal Enforced Acceleration

Nodal Von Mises stresses of the most critical tank's regions are plotted as a function of frequency. Diagram 5.2 captures these regions that are constituted by the poles of the upper and the lower dome, the upper and the lower junctures, a midpoint at the cylindrical body, and the attachment points which correspond to the mounting and the main deck ring of the frame respectively. A typical example of stress distribution on the tank structure throughout the frequency range of interest, is shown at Figure 5.9.

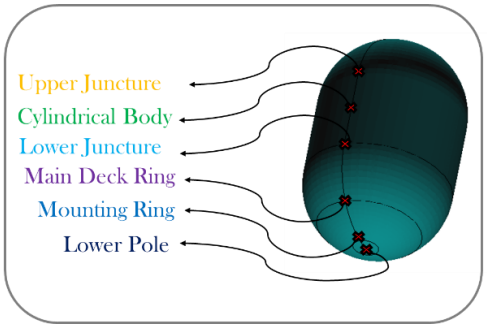

Figure 5.10 Critical Regions of the Tank

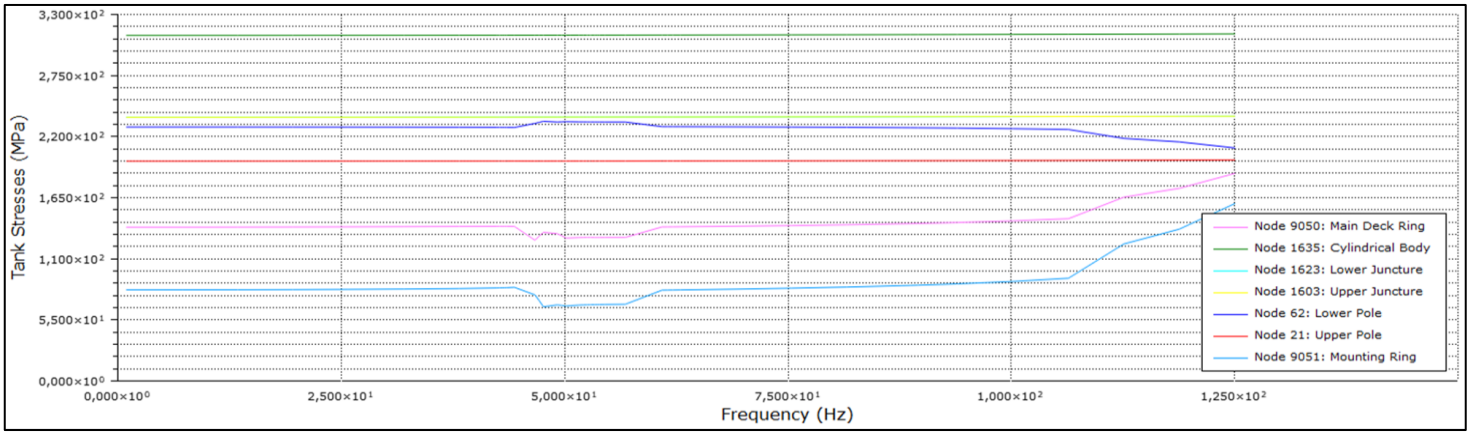

Diagram 5.2 Tank Stresses Vs Frequency

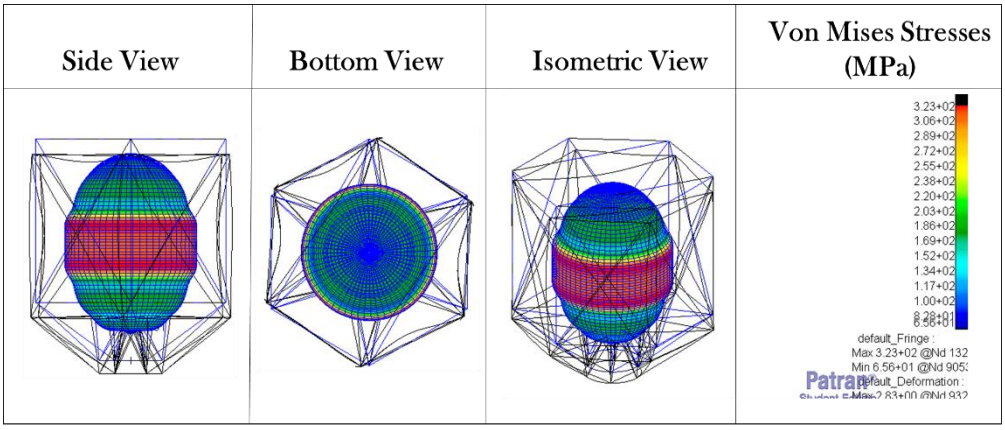

Figure 5.9 Von Mises Stress Distribution

On the other hand, considering the frame structure, the examination of the maximum stresses throughout the frequency range is divided into six steps depending on the different region of the frame. Consequently, excitation frequencies for the peak stress responses are established for the entire structure.

Upper Bulkhead Region:

Diagram 5.3 and Diagram 5.4 illustrate the nodal axial and the bending stresses developed on the highlighted upper bulkhead nodes (6592, 6602, 6631, 6669, 6707 and 6736). The maximum axial stress response does not exceed 33 (MPa) and occurs at the excitation frequency of 47.17 (Hz). The maximum bending stress response does not exceed 125 (MPa) and occurs at the excitation frequency of 49.68 (Hz).

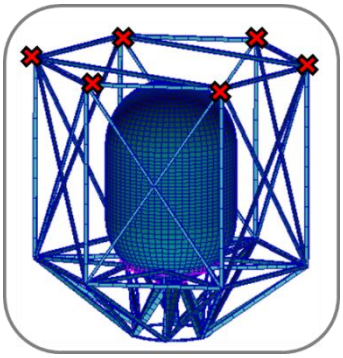

Figure 5.11 Upper Bulkhead Region

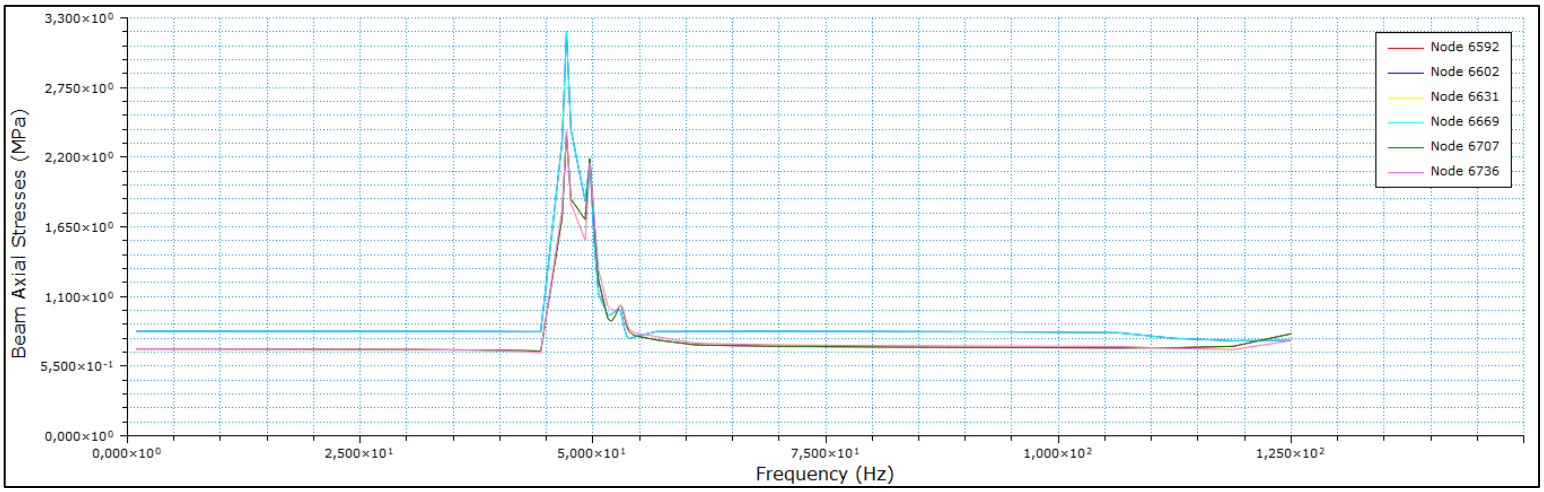

Diagram 5.3 Axial Stresses Vs Frequency

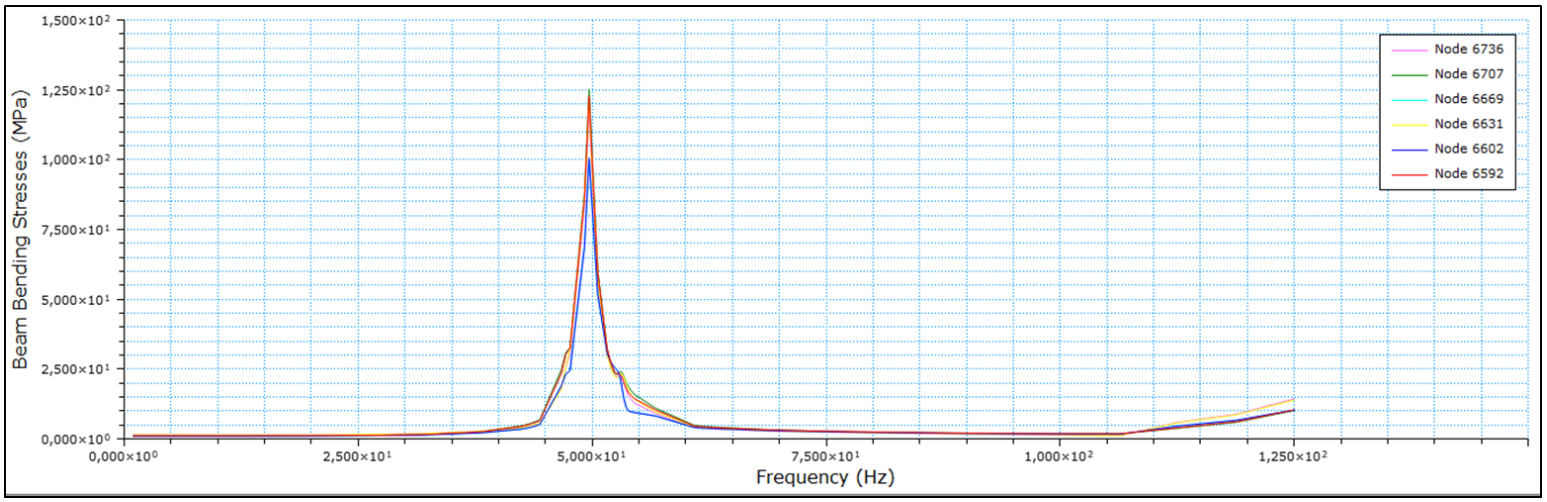

Diagram 5.4 Bending Stresses Vs Frequency

Lower Bulkhead Region:

Diagram 5.5 and Diagram 5.6 illustrate the nodal axial and the bending stresses developed on the highlighted upper bulkhead nodes (6392, 6391, 6030, 6020, 6019 and 6000). The maximum axial stress response does not exceed 39 (MPa) and occurs at the excitation frequency of 47.17 (Hz). The maximum bending stress response does not exceed 85 (MPa) and occurs at the excitation frequency of 49.68 (Hz)

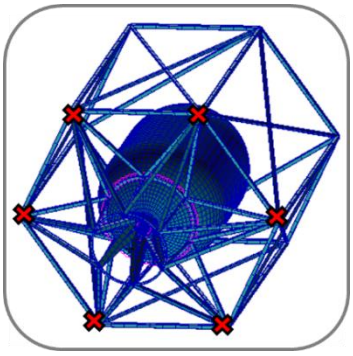

Figure 5.12 Lower Bulkhead Region

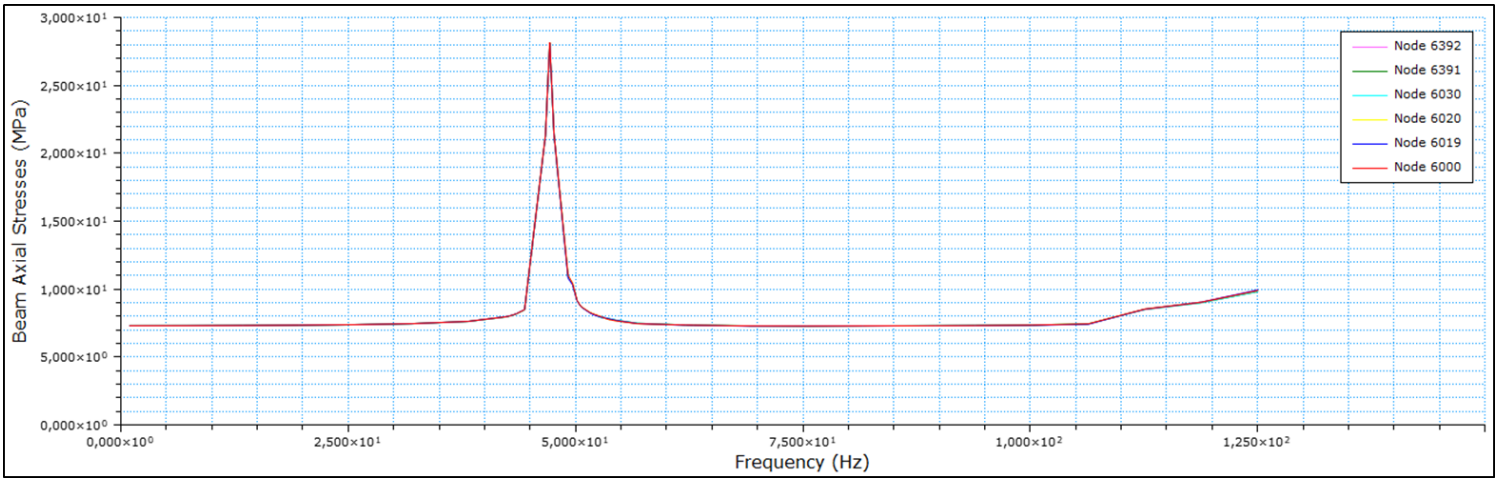

Diagram 5.5 Axial Stresses Vs Frequency

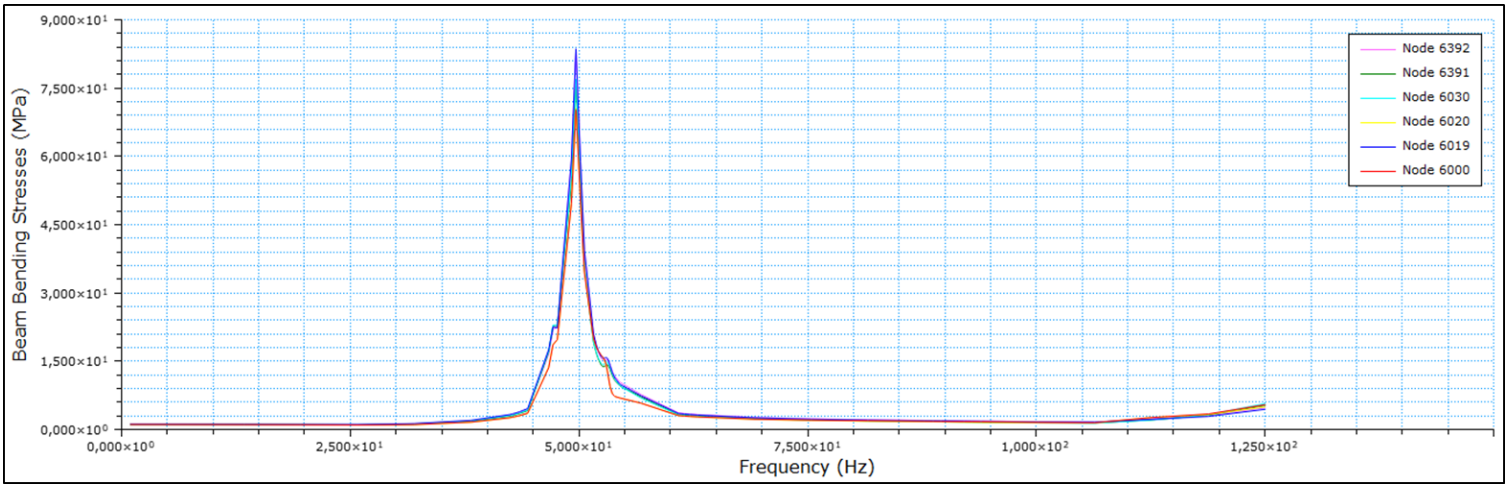

Diagram 5.6 Bending Stresses Vs Frequency

Lateral Struts Region:

Diagram 5.7 and Diagram 5.8 illustrate the nodal axial and the bending stresses developed on the highlighted upper bulkhead nodes (6746, 6717, 6688, 6650, 6573). The maximum axial stress response does not exceed 33 (MPa) and occurs at the excitation frequency of 47.17 (Hz). The maximum bending stress response does not exceed 125 (MPa) and occurs at the excitation frequency of 49.68 (Hz)).

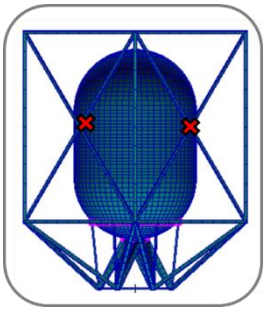

Figure 5.13 Lateral Struts Region

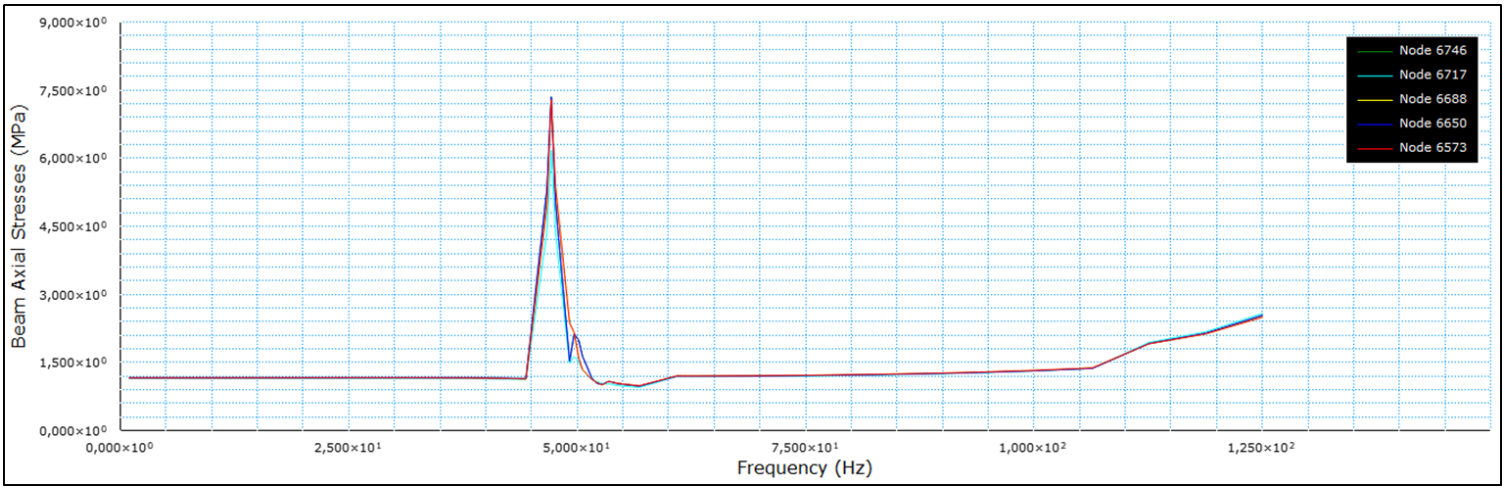

Diagram 5.8 Axial Stresses Vs Frequency

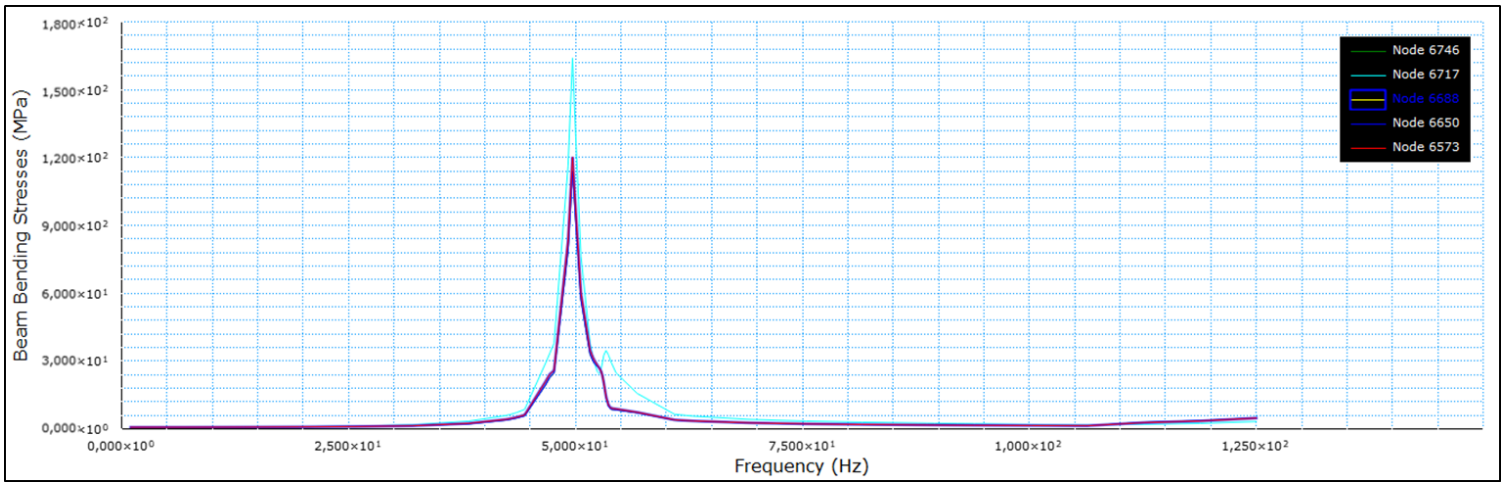

Diagram 5.7 Bending Stresses Vs Frequency

Mounting Ring Region:

Diagram 5.9 and Diagram 5.10 illustrate the nodal axial and the bending stresses developed on the highlighted upper bulkhead nodes (9131, 9129, 9128, 9127, 9126 and 9125). The maximum axial stress response occurs at the maximum frequency of the low operational frequency domain and it does not exceed 48 (MPa). Definitely, there is an excitation frequency above 125 (Hz) which leads to a greater peak stress response comparatively to the respective response of 47.17(Hz). The maximum bending stress response does not exceed 39 (MPa) and occurs at the excitation frequency of 49.68 (Hz).

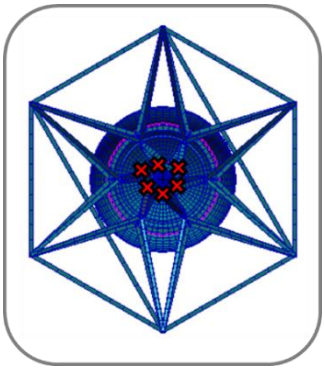

Figure 5.14 Mounting Ring Region

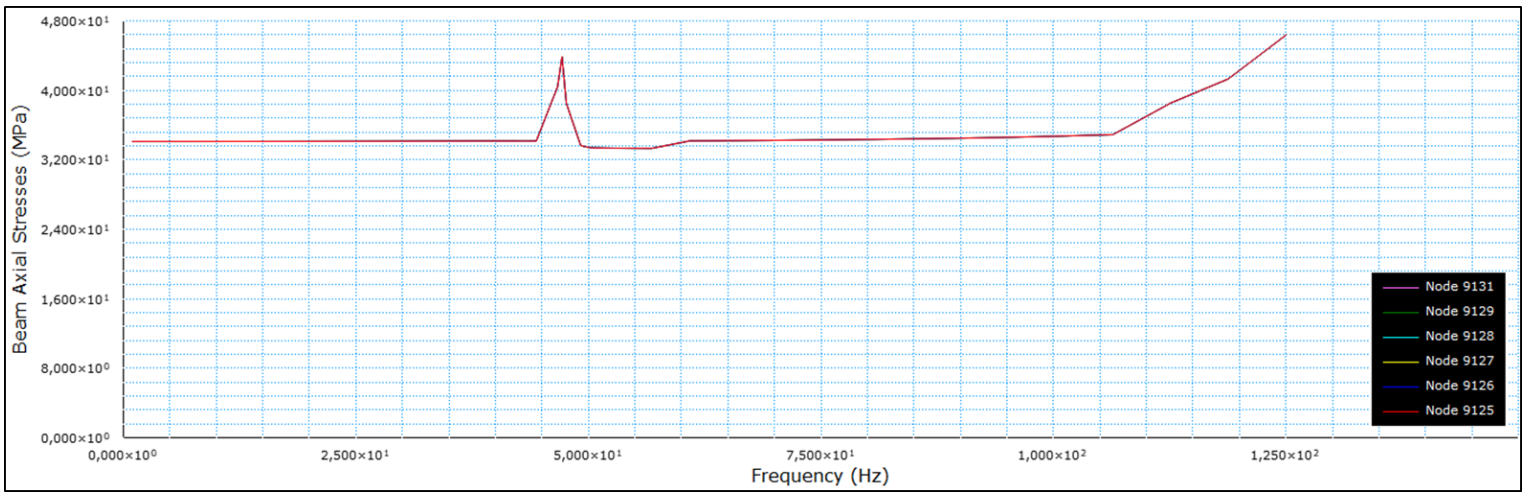

Diagram 5.9 Axial Stresses Vs Frequency

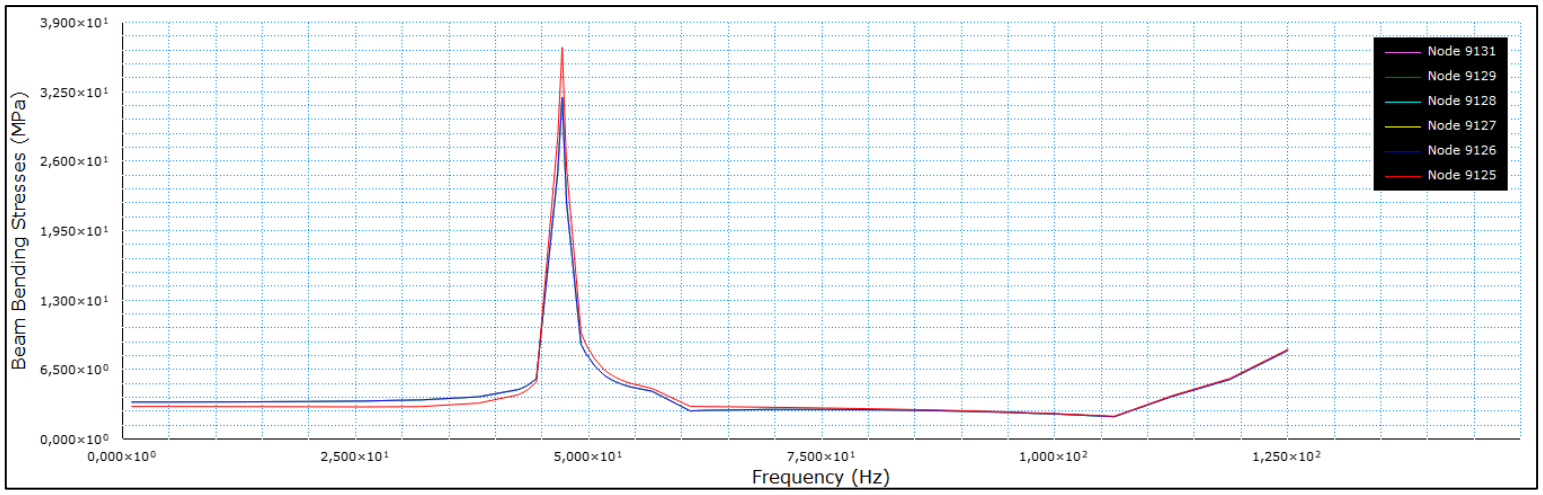

Diagram 5.10 Bending Stresses Vs Frequency

Main Deck Region:

Diagram 5.11 and Diagram 5.12 illustrate the nodal axial and the bending stresses developed on the highlighted upper bulkhead nodes (9130, 9124, 9123, 9122, 9121 and 9120). The maximum axial stress response does not exceed 33 (MPa) and occurs at the excitation frequency of 47.17 (Hz). The maximum bending stress response occurs the maximum frequency of the low operational frequency domain and does not exceed 18 (MPa). Definitely, there is an excitation frequency above 125 (Hz) which leads to a greater peak stress response comparatively to the respective response of 49.68 (Hz).

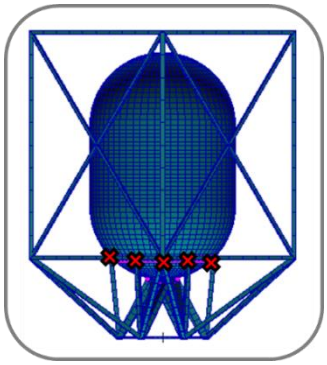

Figure 5.15 Main Deck Ring Region

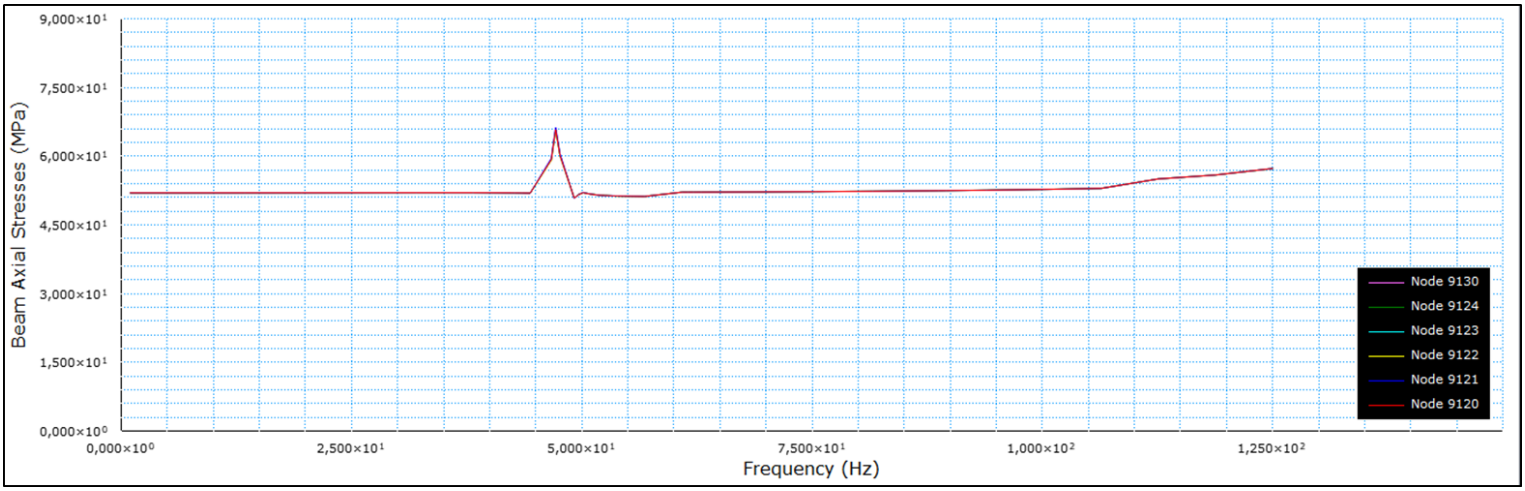

Diagram 5.11 Axial Stresses Vs Frequency

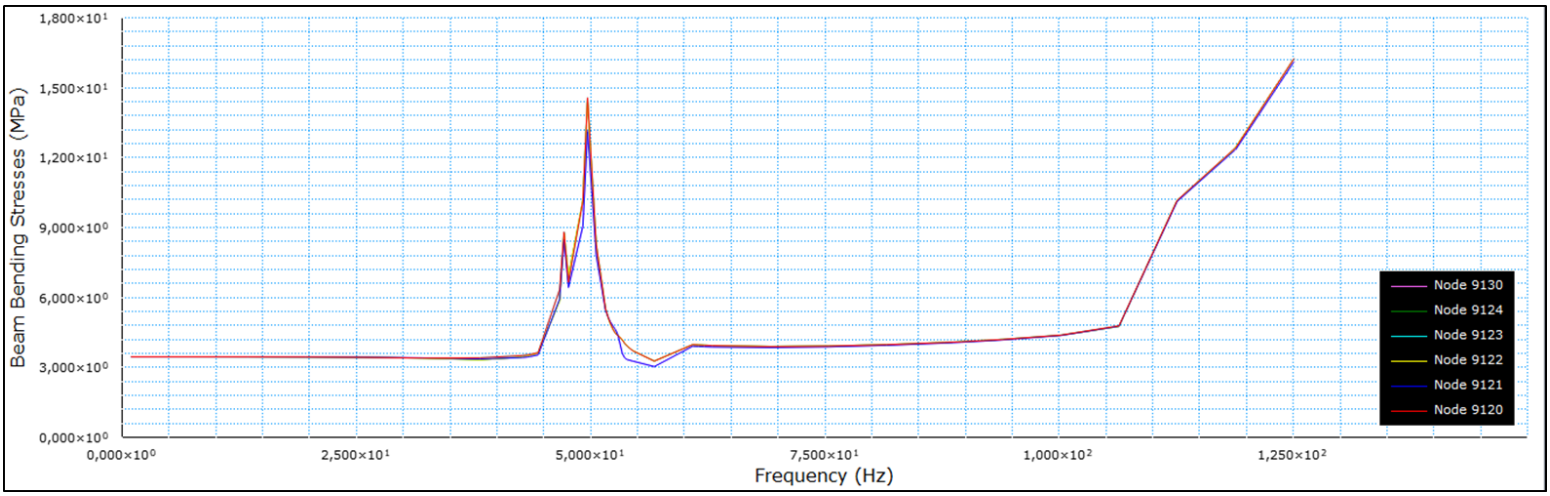

Diagram 5.12 Bending Stresses Vs Frequency

Adapter Ring Region:

Diagram 5.13 and Diagram 5.14 illustrate the nodal axial and the bending stresses developed on the highlighted adapter ring nodes (6427, 6233, 6213, 6182, 6163 and 6153). The maximum axial stress response does not exceed 34 (MPa) and occurs at the excitation frequency of 47.17 (Hz). The maximum bending stress response does not exceed 30 (MPa) and occurs at the excitation frequency of 47.17 (Hz) as well.

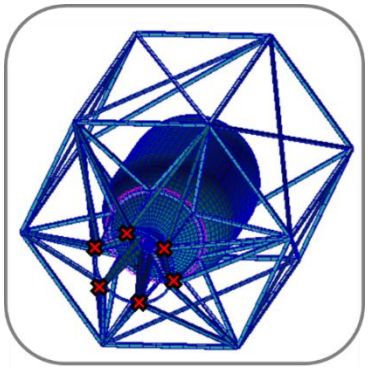

Figure 5.16 Adapter Ring Region

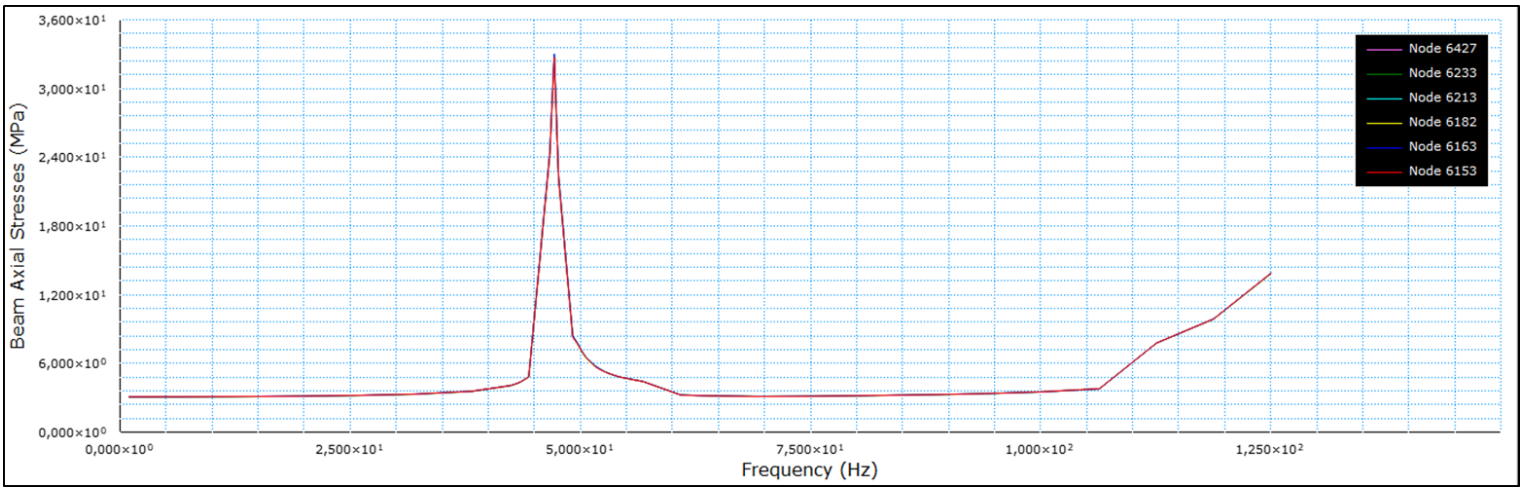

Diagram 5.13 Axial Stresses Vs Frequency

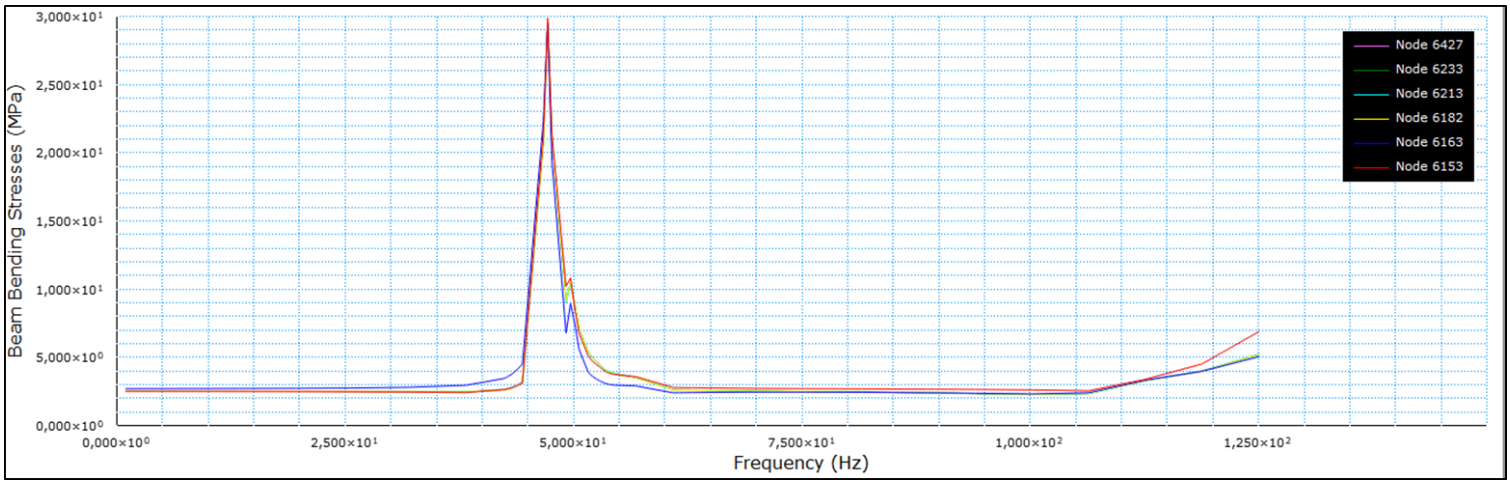

Diagram 5.14 Bending Stresses Vs Frequency

By examining the stresses developed on the frame structure throughout the frequency domain of interest, it can be clearly observed that the peaks in stress responses tend to occur only at the frequency of 47.17 (Hz) and 49.68 (Hz). Among them, the first frequency corresponds to the twenty-first natural frequency, leading to a torsional mode shape. The second one, corresponds to the twenty-fourth natural frequency of the structure, leading to lateral struts breathing mode. Axial and bending stress plots at those particular frequencies are presented below, in order to define the magnitude and the location of the maximum combined stresses on the frame structure.

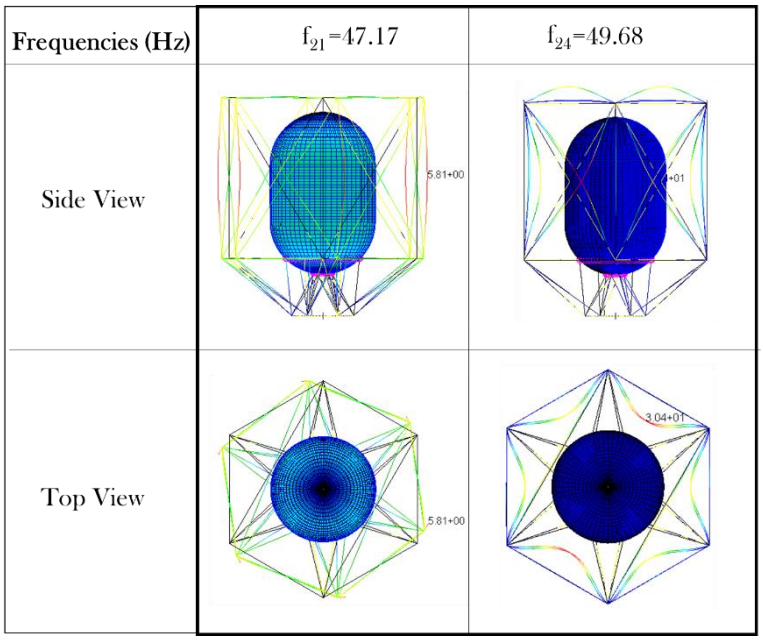

Figure 5.17 Peak Excitation Frequencies

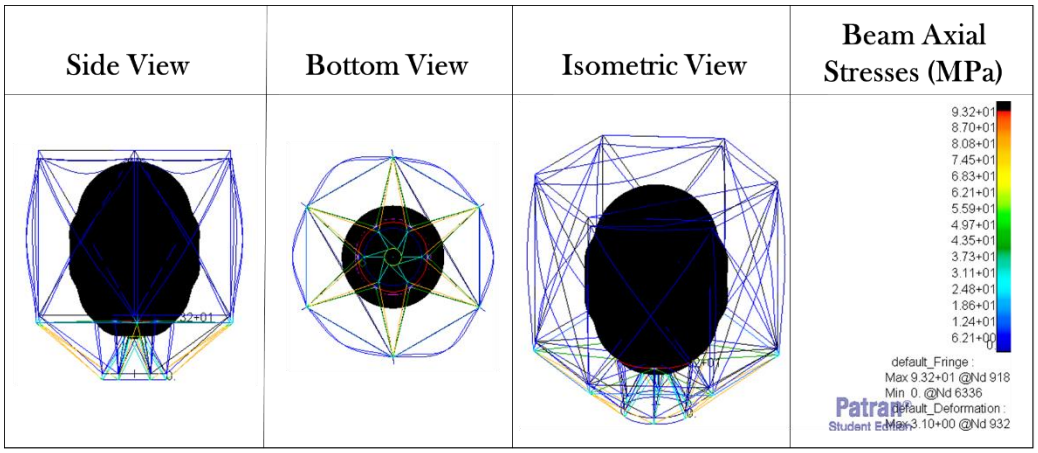

Figure 5.18 Axial Stresses of the Beam Members at Frequency 47.17 (Hz)

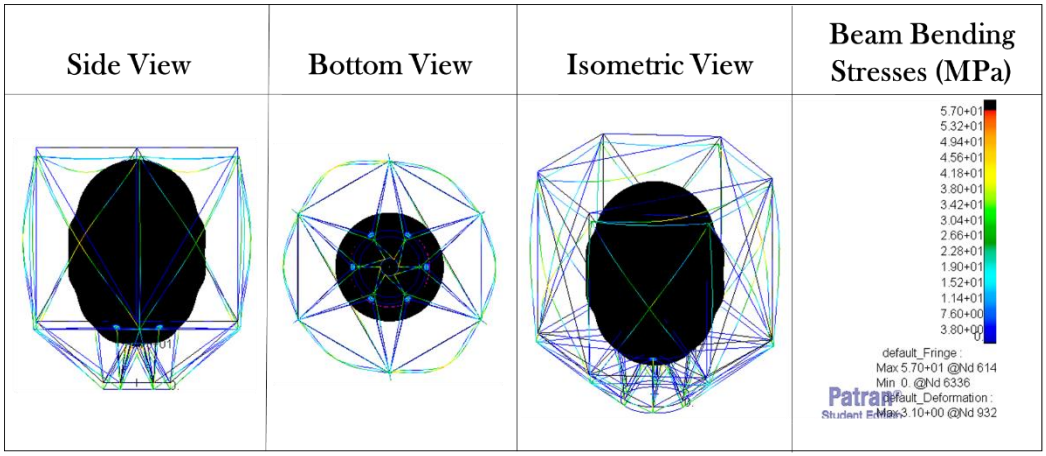

Figure 5.19 Bending Stresses of the Beam Members at Frequency 47.17 (Hz)

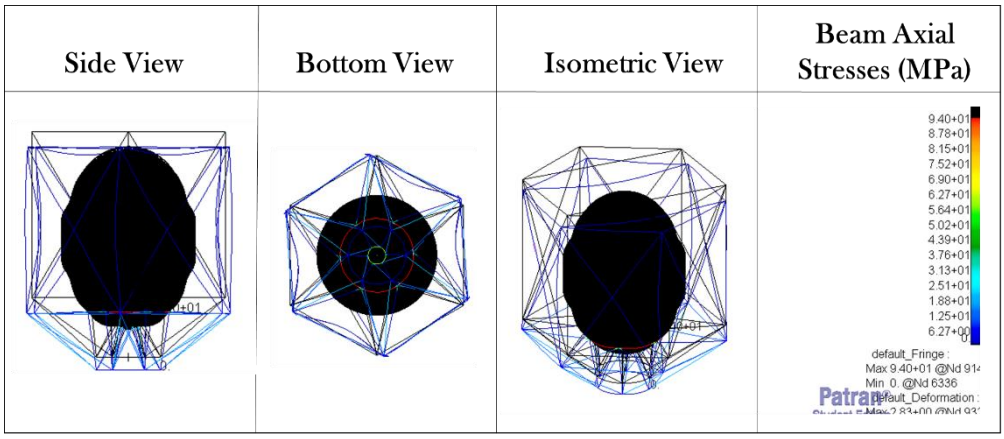

Figure 5.21 Axial Stresses of the Beam Members at Frequency 49.68 (Hz)

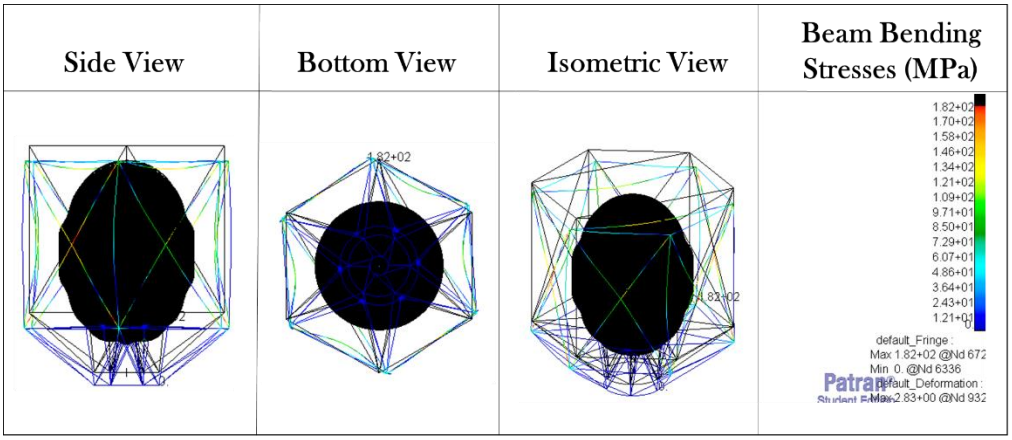

Figure 5.20 Bending Stresses of the Beam Members at Frequency 49.68 (Hz)

For both structures, the stress results at peak excitation frequencies, considering the case of the longitudinal enforced acceleration, are presented in the following tabular form.

		Tank		Frame					
Frequency (Hz)	Shape Mode	Maximum Von Mises Stress (MPa)	Region	Maximum Axial Stress (MPa)	Region	Maximum Bending Stress (MPa)	Region	Maximum Combined Stress (MPa	Region
47.17	Torsional	323	Cylindrical Body	93.2	Main Deck Ring	57	Support Struts	108.4	Main Deck Ring
49.68	Lateral Struts Breathing	323	Cylindrical Body	93.4	Main Deck Ring	182	Lateral Struts	188.3	Lateral Struts

Table 5.10 Stress Results at Peak Excitation Frequencies

Apparently, the maximum combined stresses on the frame, throughout the frequency range between 5 (Hz) to 125 (Hz), equals to 188 (MPa) and occurs at a lateral strut beam member.

Design Iteration	Maximum Combined Stress (MPa)	Frequency (Hz)	Region	Margin of Safety	Acceptance /Reject
1	188	∀	Lateral Struts	0.3324	✔

Table 5.11 Maximum Combined Stresses on the Frame

5.2.1.2. Lateral Enforced Acceleration

According to Table 5.8, Diagram 5.15 illustrates the lateral enforced acceleration amplitude as a function of frequency, which is the second and final load case for sizing the frame structure with regards to the sinusoidal vibration analysis.

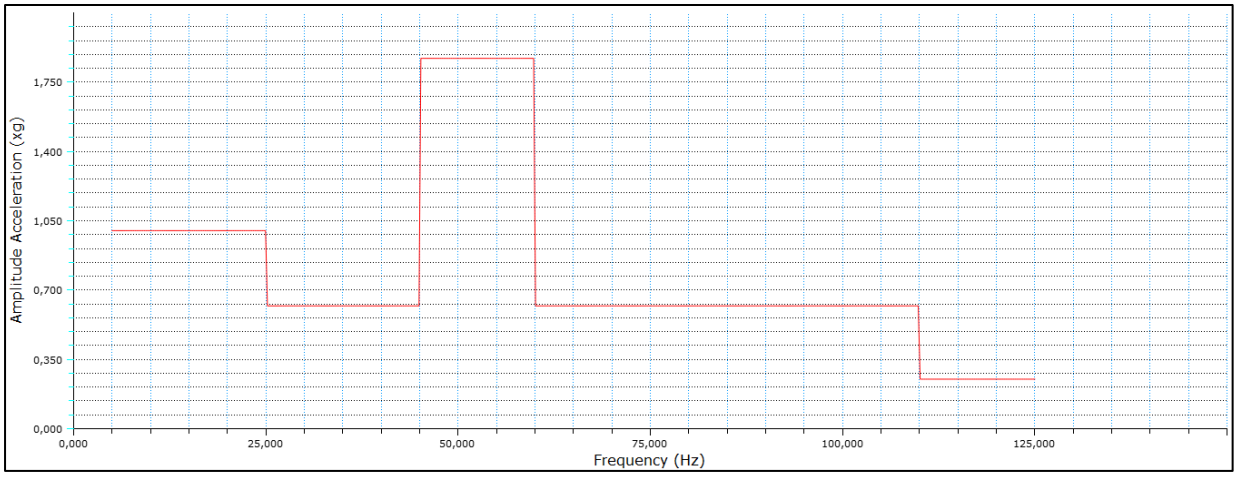

Diagram 5.15 Lateral Acceleration Amplitude vs Frequency [Credits: Arianespace]

The design process is terminated after three iterations, verifying that tank's safe operation under the above acceleration input. Similar to the previous load case, the maximum Von Mises stresses are developed on the cylindrical body of the tank.

Design Iteration	Maximum Von Mises Stress (MPa)	Frequency (Hz)	Region	Margin of Safety	Acceptance /Reject
1	2010	115.87	Attachment Points/Mounting Ring	-0.8376	✗
2	1830	122.84	Attachment Points/Mounting Ring	-0.8217	✗
3	324	∀	Cylindrical Body	0.042	✔

Table 5.12 Results of the Tank Response upon Longitudinal Enforced Acceleration

It can be observed, even after the first design iteration, unacceptable shell stresses are developed along the attachment region of the tank, which correspond to the mounting ring of the frame.

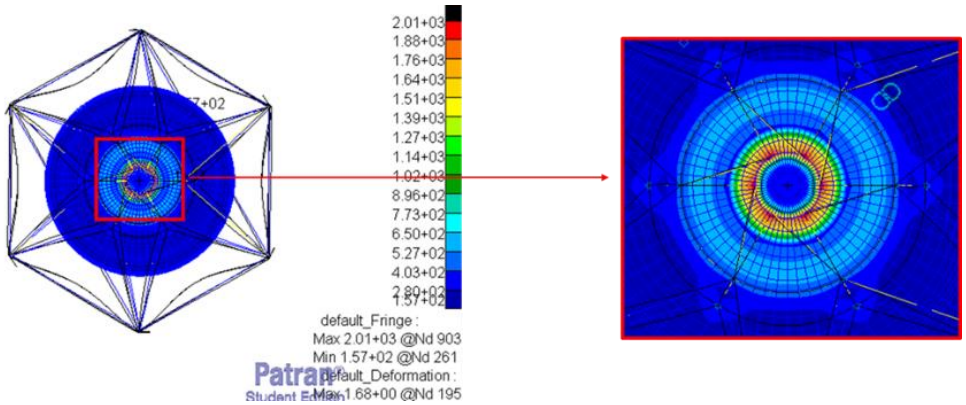

Figure 5.22 Von Mises Stresses on the Tank

Nodal Von Mises stresses of the most critical tank's regions are plotted as a function of frequency. Diagram 5.16 captures the unacceptable stress peak, which is developed on the attachment region of the tank, at the excitation frequency of 115 (Hz).

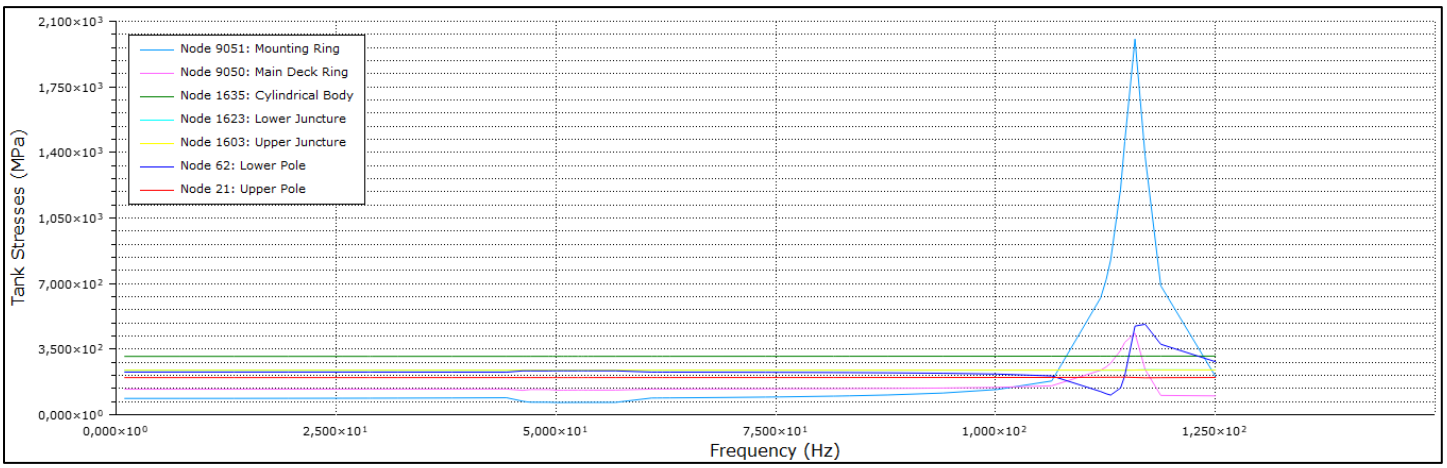

Diagram 5.16 Tank Stresses Vs Frequency

Two cross-sectional modifications have been applied for the adapter ring and the supplemental support struts. The finalized cross-sectional area for the beam member groups are (20x2) and (20x2) respectively.

Design Iteration	Member Modification	Cross-sectional Modification
1	Adapter Ring & Supplemental Support Struts	(10x1) → (15x1) & (10x1) → (15x1)
2	Adapter Ring & Supplemental Support Struts	(15x1) → (20x2) & (15x1) → (20x2)
3	-	-

Table 5.13 Cross-sectional Modifications

The design sequence of the iterative process is illustrated at Figure 5.23. For each design iteration, the particular beam member groups requiring cross-sectional modifications, are marked.

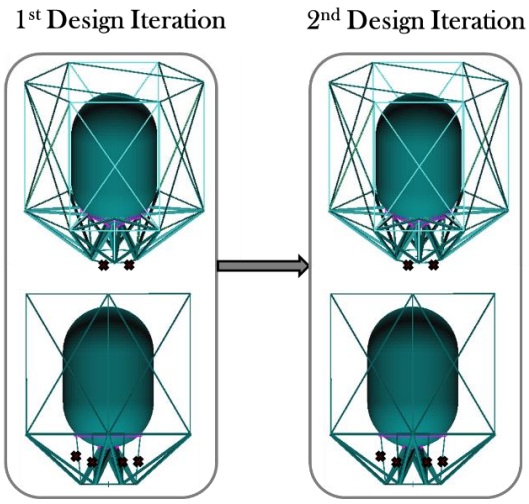

Figure 5.23 Design Sequence of the Frame Sizing for the Tension Load Case

Nodal Von Mises stresses of the most critical tank's regions are plotted as a function of frequency. Diagram 5.17 depicts the acceptable stress responses of the particular regions.

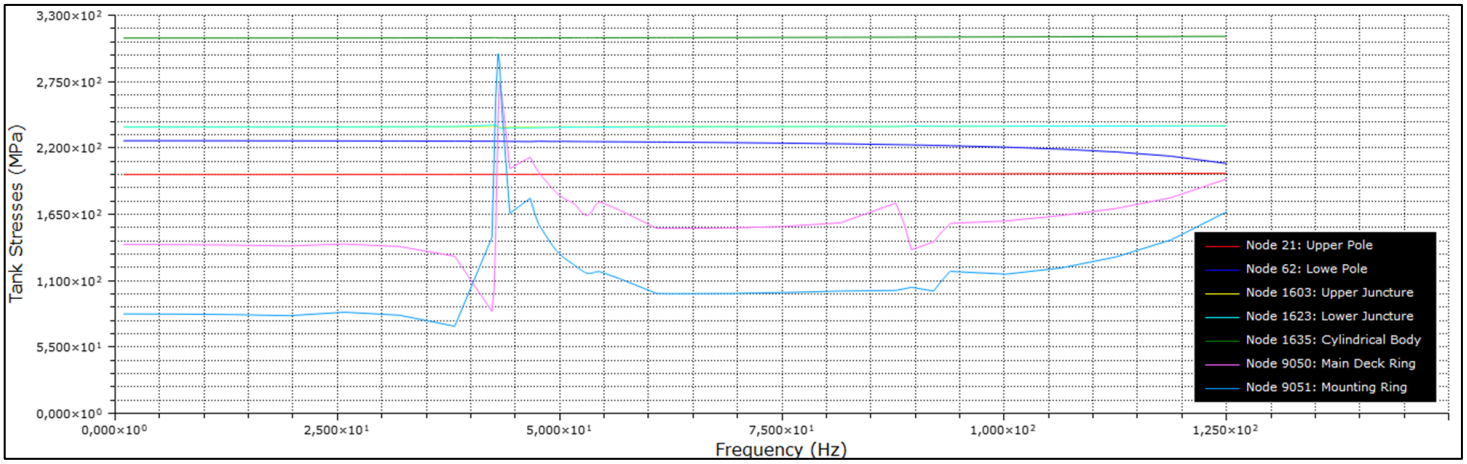

Diagram 5.17 Tank Stresses Vs Frequency

A typical example of stress distribution on the tank structure throughout the frequency range of interest, is shown at Figure 5.24 for the third design iteration.

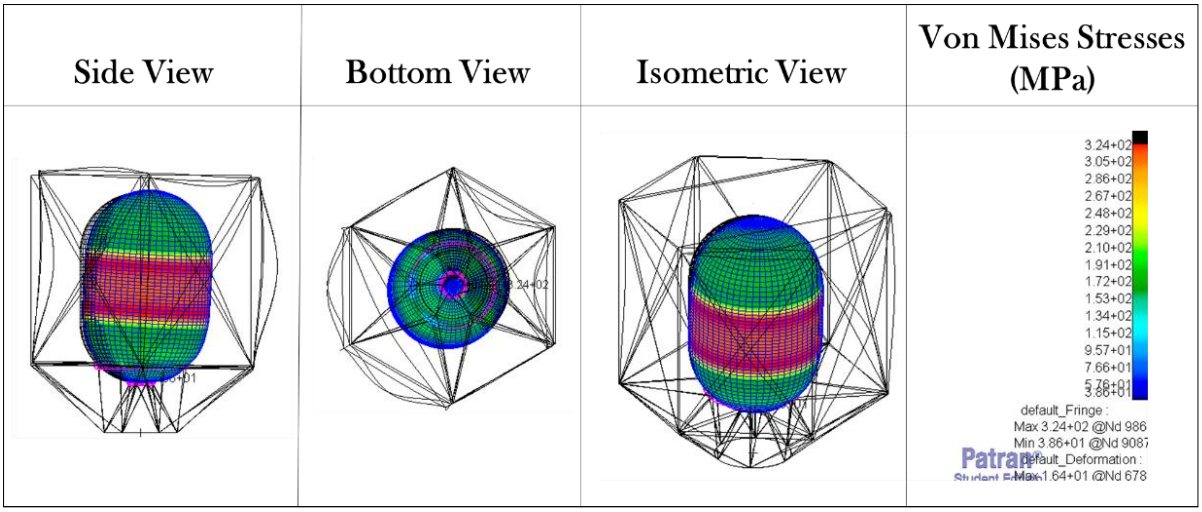

Figure 5.24 Von Mises Stress Distribution

Upper Bulkhead Region:

Diagram 5.18 and Diagram 5.19 illustrate the nodal axial and the bending stresses developed on the highlighted upper bulkhead nodes (6592, 6602, 6631, 6669, 6707 and 6736). The maximum axial stress response does not exceed 14 (MPa) and occurs at the excitation frequency of 43.07 (Hz). The maximum bending stress response does not exceed 115 (MPa) and occurs at the excitation frequency of 52.12 (Hz).

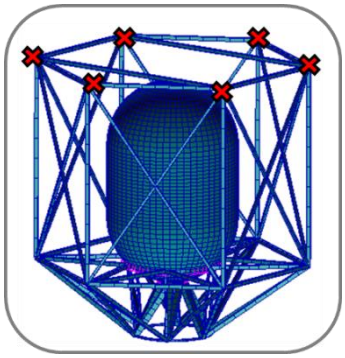

Figure 5.25 Upper Bulkhead Region

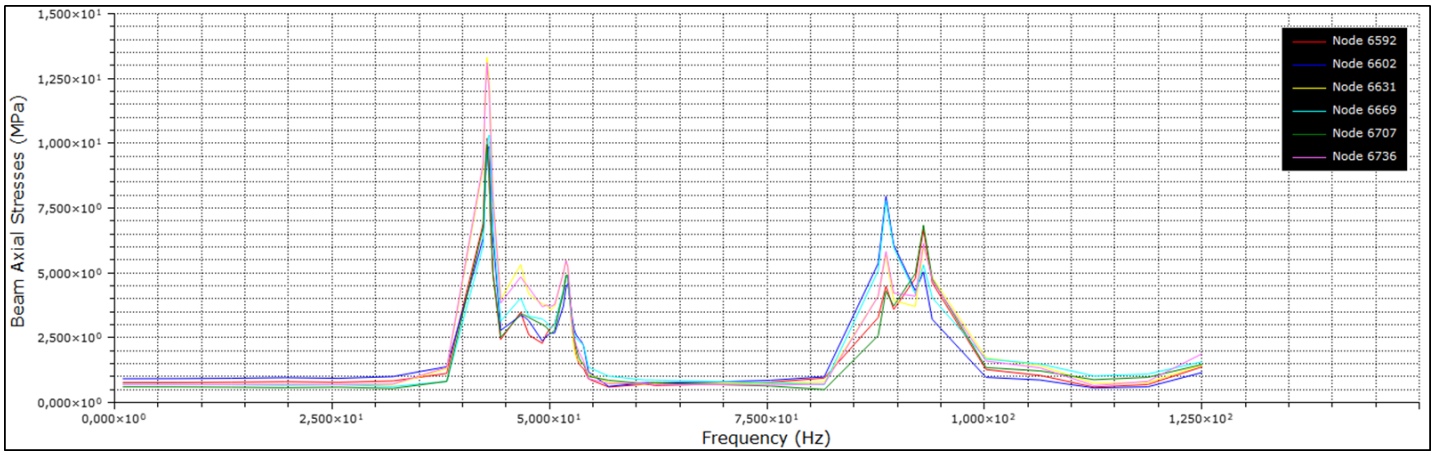

Diagram 5.18 Axial Stresses Vs Frequency

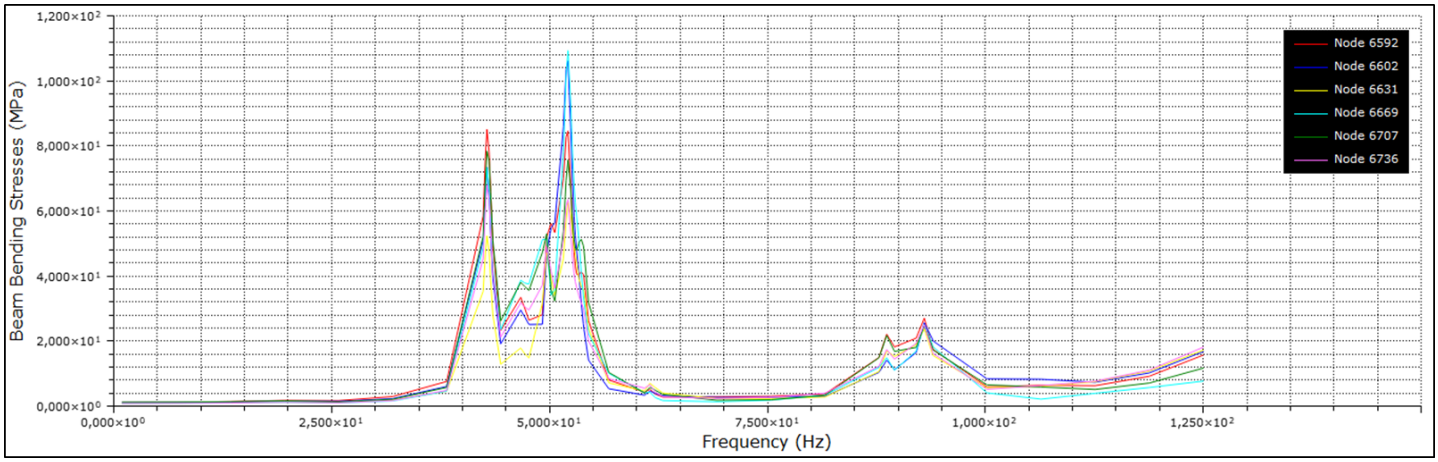

Diagram 5.19 Bending Stresses Vs Frequency

Lower Bulkhead Region:

Diagram 5.20 and Diagram 5.21 illustrate the nodal axial and the bending stresses developed on the highlighted upper bulkhead nodes (6000, 6019, 6020, 6030, 6391 and 6392). The maximum axial stress response does not exceed 32 (MPa) and occurs at the excitation frequency of 43.07 (Hz). The maximum bending stress response does not exceed 75 (MPa) and occurs at the excitation frequency of 52.12 (Hz).

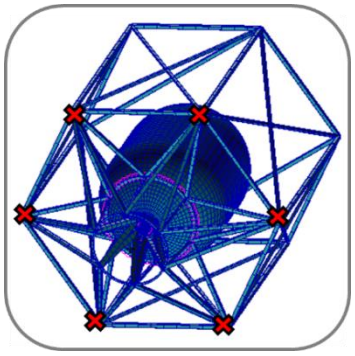

Figure 5.26 Lower Bulkhead Region

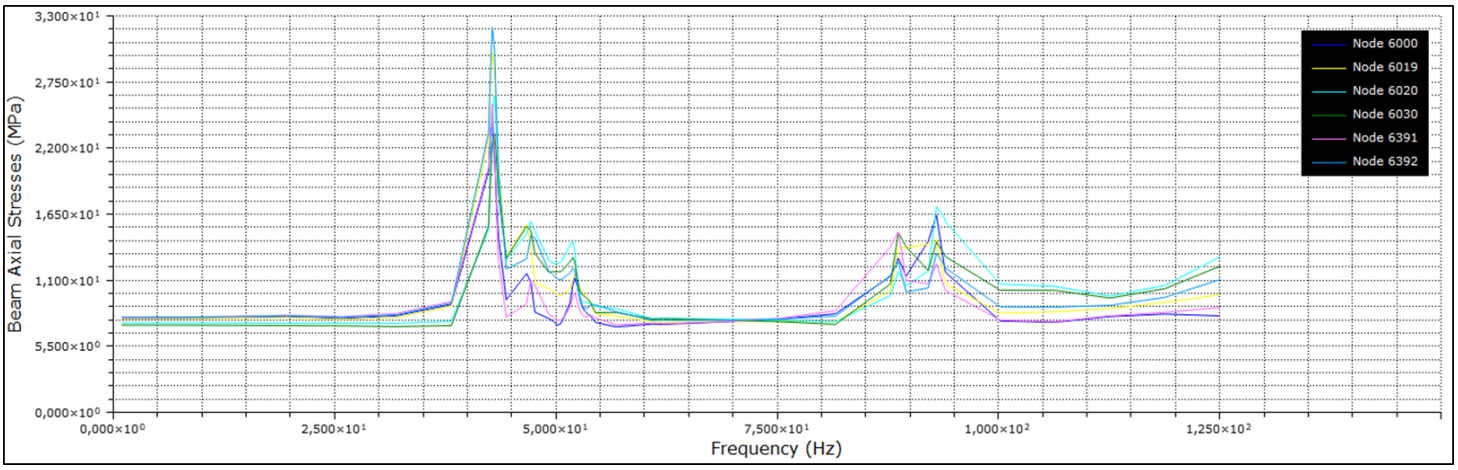

Diagram 5.20 Axial Stresses Vs Frequency

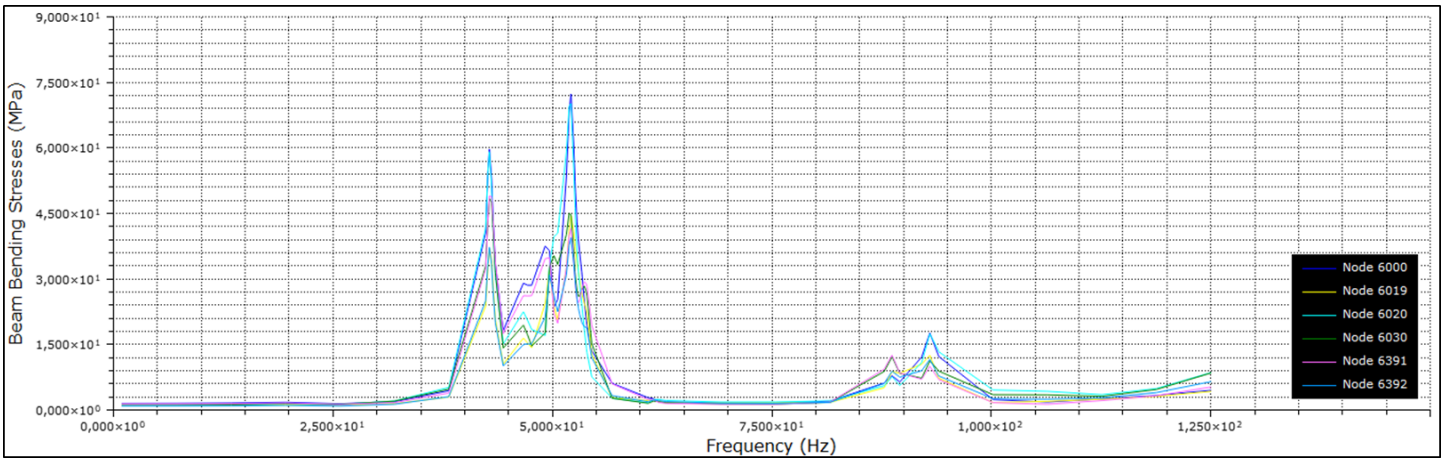

Diagram 5.21 Bending Stresses Vs Frequency

Lateral Struts Region:

Diagram 5.22 and Diagram 5.23 illustrate the nodal axial and the bending stresses developed on the highlighted upper bulkhead nodes (6573, 6612, 6650, 6888, 6717 and 6746). The maximum axial stress response does not exceed 35 (MPa) and occurs at the excitation frequency of 43.07 (Hz). The maximum bending stress response does not exceed 180 (MPa) and occurs at the excitation frequency of 52.12 (Hz).

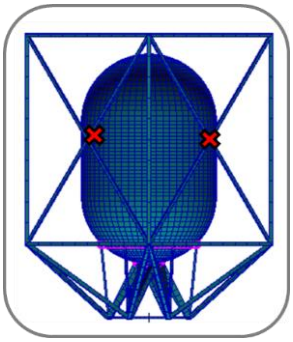

Figure 5.27 Lateral Struts Region

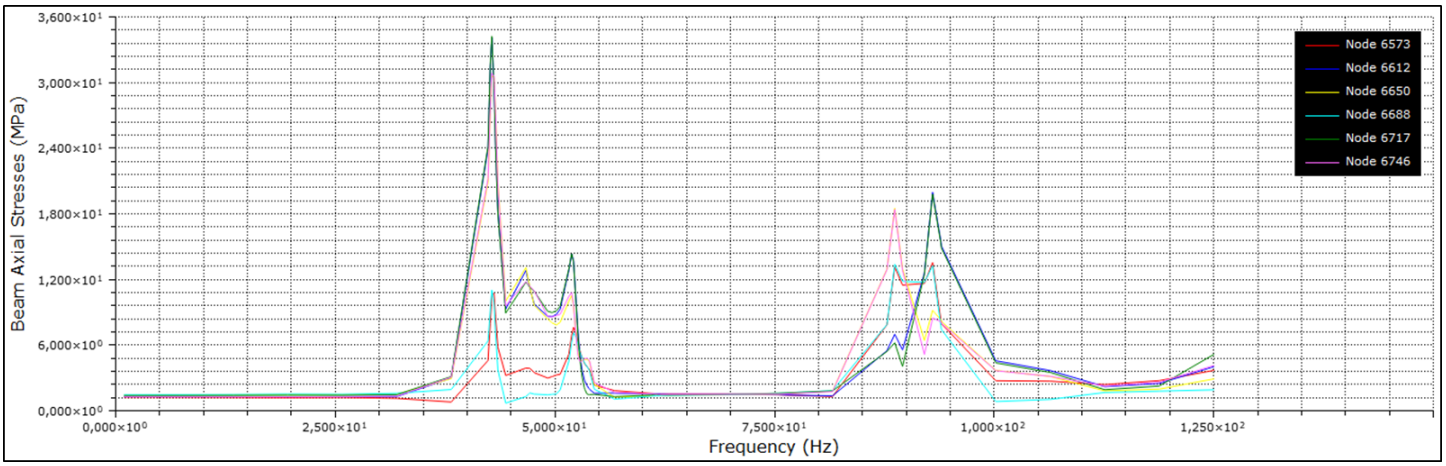

Diagram 5.22 Axial Stresses Vs Frequency

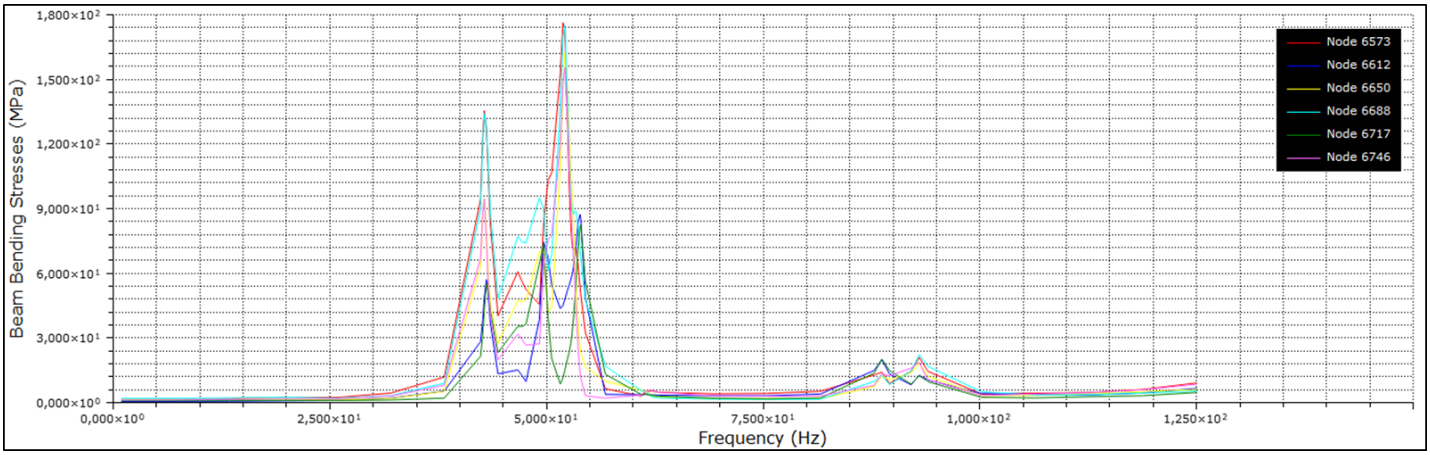

Diagram 5.23 Bending Stresses Vs Frequency

Mounting Ring Region:

Diagram 5.24 and Diagram 5.25 illustrate the nodal axial and the bending stresses developed on the highlighted upper bulkhead nodes (9125, 9126, 9127, 9128, 9129 and 9131). The maximum axial stress response does not exceed 120 (MPa) and occurs at the excitation frequency of 43.07 (Hz). The maximum bending stress response does not exceed 125 (MPa) and occurs at the excitation frequency of 43.07 (Hz) as well.

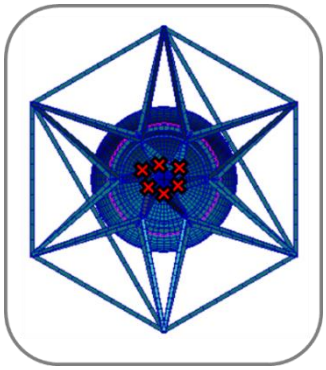

Figure 5.28 Mounting Ring Region

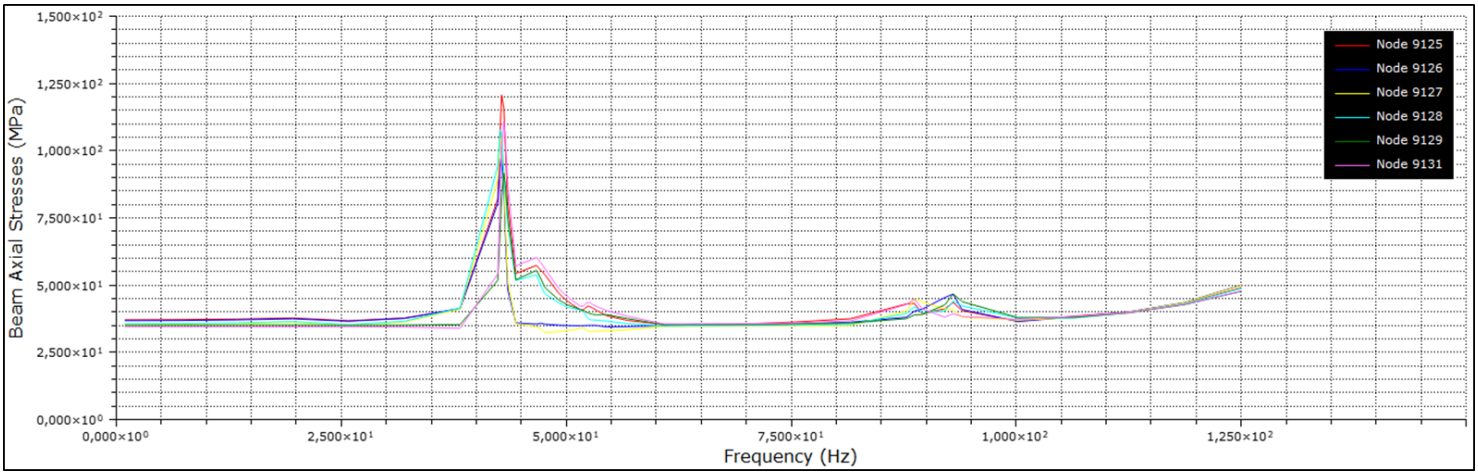

Diagram 5.24 Axial Stresses Vs Frequency

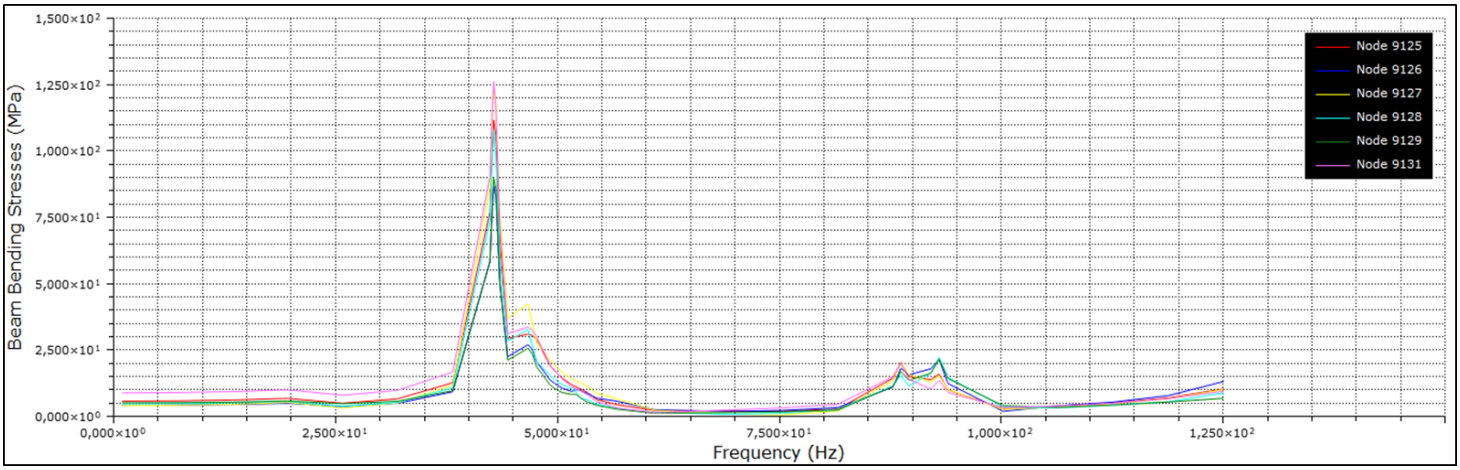

Diagram 5.25 Bending Stresses Vs Frequency

Main Deck Region:

Diagram 5.26 and Diagram 5.27 illustrate the nodal axial and the bending stresses developed on the highlighted upper bulkhead nodes (9120, 9121, 9122, 9123, 9124 and 9130). The maximum axial stress response does not exceed 110 (MPa) and occurs at the excitation frequency of 43.07 (Hz). The maximum bending stress response does not exceed 95 (MPa) and occurs at the excitation frequency of 43.07 (Hz) as well.

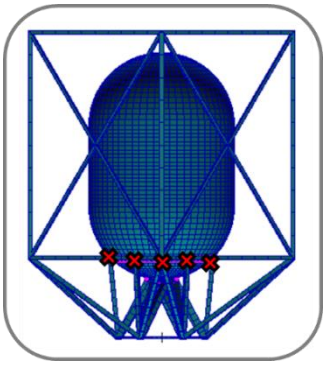

Figure 5.29 Main Deck Ring Region

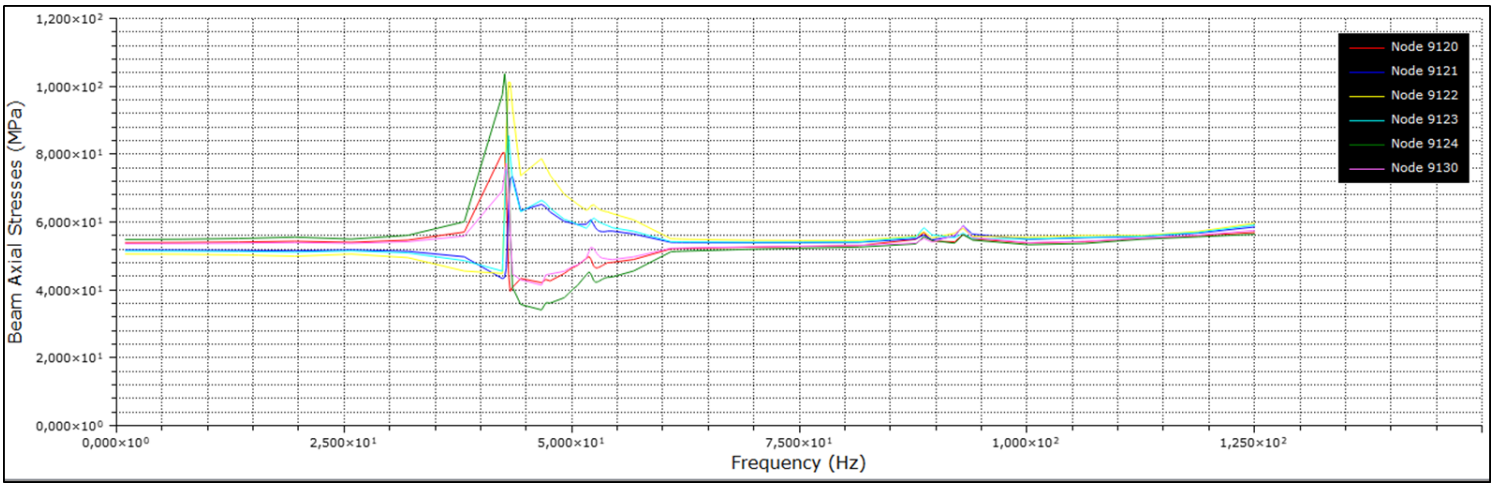

Diagram 5.26 Axial Stresses Vs Frequency

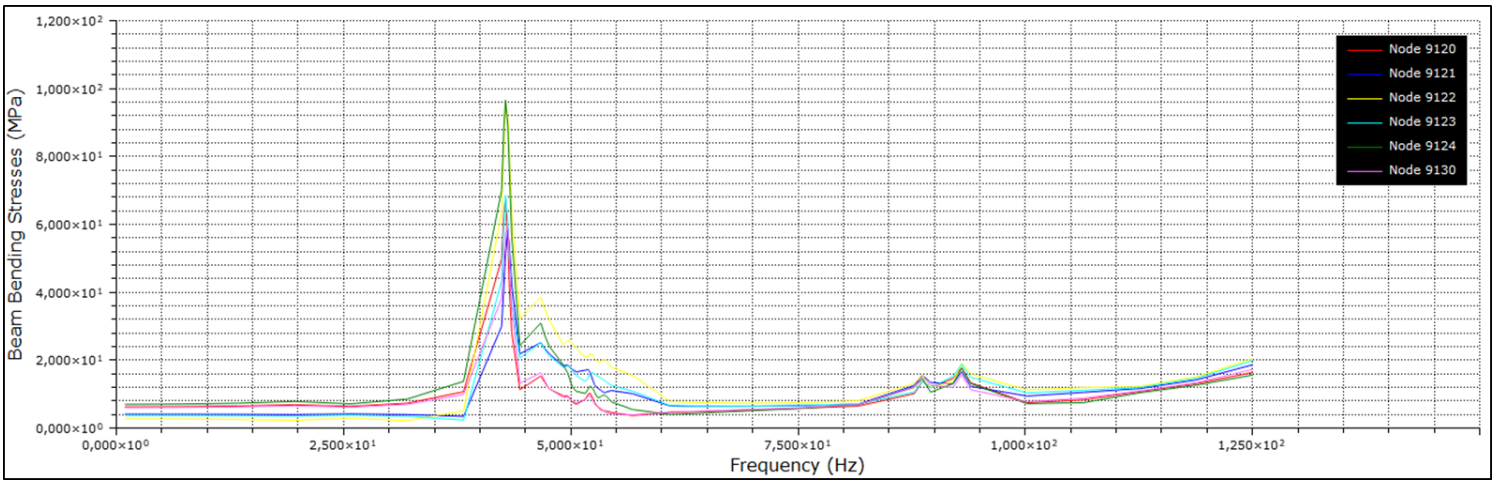

Diagram 5.27 Bending Stresses Vs Frequency

Adapter Ring Region:

Diagram 5.28 and Diagram 5.29 illustrate the nodal axial and the bending stresses developed on the highlighted upper bulkhead nodes (6153, 6163, 6182, 6213, 6233 and 6247). The maximum axial stress response does not exceed 135 (MPa) and occurs at the excitation frequency of 43.07 (Hz). The maximum bending stress response does not exceed 50 (MPa) and occurs at the excitation frequency of 43.07 (Hz) as well.

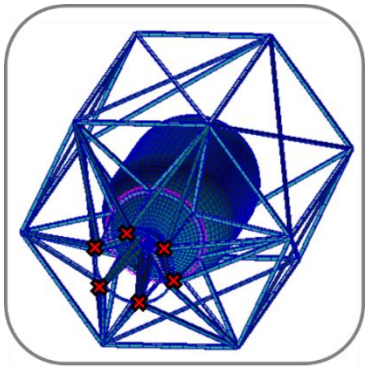

Figure 5.30 Adapter Ring Region

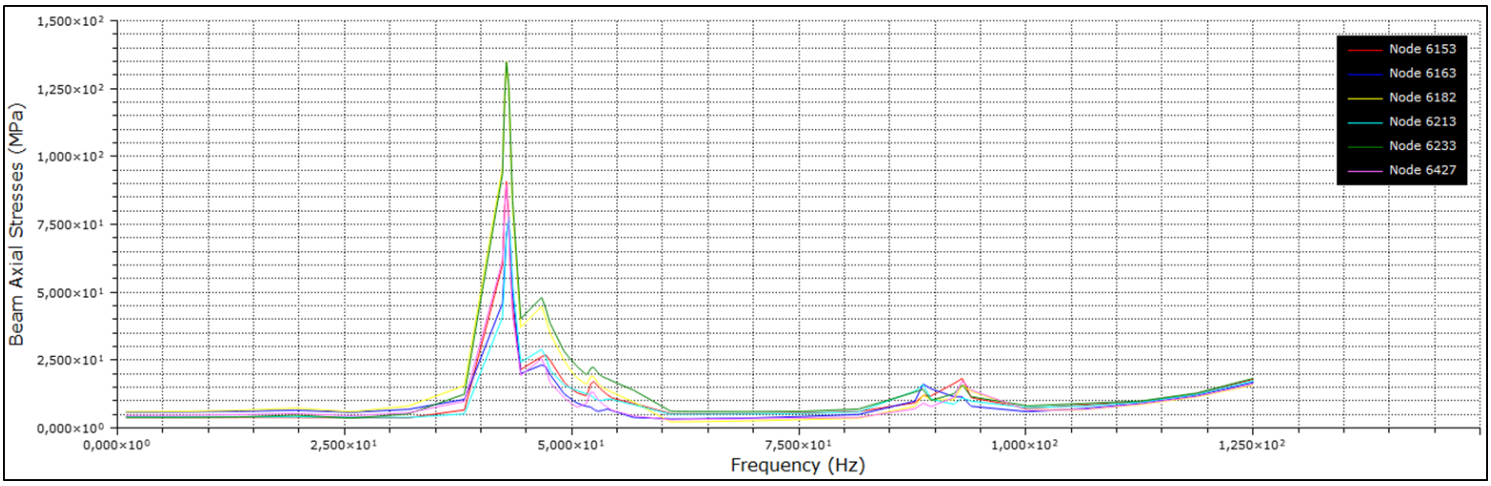

Diagram 5.28 Axial Stresses Vs Frequency

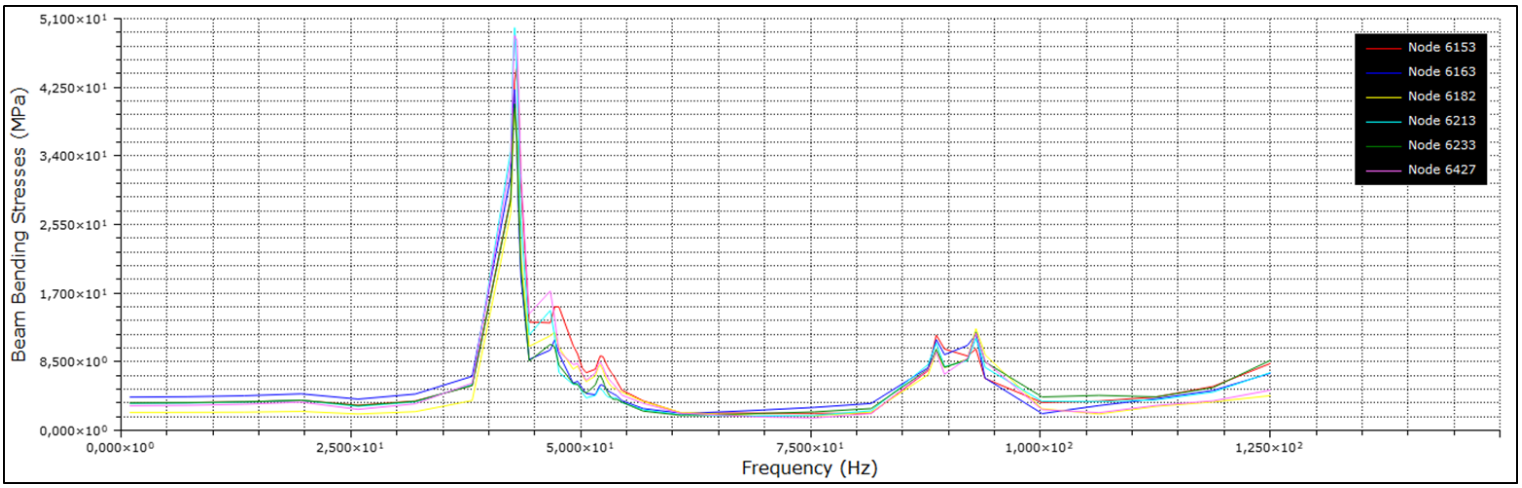

Diagram 5.29 Bending Stresses Vs Frequency

By examining the stresses developed on the frame structure throughout the frequency domain of interest, it can be clearly observed that the peaks in stress responses tend to occur at specific frequencies, such as 43.07 (Hz), 52.12 (Hz), 86.47 (Hz) and 94.91 (Hz). Among them, the first one corresponds to the second natural frequency, leading to a lateral mode shape. The second one, corresponds to the fifth natural frequency of the structure, leading to lateral struts breathing mode. The last two correspond to the twenty-second and twenty-fourth natural frequencies respectively leading to longerons breathing mode.

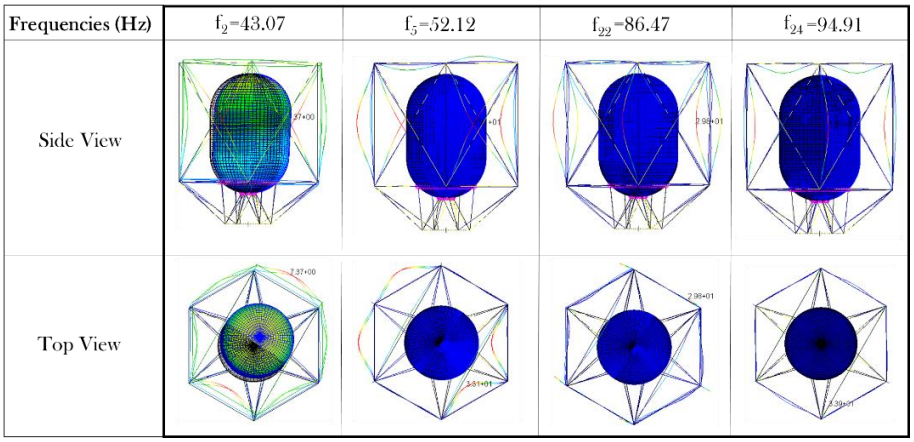

Figure 5.31 Peak Excitation Frequencies

Axial and bending stress plots, at those particular frequencies, are presented below, in order to define the magnitude and the location of the maximum combined stresses on the frame structure.

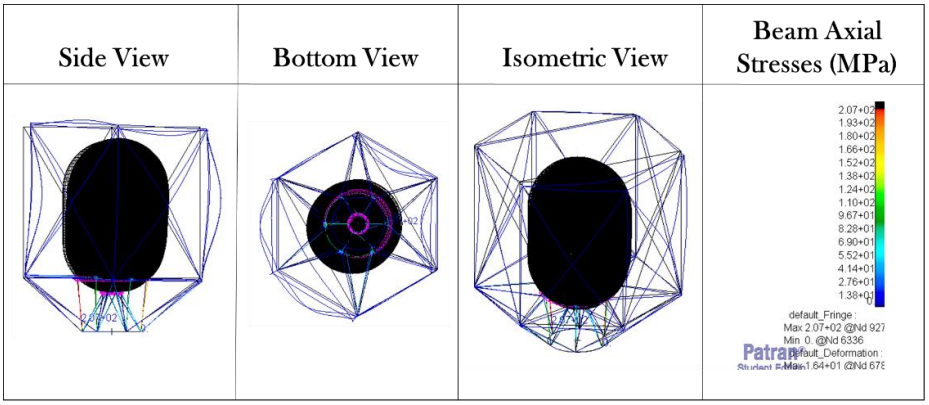

Figure 5.32 Axial Stresses of the Beam Members at Frequency 43.07 (Hz)

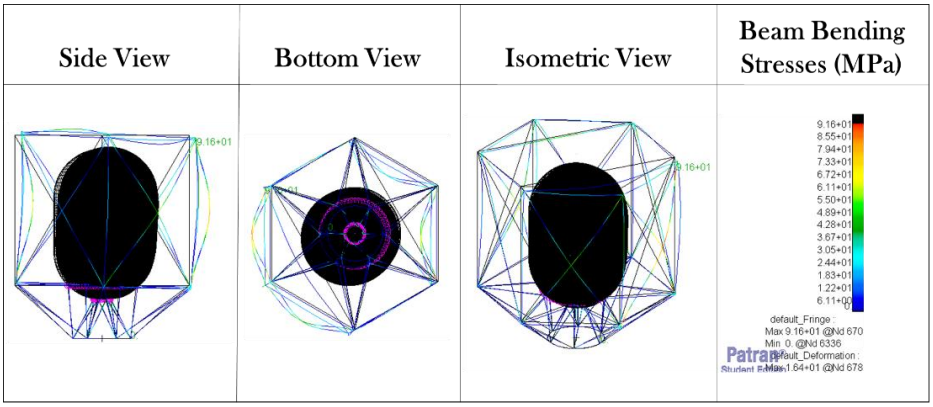

Figure 5.33 Bending Stresses of the Beam Members at Frequency 43.07 (Hz)

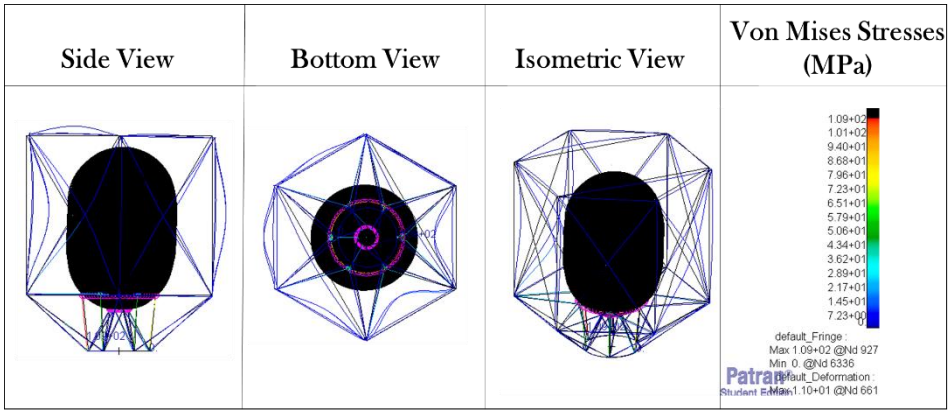

Figure 5.34 Axial Stresses of the Beam Members at Frequency 52.12 (Hz)

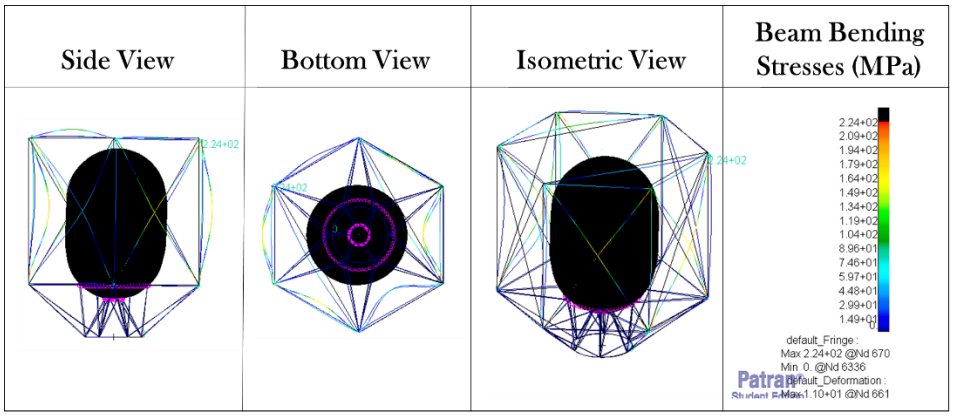

Figure 5.35 Bending Stresses of the Beam Members at Frequency 52.12 (Hz)

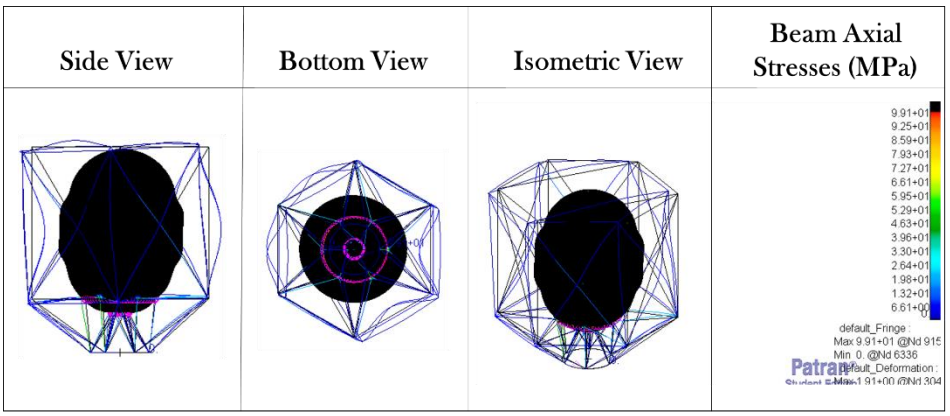

Figure 5.36 Figure 5.59. Axial Stresses of the Beam Members at Frequency 86.47 (Hz)

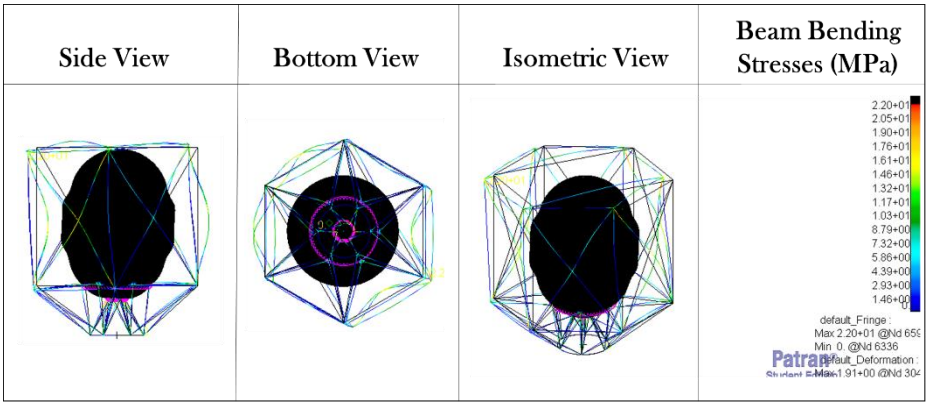

Figure 5.37 Bending Stresses of the Beam Members at Frequency 86.47 (Hz)

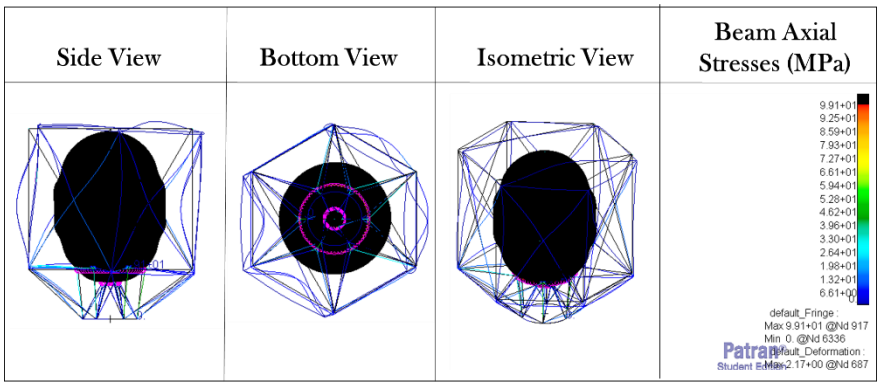

Figure 5.38 Axial Stresses of the Beam Members at Frequency 94.91 (Hz)

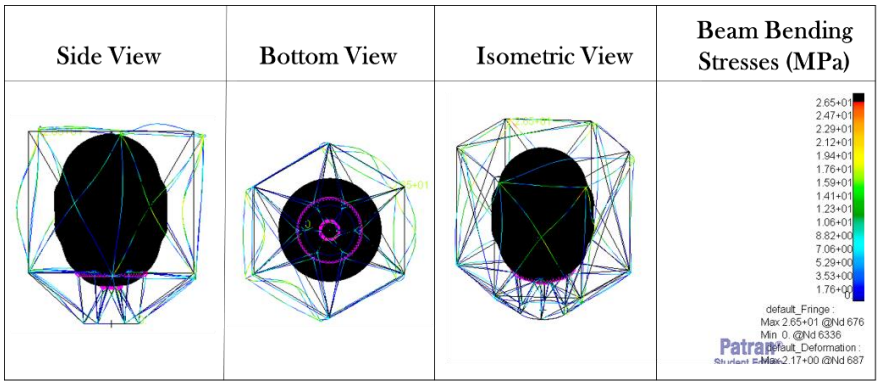

Figure 5.39 Axial Stresses of the Beam Members at Frequency 94.91 (Hz)

For both structures, the stress results at peak excitation frequencies, considering the case of the longitudinal enforced acceleration, are presented in the following tabular form (Table 5.14)

		Tank				Frame			
Frequency (Hz)	Shape Mode	Maximum Von Mises Stress (MPa)	Region	Maximum Axial Stress (MPa)	Region	Maximum Bending Stress (MPa)	Region	Maximum Combined Stress (MPa)	Region
43.07	Lateral Struts Breathing	324	Cylindrical Body	207	Support Struts	91.6	Lateral Struts	234.6	Support Struts
52.12	Lateral Struts Breathing	324	Cylindrical Body	109	Support Struts	224	Lateral Struts	238	Lateral Struts
86.47	Longerons Breathing	324	Cylindrical Body	99.1	Main Deck Ring	22	Lateral Struts	104.9	Main Deck Ring
94.91	Longerons Breathing	324	Cylindrical Body	99.1	Main Deck Ring	26.5	Lateral Struts	104.4	Main Deck Ring

Table 5.14 Stress Results at Peak Excitation Frequencies

Design Iteration	Maximum Combined Stress (MPa)	Frequency (Hz)	Region	Margin of Safety	Acceptance /Reject
3	238	∀	Lateral Struts	0.0542	✔

Table 5.15 Maximum Combined Stresses on the Frame

Apparently, the maximum combined stresses on the frame, throughout the frequency range between 5 (Hz) to 125 (Hz), equals to 188 (MPa) and occurs at a lateral strut beam member.

5.3. Evaluation of Dynamic Analysis Results

After the completion of the sizing procedure for both structural modules of the tanker spacecraft through dynamic strength analysis, mass properties are reported and evaluated in order to ensure that the design requirements for mini passengers are met. The mass and the center of gravity position of the tanker spacecraft are listed below:

Tank Modules	Thickness (mm)
Upper Dome	6.5
Lower Dome	6.5
Cylindrical Body	6.5
Total Structure Mass (kg)	44.41

Table 5.16 Tank Structure Properties

Center of Gravity	
$x_{C.o.G}$ (mm)	0
$y_{C.o.G}$ (mm)	0
$z_{C.o.G}$ (mm)	546

Table 5.18 Center of Gravity Position

Frame Bram Groups	Cross-sectional Area
Adapter Ring	(20x2)
Support Struts	(30x3)
Supplemental Support Struts	(20x2)
Mounting Ring	(34x3)
Connection Struts	(20x2)
Main Deck Struts	(20x2)
Main Deck Ring	(20x2)
Upper/Lower Bulkhead	(20x2)
Lateral Struts	(15x1)
Longerons	(20x2)
Upper Struts	(20x2)
Total Structure Mass (kg)	17.89

Table 5.17 Frame Structure Properties

It can be observed that the combined mass of the storage tank and the frame is 59.30 (kg) which corresponds to the 14.83% of the maximum possible mass.
It should be pointed out that both constraints induced by Center of Gravity position of the structure are satisfied, as its height does not exceed 900(mm) from the mounting plane of the spacecraft and its static unbalance does not exceed 15 (mm).

6. Conclusions and Recommendations

6.1. Conclusions Drawn by the Results

It is of great importance that a summary of the most significant findings of this thesis work be reported by taking into account all the steps that have been made upon proceeding with the structural design of the tanker spacecraft.

First of all, the study initiated with the conceptual design of the tanker spacecraft's payload and its primary structure. The payload is considered to be the storage tank, including the contained propellant. The proposed configuration for the storage tank is a cylindrically shaped main body combined with hemispherical domes. This type of tank configuration is selected due to mass and volume efficiency considerations. On the other hand, the configuration of the primary structure is carried out by developing skeletal network of beams. Following previous successful structural design concepts for small spacecrafts, the proposed configuration of the frame is a symmetrical structure, formed by the combination of a hexagonal beam box and a conical interface beam tower. The cross-sectional profile selected for the frame beams is hollow rectangular. The construction materials for both structures are selected with the intention of satisfying multiple criteria regarding strength mass and manufacturing efficiency. Consequently, aluminum alloys have been capitalized as candidate materials for manufacturing the structural modules of the tanker spacecraft.

The mathematical representation of the envisaged structures, plays a vital role in predicting their structural response under both static and dynamic loads. In particular, it is achieved utilizing the finite element method, which enjoys predominance among the numerical methods, mainly in solving complex structural mechanics problems. The selected software for performing finite element analysis is the academic version of MSC Patran and Nastran Software, 2018. The storage tank is modelled with three-nodded and four-nodded isoparametric shell elements and the frame structure with two-nodded beam elements. The welded type rigid connection between the two structures is achieved via rigid elements.

The thickness and the preliminary cross-sectional dimensions of the beam members have been established by an iterative linear static strength analysis procedure which have ensured that both structures are capable of withstanding the maximum static and quasi-static loads, preventing material yielding. Additionally, linear buckling analysis has been performed separately for each structure, showing that no buckling will occur neither for the tank nor for the frame, under worst-case scenarios. Delving into the design of the tank structure, a supplemental finite element model is developed, exploiting the structure's symmetry. The analysis proved that the internal pressure acting on it, is the most critical design load. Considering its ultimate magnitude, an elastoplastic analysis of the tank is conducted, showing that its thickness is sufficient in order to prevent the structure from ultimate failure. Another significant conclusion drawn, by this particular analysis, the determination of the magnitude of internal pressure which induce the initiation of plastic deformation and finally the excessive yielding. After the completion of static strength analysis, both center of gravity and mass requirements are satisfied.

The second part of the structural design process entails the dynamic analysis of the tanker spacecraft. Initially, modal analysis has been performed suggesting particular design and cross-sectional modifications on the frame, in order to increase the overall stiffness of the structure at both longitudinal and lateral direction and simultaneously to satisfy the

natural frequency requirements. The finalized dimensions of the cross-sectional areas of the beam members are determined by subjecting the tanker spacecraft to sinusoidal vibration. Enforced acceleration has been applied on longitudinal and lateral axis of the structure separately and its dynamic structural response was accessed by an iterative sizing procedure. After the completion of dynamic strength analysis both center of gravity and mass requirements are satisfied.

6.2. Limitations

Throughout this thesis work, significant limitations have been encountered, concerning the design and the analysis of the proposed tanker spacecraft. First of all, the complexity, induced by the combination of multiple disciplines influencing the spacecraft design, play a determinative role in proceeding with a simplistic approach in sizing, only the most critical structures. As a result, the structural design process is limited to the storage tank and the frame exclusively.

Secondly, individual aluminum alloys are selected for each structural module of the spacecraft. Therefore, the results drawn from the finite element analysis are limited only for these specific materials. An additional limitation is introduced upon selecting cross-sectional profiles for the beam members of the frame. Specifically, hollow rectangular cross-section profile is utilized for the frame beams in their entirety.

Finally, the academic version of MSC Patran and Nastran Software restrict the developed finite element models to the limited number of, only, 5000 computational nodes. Based on this particular limitation the envisaged structures are discretized with the finest possible mesh.

6.3. Recommendations for Future Research

Trying to encounter the aforementioned limitations, valuable findings could also be drawn in case of delving deeper into extending this thesis research. It would be beneficial if the finite element model of the tanker spacecraft is complemented with additional structural modules so as to achieve a more realistic approach of the tanker spacecraft concept. A prime example of this kind, could be the implementation of a skin-frame structure which incorporates honeycomb sandwich panels. Additionally, supplemental subsystems of the spacecraft, such as mission-oriented instruments, electronic boxes etc., could be included in the finite element model as non-structural masses.

Furthermore, it is recommended that exactly the same design procedure be repeated, in order to examine how a different material selection affects the structural response of both examined structures. It would be valuable, if the finite element model is updated with a data base of candidate materials so as to perform a comparative analysis and finally to select the optimum candidate material. The concept of updating the finite element model, could also be extended by selecting an alternative cross-sectional profile of the beam members of the frame.

A final recommendation for future research, concerns the improvement of the overall sizing procedure by updating the iterative trial and error design concept-assuming the same design variables and constraints-to a deterministic optimized design. This particular recommendation could be carried out via an alternative open source software for finite element computations. It is of great significance to mention that this approach can benefit the analysis of the existing finite element model by simultaneously inducing a massive increase in the number of the computational nodes and hence tackling the limitation, encountered in the academic 2018 version of MSC Patran and Nastran Software.

Bibliography

[1] B. Benedict, "Rationale for Need of In-Orbit Servicing Capabilities for GEO Spacecraft," in *AIAA Space Forum* , San Diego, California , 2013.

[2] B. Benedict, "Investing in Satellite Life Extension - Fleer Planning Options for Spacecraft Owner/Operators," in *AIAA Space Forum*, San Diego, California, 2014.

[3] Arianespace Servise & Solutions , Auxiliary Passengers using Arianespace Systems, Evry Cedex, France, 2017 .

[4] D. Huzel and D. Huang, "Design of Propellant Tanks," in *Modern Engineering for Design of Liquid-Propellant Rocket Engines*, Washington DC, American Institute of Aeronautics and Astronautics, 1992, p. 287.

[5] P. Fortesque, G. Swinerd and G. Stark, "Spacecraft Structures," in *Spacecraft Systems Engineering*, West Sussex, United Kingdom, John Wiley and Sons, 2011, pp. 256-261.

[6] European Cooperation for Space Standardization, "Overview of the Loads Analysis Process," in *Space engineering: Spacecraft mechanical loads analysis handbook*, Noordwijk, Netherlands, ESA Requirements and Standards Division, 2013, pp. 23-39.

[7] P. Sforza, "General Launch Vehicle Design Considerations," in *Manned Spacecraft Design Principles*, Oxford, United Kingdom, Elsevier, 2016, p. 282.

[8] European Cooperation for Space Standardization, "Factor Values," in *Space Engineering: Structural Factors of Safety for Spaceflight Hardware*, Noordwijk, Netherlands, ESA Requirements and Standards Division, 2009, p. 21.

[9] The MSC Software Corporation, "Introduction to Linear Buckling," in *MSC Nastran Linear Static User's Guide*, Newport Beach, California, 2017, pp. 320-323.

[10] The MSC Software Corporation, "Inelastic Behavior," in *MSC Nastran Nonlinear (SOL 400) User's Guide*, Newport Beach, 2017.

[11] The MSC Software Corporation, MSC Nastran Dynamic Analysis User's Guide, Newport Beach, California, 2017.